UNIVERSITY OF BELGRADE

SCHOOL OF ELECTRICAL ENGINEERING

Vladislava N. Bobić

DECISION SUPPORT SYSTEM FOR ASSESSMENT OF PATIENTS WITH NEURODEGENERATIVE DISORDERS

Doctoral Dissertation

Belgrade, 2020.

УНИВЕРЗИТЕТ У БЕОГРАДУ
ЕЛЕКТРОТЕХНИЧКИ ФАКУЛТЕТ

Владислава Н. Бобић

СИСТЕМ ЗА ПОДРШКУ ОДЛУЧИВАЊУ, ЕВАЛУАЦИЈУ И ПРАЋЕЊЕ СТАЊА ПАЦИЈЕНАТА ОБОЛЕЛИХ ОД НЕУРОДЕГЕНЕРАТИВНИХ БОЛЕСТИ

докторска дисертација

Београд, 2020.

Подаци о ментору и члановима комисије

Ментор:

др Горан Квашчев, ванредни професор
Универзитет у Београду – Електротехнички факултет

Чланови комисије:

др Горан Квашчев, ванредни професор
Универзитет у Београду – Електротехнички факултет

академик др Дејан Поповић, редовни професор у пензији
Универзитет у Београду – Електротехнички факултет

академик др Владимир Костић, редовни професор
Универзитет у Београду – Медицински факултет

др Жељко Ђуровић, редовни професор
Универзитет у Београду – Електротехнички факултет

др Милица Ђурић-Јовичић, виши научни сарадник
Иновациони центар Електротехничког факултета у Београду

Датум одбране: _____.

Acknowledgment

I owe sincere thanks to the many people who helped me bring this thesis to its completion.

First, I would like to express my highest appreciation and gratitude to my supervisor, professor dr Goran Kvaščev, for his valuable guidance, collaboration, encouragement, and support during my Ph.D. studies and preparation of this thesis. I especially thank him for his help and advice about the intelligent algorithms presented within this thesis.

I am fortunate that I had the opportunity to work and collaborate with dr Milica Đurić-Jovičić. I thank dr Đurić-Jovičić for giving me exemplary guidance on many professional fields, for the profound collaboration, sincere support, and careful monitoring. Most of all, I am grateful for the opportunity to learn and do what I love.

I owe a great deal of gratitude to professor dr Mirjana Popović, who was my mentor at the beginning of my graduate education. Professor Popović guided me on my educational path and made it possible for me to become a member of her research team and start with an academic career.

The work presented in this thesis could not be done without a tremendous multidisciplinary collaboration with other scientific institutions. I want to thank professor dr Vladimir Kostić and his team from the Clinic of Neurology, Clinical Centre of Serbia, especially dr Nataša Dragašević-Mišković, dr Saša Radovanović, dr Iva Stanković, and dr Igor Petrović, on their collaboration, assistance with study designs and experiments, and selection of participants during our clinical studies. Moreover, I thank our partners dr Agnes Roby-Brami, dr Nathanaël Jarrassé and MSc Mathilde Lestoille from Institut des Systèmes Intelligents et de Robotique, l' Université Pierre et Marie Curie, Paris for their collaboration during our bilateral scientific projects and for sharing their valuable knowledge and experience about the advanced sensor systems.

I thank all the participants for providing me their trust, patience, and cooperation during my research studies.

Furthermore, I am very grateful to my closest colleagues and friends from the Innovation Center, School of Electrical Engineering in Belgrade, MSc Ilija Radovanović, MSc Miloš Janjić, MSc Milica Badža, and MSc Ivan Vajs for their everyday support and help, and for being my best lab partners and participants in all my ideas.

I would also like to thank professor dr Boško Nikolić and assistant professor dr Milica Janković from the School of Electrical Engineering - University of Belgrade for their sincere support

and collaboration during my Ph.D. studies. Furthermore, I owe a gratitude to professor dr Antonije Đorđević for his advice with the numerical analysis. I kindly thank professor dr Nenad Jovičić for the design and development of the inertial and force sensor systems used in this research.

Finally, I owe my deep sense of gratitude to my family and friends for all the love and support, especially my parents Biljana and Nedeljko, and boyfriend Stevan, without whom none of this would have been possible.

Vladislava Bobić

Decision support system for assessment of patients with neurodegenerative disorders

Abstract – Clinical decision support system represents a computer-aided tool that utilizes advanced technologies for influencing clinical decisions about patients. This dissertation presents research and development of a new decision support system for the assessment of patients with neurodegenerative diseases. The analysis of movements that are part of standard clinical scales or everyday activities represents the basis of the system. These movements are recorded using small and lightweight wearable, wireless sensors, which do not require complicated setup and can be easily applied in any environment. The first part of system is dedicated to the (early) recognition of Parkinson's disease (PD) based on gait analysis and deep learning algorithms. PD patients could be identified with a high accuracy. The other part of the system is dedicated to the assessment of PD symptoms, more specifically, bradykinesia, utilizing the knowledge-based reasoning. A method for analysis of bradykinesia related movements is defined and presented. Moreover, by applying different signal processing techniques, new metrics have been developed to quantify the essential characteristics of these movements. The prediction of symptom severity was performed using new expert system that completely objectified the clinical evaluation criteria. Validation was performed on the example of the finger-tapping movement of patients with typical and atypical parkinsonism. A high compliance rate was obtained compared to clinical data. The developed system is objective, automated, easy to use, contains an intuitive graphical and parametric presentation of results, and significantly contributes to the improvement of clinical assessment of patients with neurodegenerative diseases.

Keywords: decision support system; movement analysis; wearable sensors; machine learning; signal processing; expert rules; neurodegenerative disorders; Parkinson's disease, bradykinesia; clinical assessment.

Scientific area: technical sciences, electrical engineering

Specific scientific area: biomedical engineering

UDK number: 621.3

Систем за подршку одлучивању, евалуацију и праћење стања пацијената оболелих од неуродегенеративних болести

Резиме – Системи за подршку клиничком одлучивању представљају рачунарске алате који применом напредних технологија могу утицати на доношење одлука у вези са пацијентима. У овој дисертацији представљени су истраживање и развој новог система за подршку одлучивању, евалуацију и праћење стања пацијената оболелих од неуродегенеративних болести. Анализа клинички релевантних и свакодневних покрета чини основу овог система. Обрасци ових покрета снимљени су помоћу бежичних, носивих сензора малих димензија и тежине, који не захтевају компликовану поставку и могу се једноставно применити у било ком окружењу. Први део система намењен је (раном) препознавању Паркинсонове болести (ПБ) на основу анализе хода и алгоритама дубоког учења. Резултати су показали да је ПБ пацијенте могуће препознати са високом тачношћу. Други део система посвећен је праћењу симптома ПБ брадикинезије применом резоновања који се базира на знању. Представљена је метода за анализу покрета који се користе за евалуацију брадикинезије. Поред тога, применом различитих метода обраде сигнала развијена је нова метрика за квантификацију важних карактеристика ових покрета. Предикција степена развоја симптома се заснива на новом експертском систему који у потпуности објективизује клиничке евалуационе критеријуме. Валидација је урађена на примеру покрета тапкања прстију, који је снимљен на пацијенатима са типичним и атипичним паркинсонизимом. Показана је висока усаглашеност у поређењу са клиничким подацима. Развијени систем је објективан, аутоматизован, једноставно се користи, садржи интуитиван графички и параметарски приказ резултата и значајно доприноси унапређењу клиничких процедура за евалуацију и праћење стања пацијената са неуродегенеративним болестима.

Кључне речи: систем за подршку одлучивању; анализа покрета; „носиви“ сензори; машинско учење; обрада сигнала; експертска правила; неуродегенеративне болести; Паркинсонова болест; брадикензија; клиничко праћење и евалуација стања.

Научна област: техничке науке, електротехника

Ужа научна област: биомедицинско инжењерство

УДК број: 621.3

Table of Contents

Table of Figures

Table of Tables

Preface

This thesis is a part of the research on the development of systems for movement analysis and rehabilitation, with particular focus given to the development of decision support systems for more efficient diagnosis and assessment of patients with neurodegenerative disorders and assistive systems for motor functions recovery in patients with motoric impairments.

Research activities were performed at the Laboratory for eHealth and Biomedical Engineering, Innovation Center, School of Electrical Engineering in Belgrade, and Laboratory for Biomedical Engineering and Technologies (BMIT), University of Belgrade - School of Electrical Engineering. Clinical studies and clinical research activities were performed at the Clinic of Neurology, Clinical Centre of Serbia, School of Medicine, University of Belgrade, Belgrade, Serbia.

Research presented in this thesis was supported by the Ministry of Education, Science and Technological Development of the Republic of Serbia, grant #175016, "The effects of assistive systems in neurorehabilitation: recovery of sensory-motor functions" (2011-2019), PI prof. dr Mirjana Popović, and in part supported by the Ministry of Education, Science and Technological Development of the Republic of Serbia, grant #175090, "Motor and non-motor symptoms of Parkinsonism: clinical, morphological and molecular-genetic correlations" (2011-2019), PI prof. dr Vladimir Kostić.

The part of the research was also performed within the project of bilateral scientific collaboration between the Innovation Center, School of Electrical Engineering in Belgrade, and Institut des Systèmes Intelligents et de Robotique, l' Université Pierre et Marie Curie, „Development of new technologies for motor assessment of upper extremities in patients with motor impairment" (2018-2019), and within the project of bilateral scientific collaboration between the Innovation Center, School of Electrical Engineering in Belgrade and University Medical Center Göttingen (UMG), „Development of smart body-area-network system for activity tracking" (2019-2020).

Thesis outline

Chapter 1 provides information about the clinical decision support systems, their basic structure, types, and technological aspects of the work presented in this thesis. Furthermore, this Chapter also presents the medical background of the analysed problem, including details about the neurodegenerative disorders, with special focus given to Parkinson's disease, as well as clinical

procedures for assessment of these patients along with the problems that need to be resolved. At the end of the Chapter, the objectives and initial research hypotheses of the thesis are presented.

Chapter 2 presents state of the art in the field of advanced technologies that are developed and implemented to support the clinical assessment of patients with Parkinson's disease and related disorders. It reviews different methods in terms of measurement systems, experiment design, and intelligent algorithms that are developed and used for providing diagnostic recommendation or prediction of symptom severity or response to therapy.

Chapter 3 introduces a new decision support system for the assessment of patients with neurodegenerative disorders. The system is briefly explained.

Chapter 4 describes the challenges of the gait segmentation, which represents one of the most important pre-processing steps in the gait analysis. Four different segmentation methods are applied and validated using the gait data, recorded from patients with Parkinson's disease and healthy subjects. The segmentation techniques are compared in terms of their accuracy, precision, and applicability to every day clinical implementation.

In chapter 5, a new method for the identification of Parkinson's disease patients is presented. The particular focus is given to the recognition of Parkinson's disease in the early stage of its development. The method uses deep learning algorithms and gait data recorded with wearable inertial and force sensors. Two types of deep neural networks are developed and validated. The performance of the designed models is additionally examined in terms of data augmentation strategy, length of walking sequences that are used for training and testing, and walking conditions under which the gait is recorded.

Chapter 6 describes a method for analysing the amplitude of repetitive hand and leg movements that are used for the assessment of symptom severity. Furthermore, this Chapter introduces a new technique for the segmentation of repetitive movements into individual cycles.

Chapter 7 presents a new method for the evaluation of symptom severity. The first part of the method provides a detailed analysis and quantification of clinically relevant repetitive movements. A new parameterization is designed to quantify the essential kinematic, temporal and frequency movement properties objectively. The developed metrics are used as the input to the expert system for the prediction of clinical scores. The decision-making process implements expert rules that completely objectify clinical criteria for score assignment. The results are validated on data recorded during finger-tapping movement from patients with typical and atypical parkinsonism and presented in a manner that is understandable and intuitive for the potential end-users.

Chapter 8 presents the results of the developed decision support system on the example of one patient.

Finally, chapter 9 summarizes the results and contribution of the thesis and outlines the possibilities for future developments of the developed and proposed decision support system.

Publications presented in the thesis

The thesis is based on the publications listed below:

I. International journal papers

[1] **V. Bobić**, M. Djurić-Jovičić, N. Dragašević, M. B. Popović, V. S. Kostić, and G. Kvaščev, "An Expert System for Quantification of Bradykinesia Based on Wearable Inertial Sensors," *Sensors*, vol. 19, no. 11, p. 2644, Jun. 2019, doi: 10.3390/s19112644. **(M21)**

[2] M. Belić, **V. Bobić**, M. Badža, N. Šolaja, M. Đurić-Jovičić, and V. S. Kostić, "Artificial intelligence for assisting diagnostics and assessment of Parkinson's disease—A review," *Clinical Neurology and Neurosurgery*, vol. 184. Elsevier B.V., p. 105442, Sep. 01, 2019, doi: 10.1016/j.clineuro.2019.105442. **(M23)**

[3] **V. Bobic,** M. Djurić-Jovičić, N. Jarrasse, M. Ječmenica-Lukić, I. N. Petrović, S. M. Radovanović, N. Dragašević, and V. S. Kostić, "Spectral parameters for finger tapping quantification," *Facta Univ. - Ser. Electron. Energ.*, vol. 30, no. 4, pp. 585–597, 2017, doi: 10.2298/fuee1704585b. **(M24)**

II. International conference papers

[1] **V. N. Bobic**, M. D. Djuric-Jovicic, S. M. Radovanovic, N. T. Dragasevic, V. S. Kostic, and M. B. Popovic, "Challenges of Stride Segmentation and Their Implementation for Impaired Gait," in *Proceedings of the Annual International Conference of the IEEE Engineering in Medicine and Biology Society, EMBS*, Oct. 2018, vol. 2018-July, pp. 2284–2287, doi: 10.1109/EMBC.2018.8512836 **(M33)**

[1] **V. N. Bobić**, M. D. Djurić-Jovičić, N. Jarrasse, M. Ječmenica-Lukić, I. N. Petrović, S. M. Radovanović, N. Dragašević, and V. S. Kostić, "Frequency analysis of repetitive finger tapping – extracting parameters for movement quantification," in *Proc of the 3rd International Conference on Electrical, Electronic and Computing Engineering*, Jun. 2016, p. MEI2.2 1-MEI2.2 5. **(M33)**

1. Introduction

1.1. Decision support systems for clinical practise

Clinical decision support system (DSS) refers to any computer-aided tool that is developed to influence clinical decision making about patients [1]. Although human expertise represents an essential part of any clinical decision-making process, computational methods and precise sensor systems can support the whole process with objective measures of patients' state and behaviour that cannot be otherwise observed by a human eye. The significance of clinical DSS is manifold – these systems can improve health care and contribute to a better understanding of medical problems that need to be resolved and contribute to the design of clinical reasoning models [2]. The necessity for these systems has been further recognized in the past decades due to growth in health care costs and complexity, challenges that are related to the management of clinical knowledge and information, adoption of electronic medical records, and increased need for personalized medicine [2].

The literature suggests that a DSS should have different important characteristics, which could be grouped into three main components: 1) data management; 2) decision-making process; and 3) user-interface [3].

1.1.1. Data management

Having good data management capabilities represents a prerequisite to a reliable decision-making process. This includes access to both internal and external data and information [3]. In the sense of modern clinical DSS, data management requires effective techniques for acquiring large and complex electronic health data (or **big data**) that is represented in a standardized form and enables fast, accurate, and efficient processing [1], [2]. The choice of the data representation scheme is influenced by the problem that the intelligent system tries to solve.

Over the last few decades, researchers have developed different techniques for capturing relevant clinical data, ranging from simple keyboard data entries, speech or image inputs, scannable forms, various physiological data to real-time data monitoring. With the recent technological advancements, an especially important role for the acquisition of clinical data belongs to wearable systems. **Wearable systems** represent sensor devices that can continuously measure human physiology, such as electrocardiography (ECG), heart rate, blood pressure and oxygen saturation, body temperature, electromyography (EMG), electroencephalography (EEG), and body, head and eye movements [4]. A typical wearable system consists of 1) sensors that produce analog or digital data; 2) a processing unit that collects and transforms raw data; and 3) a display that shows acquired

and processed data [5]. In the case of wireless wearables, the system also comprises a transceiver that wirelessly sends data to a central unit. Furthermore, data processing can be completely performed at the sensor unit, or it can be partially performed, transmitted to the computer, and then processed [5]. Regarding the design requirements, these systems should 1) be low-cost to increase their potential for large scale applications, 2) be small and lightweight to allow monitoring of human physiology in an unobtrusive manner, 3) provide safe operating and positioning on a human body, 4) provide low-energy operation and communication and 5) simple and flexible setup that can be easily adapted for a new user [5]. The integration of wearable technologies into healthcare can help with relocating the resources, active engagement of patients in the disease management process, increase of the flexibility of regular clinical procedures, and reduction of the need for continuous supervision [4].

A wireless **inertial measurement unit (IMU)** is a wearable sensor module that typically comprises a 3-axial accelerometer and 3-axial gyroscope sensors (and sometimes magnetometers). The accelerometer represents an electronic sensor that allows determination of the object's position and movement in space. It measures total acceleration forces that are exerted upon an object, including both static (such as gravity) and dynamic (causing the object to move) forces. Measured accelerations are provided through the components of the IMU's local coordinate system. The rotational movement of an object can be detected with a gyroscope sensor. The gyroscope measures the rate at which the object changes its orientation (i.e., angular velocity) around the three axes of the IMU's local coordinate system. Magnetometer sensors measure the direction, strength, or relative change of the Earth's or any other magnetic field. Typically magnetometer is used for determining the movement heading reference. By placing IMUs on a human body, analysis of body kinematics can be performed. IMUs are easy to apply and they allow for recording for a long time and in any space. Additionally, the quality of these sensors is continuously increasing, while their price and size are being reduced, improving their applicability for everyday and clinical use [6]. Their applicability has been further extended with inertial sensors embedded in smartphones, which are now widespread, low-cost, and unintrusive [7].

1.1.2. Decision-making process

Artificial intelligence (AI) is the core of the DSS. Different definitions of AI are discussed in the literature. In a broad sense, AI is the intelligence demonstrated by machines. Russell and Norvig [8] defined AI as the study of intelligent agents. An intelligent agent represents anything that perceives the environment through sensors and performs subsequent actions upon it through actuators. In that context, behaviour of agents is defined by agent functions that perform a mapping from perceived information to actions. In another approach, AI is described as the field of computer science dedicated to designing intelligent computer systems that can perform functions associated with human behaviour, such as learning, reasoning, problem solving, and others [9]. The two most important sub-fields of AI are expert systems and machine learning.

Expert systems represent computational systems that are designed to solve different problems in a manner that is similar to the reasoning of a human expert [10]. The basic idea behind the expert systems is to encompass domain-specific human knowledge and expertise and to serve as a tool for non-expert users looking for advice on the subject matter. Two main components of expert systems are a knowledge base and an inference engine [9]. The knowledge base comprises instances of domain-related knowledge and information. Knowledge bases typically comprise certain pieces of knowledge (such as rules), and a system could contain several knowledge bases with different types

of knowledge [11]. The inference engine comprises information-processing units (inferences) that perform simple reasoning tasks [11]. The inferences use knowledge from a knowledge base to provide new information based on the given input. DENDRAL [12], MYCIN [13], and PROSPECTOR [14] were the first examples of the expert systems that were successfully developed and applied for resolving domain problems. MYCIN was dedicated to the diagnosis of blood infections and comprised a knowledge base of about 450 rules, which were acquired from extensive interviews with experts, textbooks, and experience with diagnosis [8]. Furthermore, the system embodied a calculus of uncertainty of medical knowledge called certainty factors.

Machine learning (ML) comprises algorithms that are able to learn from data [15]. The learning represents the process that enables algorithms to perform some task. Given some input data, ML can resolve different tasks; classify objects belonging to different categories, predict numerical values, find natural grouping among unlabelled data, transcribe or translate data from one form to another, detect atypical or abnormal events (anomalies), synthesize new similar samples based on the existing data, insert missing data values, and other [15]. Based on a learning principle, ML algorithms can be divided into two main groups: supervised and unsupervised learning algorithms [15]. Unsupervised learning algorithms process unlabelled multidimensional data to find and explore the distribution of data or some properties of that distribution. In contrast, supervised learning algorithms process multidimensional data that is associated with some labels or targets, which "teach" the ML algorithm what to do. There are some other types of learning algorithms, including semi-supervised learning algorithms, which use partially labelled data, or reinforcement learning algorithms, which use a feedback loop to interact with the environment during the learning process [15].

The performance of ML algorithms is typically measured with some quantitative metrics. Accuracy represents the most common metric for evaluating the performance of classification tasks; however, other measures are used as well, including sensitivity, specificity, precision, F1-score, and area under the curve [16]. The basic idea behind the ML is to examine the algorithm's ability to generalize and evaluate how well these algorithms are performing on previously unseen data [15]. Because of that, input data is split into training data, used for algorithm learning, and test data, used for examining the algorithm's ability to generalize. In the literature, different validation techniques and methods for data division are proposed and implemented depending on the task, data type, database size, and used algorithm.

Input data usually represents some set of features that are specifically captured or designed to solve the problem of interest. It is usually provided in the form of a multidimensional vector, where rows indicate different examples, and columns correspond to features. Appropriate data representations are typically obtained using various signal processing techniques. In a broad sense, **signal processing** is defined as the implementation of analog or digital techniques for improving the functionality of data [17]. Analog techniques process time-varying electrical signals, whereas the digital techniques utilize data provided in the form of an array of numbers. In biomedical engineering, these techniques are applied to provide diagnostic or any other relevant clinical information [17]. For these applications, the following techniques may be important: advanced spectral methods, time-frequency analysis, wavelets (both continuous and discrete), advanced filters, and multivariate analysis.

The recent achievements in the field of AI have been mostly brought by a subset of ML called deep learning (DL). The main limitation of the conventional ML algorithms is their inability to

process raw data. These algorithms need to be fed with features that faithfully portray the desired patterns in data in order to recognize them [18]. The extraction of suitable attributes is not a trivial task – it requires dedicated work and high-level engineering skills. With bigger datasets or a larger number of groups being analysed, creating proper data representations becomes even more complex and demanding. DL comprises a set of algorithms that can process raw data and automatically extract features for efficient classification or detection of objects [18]. These algorithms have shown amazing capabilities for different classification tasks; however, the first breakthrough was seen in image and speech recognition tasks [19]–[22].

The reasoning (inference) system and knowledge base on which that system operates represent the most important part of the clinical DSS [2]. Based on the used reasoning, clinical DSS could be divided into two main groups: knowledge-based and nonknowledge-based [1]. The concept of the **knowledge-based clinical DSS** arose from the idea of expert systems that are designed to simulate the decision-making process of a human expert [1], [10]. The knowledge base of these clinical DSS contains information about diseases and their symptoms and other relevant clinical information, which is typically expressed as production (or "if-then") rules. The inference engine of these systems usually associates the knowledge base with the patient data. These systems require a priori knowledge in order to provide the correct answers to specifically designed medical questions [1]. The earliest of these systems were dedicated to the provision of diagnostic support, but not in the manner that simply mimics and replaces the human reasoning but instead gives information that assists the decision-making process of clinical workers. On the other hand, **the nonknowledge-based clinical DSS** use machine learning algorithms for finding patterns in clinical data These models do not require any a priori knowledge - the DSS is designed to find new patterns and relationships in given datasets, which are then applied to previously unseen data. This is especially important for the cases when a priori knowledge is limited or non-existent. A combination of different reasoning methods results in a **hybrid clinical DSS** [23]. The hybrid systems can utilize the best of any methods and provide an optimal solution for a concrete problem.

1.1.3. User interface

Communication with a user is derived through a user interface. The user interface should have a powerful but also simple design [3]. It should enable interaction through queries, reports, and graphs.

The use of a **Web-based interface** extends the usability of DSS systems to a large number of users [3]. In this way, developers can introduce and utilize new technologies at their site. Furthermore, Web browser user interfaces facilitate adoption among users: they do not require extensive training, they increase profitability and speed of decision-making processes, and they can be used with no geographic limitations [3].

Mobile platforms and technologies have been increasingly adopted and implemented in the field of medicine, enhancing the possibilities of the existing systems. In general, the mHealth represents the health practise that is supported by mobile devices [24]. The rise of **mHealth** technologies has been guided by the development of smartphones and tablets, as well as advances in mobile platforms, most significantly Android and iOS, and mobile communication technologies, such as 3G, 4G, Bluetooth, Zigbee, Radio-frequency Identification (RFID), and others. The use of mobile

user interface in clinical DSS increases their portability and possibility for customization. Furthermore, these tools are available "at hand" every time the physicians need it at a low-cost [25].

1.1.4. Applications

Based on the clinical problem that a clinical DSS tries to solve, there are four categories of these systems [1]:

1. Alerting systems are programs that continuously monitor and test the patient's clinical data according to the previously defined clinical criteria. Alert is activated when data meet the set criteria. The design and timing of alerts depend on the goal.
2. Critiquing systems respond to entered information about a medical intervention by identifying inconsistencies between the entered data and an internal definition or by indicating an alternative treatment approach.
3. Suggestion systems represent the third category of clinical DSS, which are designed to interactively support the clinical decision-making process, by answering to physician's request for assistance. In these systems, the clinicians use the DSS, enter the relevant clinical data, the system process the data, and composes a suggestion.
4. Retrospective quality assurance programs utilize patient's clinical data and formulate decisions about the quality of care and send them back to physicians.

The clinical DSS has been developed for many clinical areas, including neurology. In the next section, the medical background of the thesis and need for the development of new DSS for assessment of neurodegenerative disorders are described.

1.2. Understanding the medical background of the analysed problem

Neurodegenerative disorders represent progressive and incurable diseases, which are causing degeneration or complete death of nerve cells [26]. These conditions can produce problems with motor or mental functioning. Parkinson's disease (PD) is the second most common neurodegenerative disorder in the world. According to some sources [27], the prevalence of PD in 2016 was estimated as 6.1 million (95% uncertainty interval 5.0–7.3) cases worldwide. In the same study, it was reported that 16,702 (95% uncertainty interval 12,943 to 20,877) individuals were diagnosed with PD in Serbia, which represented 0.24% of the total population of the Republic of Serbia at a time [28]. These numbers are showing a significant growth compared to data reported for 1990: the prevalence of PD increased 2.4 times over 26 years [27]. It is expected that the number of individuals diagnosed with PD will continue to increase, and it will affect between 8.7 and 9.3 million people in the world by the year 2030 [29].

1.2.1. Symptomatic expressions of neurological disorders of parkinsonian type

PD occurs from the progressive loss of dopaminergic neurons in the basal ganglia structure called substantia nigra [30]. The disease is characterized by diverse motor and non-motor symptoms (Figure 1.1) that are affecting the physical and mental abilities of PD patients and violating their everyday life, routines, and activities. The most notable PD clinical motor representations are bradykinesia, rest tremor, rigidity, and postural instability [31], [32]. Bradykinesia (or slowness of

movements) is one of the most recognizable and characteristic symptoms of PD, expressed with difficulties in planning, initiating, and executing motions, especially in tasks that require sequential motor performance [33]. Because of that, bradykinesia is assessed and evaluated using fast, repetitive hand and leg movements, including finger-tapping, hand opening-closing, hand pronation-supination, and toe-tapping. Although they are not cardinal PD symptoms signs, gait disturbances represent one of the most incapacitant motor signs, characterized by decreased stride length and walking speed, festinating gait, and increased stride variability [34]. Abnormal changes in the gait pattern may be visible from the early stages of disease development.

In addition to the primary parkinsonism type (referred to as the Parkinson's disease or idiopathic Parkinson's disease), there are also some atypical syndromes, such as progressive supranuclear palsy (PSP), multiple system atrophy (MSA), corticobasal degeneration (CBD) and dementia with Lewy bodies (DLB) [35], [36]. These syndromes are characterized by similar symptoms, especially in the early stage of disease; however, atypical parkinsonism is much more progressive than idiopathic PD and requires different treatment [36].

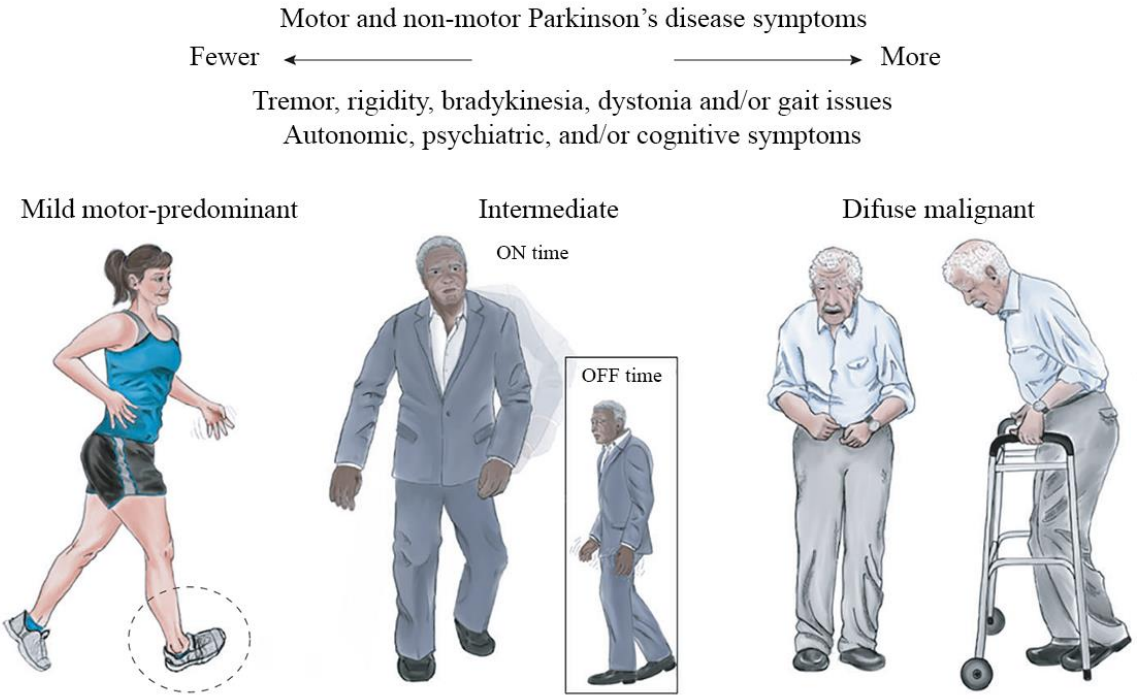

Figure 1.1 Illustration of Parkinson's disease symptoms in different disease stages (image adapted from [37]).

1.2.2. Clinical assessment

There is no specific test that can provide a definite PD diagnosis [31]. For that reason, the recognition of PD is not a trivial task, especially in the early stage of disease development. PD is usually diagnosed using the UK Parkinson's Disease Society Brain Bank criteria based on the presence of specific symptoms [38]. Some studies examined the reliability of the clinical PD diagnosis [39]. Post-mortem neuropathological examination was performed on 232 cases of parkinsonism, of whom 131 with idiopathic PD and 101 cases with other types of parkinsonism. The clinical diagnosis was correctly given in only 26% of cases when observing individuals who did not show a clear response or did not receive standard therapy. For people in the advanced stage of the disease development (>5 years disease duration), diagnostic accuracy achieved 88%; however, only

53% of individuals diagnosed in the early stage (<5 years disease duration) have been confirmed as PD.

The severity of PD is often evaluated using the Hoehn and Yahr (H&Y) scale [35]. Initially, the H&Y scale had five scores (from 1 to 5), but later it was complemented with two additional ratings (1.5 and 2.5) for more precise quantification of PD severity level [40]. Assessment of parkinsonism signs and evaluation of both motor and non-motor clinical symptoms is performed using the standardized clinical scale named the Unified Parkinson's disease rating scale (UPDRS) [41], [42]. Motor symptoms are assessed with a set of tests designed to provide more detailed insight and evaluation of these symptoms.

However, neurologists cannot objectively measure human behaviour or physiology; they can only observe (hear or see) patients and assess them based on their knowledge and experience. Such an assessment may result in subjective and rough evaluation. Furthermore, human judgement can change over time (due to their current mood, fatigue, or their focus) and result in an inconsistent assessment of patients [43]. Due to the mentioned issues, there is a strong need for the development of new systems that can support the clinical decision-making process and provide an objective and automatic assessment of patients with neurodegenerative disorders.

1.3. Objectives of the thesis

The goal of the research is to design a new clinical decision support system that can contribute to the development of objective, automatized, and improved assessment of patients with neurodegenerative diseases. The system is based on the analysis of clinically relevant repetitive movements that are recorded using small and easy to use wireless wearable sensors and processed using different signal processing techniques and artificial intelligence algorithms.

The importance of research is reflected in the practical and scientific potential of the obtained results that improve and facilitate the everyday clinical decision-making process. Achieved improvements refer to a complete understanding of all phases and changes of the movements being analysed and the design of metrics that thoroughly describe all specific movement characteristics. Furthermore, the advancements include the development and implementation of a new expert system and machine learning algorithms that objectify the decision-making process, together with the provision of graphical and parametric feedback in a form that is entirely understandable to potential end-users (neurologists and clinicians).

1.4. Starting hypotheses of the thesis

H1: By using the advanced algorithms, recognition of patients with neurodegenerative disorders can be improved. The work presented in this thesis is looking for answers to the following research questions:

1) Is it possible to develop a fast and easy to apply diagnostic support based on the signals that are recorded by the lightweight and small wireless wearable sensors while performing clinically relevant repetitive movements?
2) Can applied machine learning algorithms achieve results that improve diagnostic accuracy compared to the results presented in the literature?

H2: It is possible to achieve objective evaluation and quantification of the degree of motoric impairments in patients with neurodegenerative disorders. The work presented in this thesis is looking for answers to the following research questions:

1) Can small and lightweight wireless inertial measurement units be used to record clinically relevant repetitive movements for evaluating the severity of motor impairment in patients with neurodegenerative diseases?
2) Can the selected signal processing techniques be used to analyse the recorded signals and to develop new metrics that contribute to a better understanding of the observed movements and quantification of essential movement properties, such as motor blocks, amplitude, speed, amplitude decrease, and others?

H3: It is possible to develop a new expert system for objective prediction of clinical motor scores. The work presented in this thesis is looking for answers to the following research questions:

1) Is it possible to develop an objective and automatic support for the assessment of motor symptom severity that is based on the introduced parameterization and a new expert system that fully objectify standardized clinical evaluation criteria?
2) What are the results of the expert system compared to the benchmark data given by several neurologists who have years of experience in diagnosing, assessing, and evaluating patients with neurodegenerative diseases?

2. Advanced technologies for supporting the clinical assessment: State of the art

Lack of objectivity and reliability in the adopted and standardized clinical procedures for PD assessment has been a strong motivation for researchers to design and develop new systems that can support and improve clinical diagnosis and evaluation of disease progression and symptoms severity [44]. The methods proposed in the literature vary in terms of used instrumentation, observed tests and experiment protocols, the number of included patients, and applied analysis. In the next few sections, a comprehensive overview of the literature is provided and organized based on various essential aspects of the performed analysis.

2.1. Measurement systems for capturing relevant clinical data

When it comes to the assessment of PD patients, researchers most frequently focused their studies on analysing clinical signs. Motor representations of this disease were especially studied since they represent the most cardinal and recognizable PD signs. Degrading vocal performance in PD patients was suggested as one of the supporting pieces of evidence of PD progression, and as such, was addressed in a number of research studies for providing objective PD assessment. Multiple types of voice measurements were recorded using the head-mounted microphone [45] or a telemonitoring system [46]. Some researchers focused on the analysis of handwriting images or handwriting dynamics recorded with a smartpen [47], [48], whereas the others analysed clinically relevant hand and leg movements captured with different sensor systems, including optical systems [49]–[52], smartphone integrated sensors [53]–[55], wearable force and inertial sensors [56]–[64], force platforms [65], [66], standard computer keyboards [67], [68], or electromagnetic sensors [69], [70]. The number of studies utilizing the wearable wireless sensors for analysis of physiological signals in PD patients is increasing during the past years. Unlike optical systems, wearables are small and compact, often inexpensive, and do not require dedicated space for recording. IMUs are particularly significant; these sensor units are suitable for capturing and analysing clinically relevant movements of the head, trunk, upper and lower extremities that are especially important in the assessment of parkinsonism. Inertial sensors have been applied for recording body movements during gait [61], finger-tapping [60], [71], hand opening-closing [72], hand pronation-supination [58], [59], [73], toe or foot-tapping [74], [75], or for tremor analysis [64], [76], [77]. Sometimes, these sensors have been combined with other sensor modules for providing an in-depth analysis of patients' state, including force sensors [78], EMG sensors [79], or ambient sensors [80]. However, with the higher number of

sensor modules used, the complexity of testing increases, thus reducing the convenience and practicability of such setup.

2.2. Measurement protocols and database size

Most studies utilized data recorded for that research, which resulted in a variety of implemented experimental protocols. Hand and leg movements for assessment of bradykinesia have been recorded for a concrete number of repetitions, e.g., ten times [59], [60], or for some specified period, usually 10-15 s [58], [72], [81], depending on the version of the UPDRS which was followed. The gait was also recorded under diverse conditions: some observed shorter time series recorded during short walking distances, typically 5-15 m [61], [66], whereas the others analysed few minutes long signals which described walks along tens of meters long paths [82]. The size of the used database, more specifically, the number of included subjects (patients) also varied significantly between studies: from systems demonstrated on data obtained from just a few patients [83], to those including a few hundreds of patients [61]. In some studies, healthy subjects even mimicked the impaired movement patterns of PD subjects [84]. Furthermore, the clinical characteristics of included patient groups differed significantly between the studies. Data variety could be significant for some tasks (e.g., prediction of full-scale symptom severity). However, in some cases, the developed systems should focus on some specific sub-group of patients (e.g., recognizing PD in its early stage, not in the late stages when symptoms are already too developed and easily recognizable).

Unfortunately, collecting enough data for efficient analysis and especially for implementing machine learning algorithms is a very demanding task. It requires a lot of time, multidisciplinary collaboration between different institutions, and researchers dedicated to collecting and annotating data in a standardized manner. Some freely available databases contain physiological data recorded from patients with PD and related disorders. UCI Machine Learning Repository contains several datasets with voice measurements. One of these databases represents the result of a six-month trial of a telemonitoring device that was developed to provide a system for remote monitoring of symptom progress [46]. It contains voice recordings that were automatically captured in homes of 42 early staged PD patients. This repository also includes a database with multiple types of sound recordings, which were recorded from 20 PD patients and 20 healthy controls [85], and from 23 PD patients and eight healthy controls [45]. Hand PD is another publicly available dataset that contains data collected from patients with PD [86]. The database includes drawings of four spirals and four meanders transformed to .jpg format. The drawing data is collected from 74 individuals diagnosed with PD and 18 healthy subjects [47]. An improved version of this dataset is also available at the same site [87]. The new database contains drawings from 66 individuals, namely 31 PD patients and 35 healthy subjects. The individuals were asked to perform 12 different drawing exams, and the database contains 264 images in total. The data is also complemented with handwritten dynamics data recorded with a smartpen.

The largest available open-source database that contains PD movement data is the database created in 2000, available at the PhysioNet site [88]. This database includes gait data, collected from 93 PD patients (in the early or mild stage of the disease development) and 73 healthy subjects. The data was recorded for approximately 2 minutes on level ground, using force sensing resistors placed on shoe insoles. The same research group published some other gait databases on the PhysioNet site, including the database that comprises data from 15 patients with Amyotrophic lateral sclerosis (ALS),

15 patients with PD, 20 patients with Huntington's disease (HD), and 16 healthy controls [82], [89]. The database was formed similarly as the latter one: the data was recorded for 5-minutes using force sensing resistors while walking along a 77 m long hallway. These datasets are usually complemented with demographic and clinical data of included patients.

A significant number of research groups utilized these databases in their research; however, the obtained results severely depended on the applied analysis, which will be discussed in the following section.

2.3. Intelligent algorithms for objective and automatic PD assessment

Clinical data recorded with accurate and unobtrusive systems has been processed utilizing different signal processing techniques and artificial intelligence algorithms for the provision of (early) diagnosis, monitoring of symptom progression, and response to therapy [90]. The choice of the analysis that was applied mostly depended on the desired outcome. The presented literature review focuses on the methods and results that are relevant to the topic of this thesis.

2.3.1. Provision of diagnostic recommendations

As correct diagnosis represents one of the top medical priorities, and the crucial step of the PD assessment, the development of new diagnostic tools has been a topic in many research studies. Various signal or image processing techniques were frequently combined with supervised machine learning algorithms for the recognition of patients with PD and related neurological disorders.

A study combined an open-source database containing voice measurements with fuzzy k-nearest neighbours algorithm and achieved a sensitivity, specificity, and accuracy above 95% for discriminating PD patients and healthy subjects [91]. A support vector machine algorithm (SVM), mixed with a genetic algorithm for feature extraction, also provided high accuracy results for PD recognition based on the same dataset [92].

Evolutionary algorithms applied to the finger-tapping data were able to classify healthy controls and PD patients with sensitivity, specificity, and accuracy of 94.6%, 91.8%, and 93.5%, respectively [69]. Similar results were obtained for the early-stage PD recognition - these algorithms accomplished sensitivity, specificity, and accuracy of 94.4%, 91.8%, and 92.5% [69]. Keystroke features were also analysed for the provision of accurate identification of PD [93]. An ensemble of machine learning classification models achieved sensitivity and specificity of 96% and 97%, respectively. A feature vector with 12 elements was extracted from the tremor recordings of 21 PD patients and 21 healthy control individuals using a wavelet analysis [55]. The designed set of attributes was fed to a neural network classifier, which accomplished sensitivity, specificity, and accuracy of 95%.

Interesting results have been obtained using the PhysioNet database with gait data recorded from 92 patients and 73 healthy controls [62]. Radial basis function neural network fed with gait features extracted from force data, classified patients and healthy controls with sensitivity, specificity, and accuracy of 96.77%, 95.89%, and 96.38%, respectively. In another study utilizing this database, several gait features were extracted from the recorded force profiles, including stride time, stance

time, swing time, and foot strike profile [94]. The medium gaussian SVM differentiated PD patients and healthy controls with sensitivity, specificity, and accuracy of 97%, 87%, and 94%, respectively. A 10-m long walking was recorded with the inertial sensors from a large pool of subjects (156 PD patients and 424 healthy subjects) [61]. The IMU gait measurements were processed using the Hidden Markov models, which resulted in fixed-length gait representations. Classification performance was examined using a classical k-nearest neighbour classifier, which accomplished an accuracy of 85.51%.

DL algorithms have also penetrated the field of neurology. New studies have proven their high potential for recognizing for patients with neurodegenerative disorders. The decision-making process of DL algorithms resembles the work of clinical experts – each movement pattern is rated with one output, similar to the clinical scores [90]. Furthermore, DL algorithms extend the capabilities of conventional ML with the possibility of performing a temporal analysis, which might be particularly crucial in the PD assessment [95].

Fuzzy recurrence plots of very short time series of keystroke logs data were passed as input to a long short-term memory (LSTM) network, and accomplished accuracy of 81.9% for early PD identification [68]. Several DL models were designed to recognize PD patients based on their handwriting data [48], [87], [96]. A convolutional neural network (CNN) model fed with the Hand-PD dataset accomplished an accuracy of nearly 95% [96]. Transfer learning using the Alex CNN showed even better results with an accuracy of 98.28% [48].

Various studies processed gait data for the provision of DL based support for more accurate (early) PD diagnosis. Video data captured with the Microsoft Kinect sensors system was fed to an LSTM model [52]. This approach achieved high accuracy results (98.10%). In another study, different network topologies were examined for early PD identification based on gait data recorded with the Microsoft Kinect device [97]. The best result was obtained with a convolutional LSTM network (accuracy of 83.40%). Several research groups developed DL models utilizing the above mentioned publicly available PhysioNet database, which contained gait data from 92 patients and 73 healthy controls [63], [95], [98]. A new CNN network was fed with force data transformed to spectrogram images and trained for PD identification [98]. This approach accomplished an accuracy of 88.17% for one data division. A two-channel model (consisted of both LSTM and CNN) extracted patterns from the gait data and enabled recognition of PD with accuracy above 96% [95]. The network with 18 parallel 1-dimensional CNN blocks accomplished the best results for this database with high accuracy of 98.7% [63].

Although showing promising results in the field of deep learning-based diagnosis of PD patients, none of these studies tackled the problem of the early PD diagnosis using the data recorded with wearable sensors. Inconsistent validation techniques limit the possibilities of comparison with other methods. Furthermore, most studies evaluated their algorithms using data division performed on the record (file) level, which may cause unrealistically good results.

2.3.2. Evaluation of symptom severity

Another approach to this topic combines clinical data and intelligent algorithms for providing an objective evaluation of symptom severity or therapeutic effects. The PowerGlove system was used for quantifying several hand motor symptoms of PD patients in both OFF and ON therapy conditions and successfully measured differences between the two states [78]. The effects of deep brain

stimulation on the performance of finger-tapping movement were also examined using a method that implemented a musical keyboard for recording finger taps and five features describing biomechanical and temporal movement properties [99]. A smartphone accelerometer was used for the acquisition of hand tremor data in 52 PD patients [100]. From the recorded data, different features were extracted and fed to four different classifiers. A naive Bayes classifier achieved high accuracy results (near 100%) for the prediction of symptom severity. Small force and gyroscope sensors measured data during the reinforcement manoeuvres for quantifying the severity of rigidity at the elbow and wrist [101]. The recorded data was described with different measures of mechanical impedance. The obtained features showed agreement with the clinical data.

Bradykinesia was often analysed in the literature since it represents one of the most recognizable motor symptoms of PD. The severity of this clinical PD sign was evaluated using different clinically relevant repetitive movements, including finger-tapping [60], [71], [81], hand opening/closing [102], [103], hand pronation/supination [58], [59], [73], foot or toe-tapping [74], and by simultaneous analysis of several movements [64], [104].

From the accelerometer data of 36 PD patients and ten healthy controls, researchers extracted eighteen features describing various frequency and biomechanical movement characteristics [60]. The most relevant features were selected using an ordinal logistic regression model and a greedy backward algorithm. The performance of the designed model was compared with the scores of 3 specialists, showing high predictive power, with the Goodman-Kruskal Gamma score of 0.961 [60]. A similar approach was implemented for assessment of bradykinesia severity based on the repetitive hand opening/closing task [103]. Features describing the dominant grasping frequency and mean angle were extracted from the signals recorded with small IMUs. A regression model was fitted, and the output was compared with the clinical scores, showing high correlation expressed through the determination coefficient $r^2 = 0.99$. In another study, two time-domain and two frequency-domain features were extracted from the gyroscope data recorded during the repetitive finger-tapping movement [105]. Each feature was statistically correlated with the clinical scores (from $r = 0.73$ to $r = -0.80$). The severity of bradykinesia symptom in the finger-tapping movements was also quantified with a method that combined principal component analysis and multiple linear regression [81]. This approach predicted UPDRS finger-tapping scores with a mean square error of 0.45 compared to the benchmark clinical data. A method that used a motion capture system and dynamical analysis for providing automatic finger-tapping show strong ($r = 0.785$) and significant correlations ($p < 0.0015$) with clinical data [49]. The new performance indexes were also introduced to describe bradykinesia severity in upper limbs [58] and walking and sit-to-stand tasks [106]. The obtained indexes successfully correlated with the clinical bradykinesia scores and differentiated PD patients with and without bradykinesia [58] and ON and OFF states in patients [106].

Several studies implemented a SVM classifier for prediction of UPDRS scores [64], [72], [84]. SVM accomplished high accuracy results (sensitivity, specificity, and accuracy above 97%) for prediction of finger-tapping scores using spectral and non-linear features [84]. The features were extracted from gyro signals that were recorded in healthy subjects mimicking the impaired movements of PD patients. Error below 5% was also obtained for estimating the severity of several symptoms (bradykinesia, tremor, and dyskinesia) in 12 PD patients performing multiple movements of upper and lower extremities [64], or for estimating bradykinesia severity in 78 PD patients performing hand opening/closing for 10 s [72]. A decision tree algorithm was also applied for

predicting bradykinesia severity in a hand pronation/supination task and showed a mean agreement of 0.48 with clinical ratings [73].

Although supervised machine learning algorithms predicted clinical scores with high accuracy, the labels used for designing models were subjectively given by one or several specialists in movement disorders. The clinical scoring process severely depends on the examiner experience and knowledge, and it was shown that a high inter-rater variability exists in the given scores. The abovementioned reasons limit the applicability of these algorithms for prediction of clinical scores since this type of learning might introduce the subjectivity in the obtained results as well (the model predicts based on the scores given by a small group of physicians, not based on the rules that are used in clinical practice). Furthermore, the models were usually defined based on data obtained from a few dozens of data samples, which is not enough data for designing a clinically acceptable model. Due to those facts, some research groups implemented decision rules for describing the clinical decision-making process. Clinical scores were predicted with high accuracy (above 90%) using fuzzy rules and features related to biomechanical properties of foot-tapping [74] and hand pronation/supination movements [59]. Commercialized smartphone application Kinesia One, proposed by the Great Lake Technologies, predicted scores for several bradykinesia tasks based on data recorded with an inertial sensor placed on an index finger [107]. However, the output of these systems provided just a score evaluating the severity of a symptom; none of these systems does provide a graphical nor parametrical output of the performed movement analysis. Furthermore, most of the presented systems utilized features that were not fully describing important biomechanical features of performed movements (as they are observed in the clinical practice).

A lot of work has been done in this field; however, a need for additional improvements still exists in different aspects of these studies. The required advancements mainly apply to an early diagnosis of these diseases, especially to a diagnosis that is based on easily performable everyday tasks that can be recorded with simple and inexpensive instrumentation. Furthermore, the assessment tools for the prediction of clinical scales can also be improved in terms of developed analysis of the observed movements, applied reasoning and provision of results in a manner that is intuitive and understandable for the potential end-users.

3. Decision support system for assessment of patients with neurodegenerative disorders

This thesis presents research and development of a new decision support system for the assessment of patients with neurodegenerative disorders. The system was developed following the recommendations for having a clinical DSS with excellent performances (Figure 3.1). The proposed DSS represents a suggestion clinical DSS – it is intended for clinical professionals working in the field of neurology, more specifically for specialists in movement disorders who seek assistance or consultation while assessing the patients.

Analysis of relevant hand and leg movements represents the basis of this system. Data is recorded with lightweight and small wireless, wearable sensor systems, and analysed using advanced signal processing techniques and artificial intelligence algorithms. The developed system is a hybrid: it comprises both nonknowledge-based and knowledge-based reasoning. The choice of the reasoning depended on the system's intended result: 1) outputting the diagnostic recommendation, and 2) evaluating the symptom severity.

The first part of the support is dedicated to the identification of Parkinson's disease, with the particular focus given to the recognition of PD in an early stage of disease development. For that purpose, the nonknowledge-based reasoning was applied. Data recorded during the walking is used as the input to this part of the system. The performed analysis consists of two steps: 1) gait segmentation using different signal processing techniques, and 2) the provision of diagnostic recommendations based on deep learning.

The second part of the support utilizes knowledge-based reasoning for the assessment of symptom severity, more specifically, the severity of bradykinesia. The bradykinesia represents one of the essential parkinsonism signs. The severity of this symptom can be evaluated with four different repetitive hand and leg movement tests. The support for the assessment of symptoms is presented in two steps: 1) a method for analysing the amplitude of four repetitive movements, and 2) evaluation of symptom severity using new metrics for movement quantification and an expert system for the prediction of clinical scores.

The output of the system comprises recorded and processed data, diagnostic recommendations, metrics for movement quantification, and predicted clinical scores evaluating the

severity of the bradykinesia symptom. The output of the support is presented in a manner that is simple, intuitive, and understandable for the potential end-users.

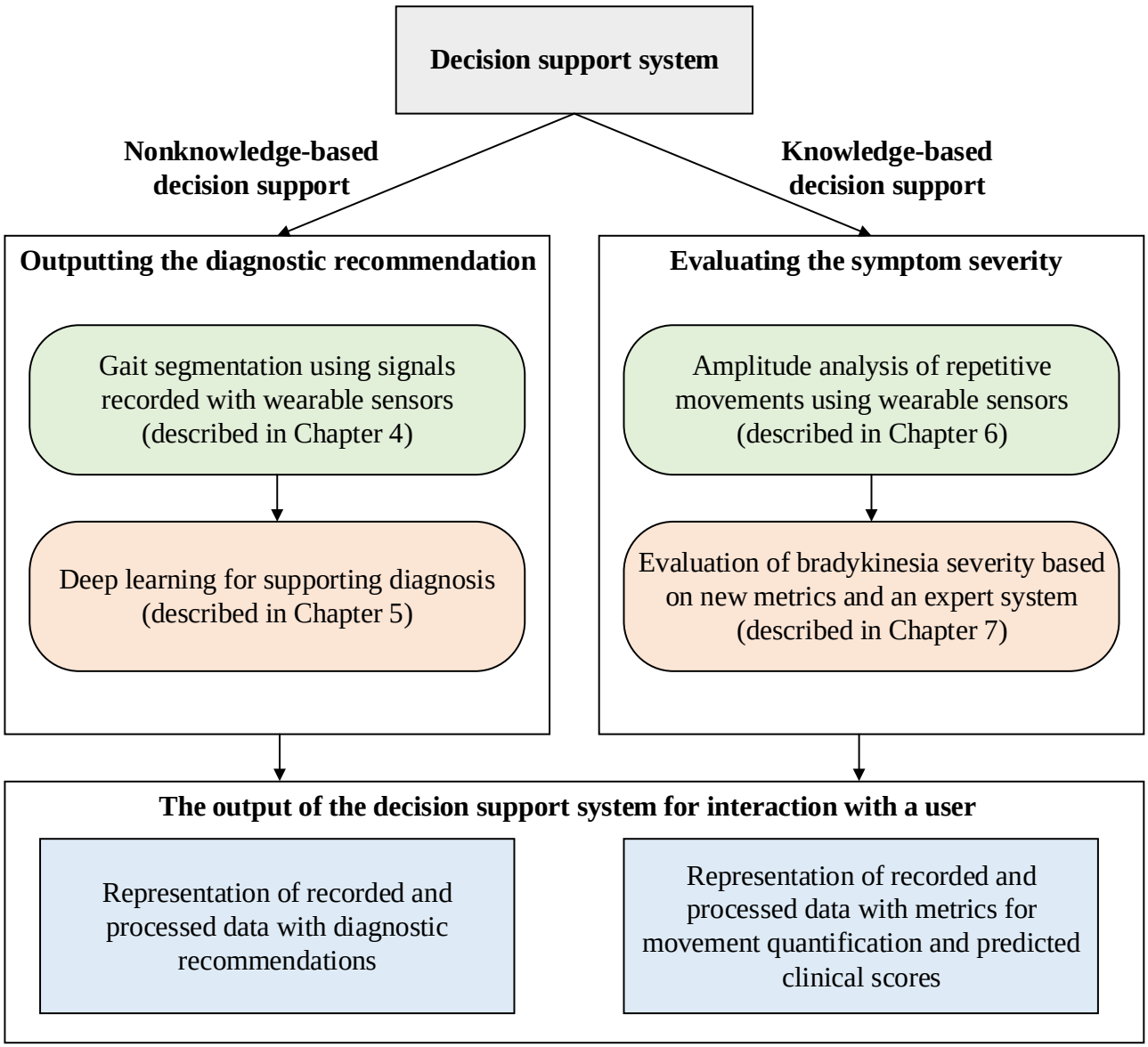

Figure 3.1 The block diagram of the developed decision support system for the assessment of patients with neurodegenerative disorders.

4. Gait segmentation using signals recorded with wearable sensors

Gait represents locomotion delivered through the motion of human limbs. Analysis of gait has become a significant tool for the clinical assessment of different disorders or injuries, allowing examination of therapy or surgery effects, disease progress and recovery. One of the essential processing steps of the gait analysis is gait segmentation. It is applied for dividing walking sequences to individual cycles or partitioning cycles to their sub-phases. Furthermore, gait segmentation enables analysis of important gait properties on the level of individual cycles (e.g., extraction of spatio-temporal parameters), detection of specific gait events, and assessment of gait intra-variability within longer walking sequences, which is important for the assessment of gait disturbances in patients with neurodegenerative disorders, and especially parkinsonism.

Each gait cycle or stride has two main phases: stance and swing [108]. The stance phase represents the period when a limb is in contact with the ground. It starts with an initial contact, usually identified with a heel strike (HS), and lasts until the foot leaves the ground, typically associated with a toe-off (TO). During the swing phase, the limb advances with the foot lifted in the air. Contrary to the stance phase, the swing begins with a TO and ends with initial contact. Two intervals at the beginning and end of the stance phase represent periods when both feet are in contact with the floor (double support). In between those two intervals, only one limb contacts the ground, providing single support. After the initial contact, initial double support begins the stance phase. When the opposite limb starts swinging (contralateral TO), the body is supported only by the original limb on the ground. By finishing the swing phase, the opposite limb strikes the ground (contralateral HS), which represents the beginning of the terminal double support period, which lasts until the original limb is lifted for a new swing (ipsilateral TO). In the normal gait cycle, the swing phase constitutes about 40% of the complete gait cycle, whereas the stance phase accounts for the other 60% (out of which 10% belong to the individual double support periods and 40% to the single support period).

Although recognition of gait events and phases may seem straightforward and visually recognizable; reliable, and precise segmentation is not a trivial and straightforward task. Gait patterns can be very variable even in healthy subjects. The diversity of gait patterns becomes even more prominent in patients with motor impairment where altered motor control (due to some trauma or disorder) can significantly change the biomechanics of their movements. Therefore, developing a precise algorithm for automatic gait segmentation that can work for any subject (regardless of their health status and type of motor disability they may experience) represents a complicated task, and different solutions have been proposed to solve this problem. Setting a threshold for the detection of

specific gait events represents one of the most common gait segmentation techniques. This method has been implemented for discriminating the swing and stance phases from the signals acquired with force sensors [109]. Others used it for detecting event-related peaks [110] or identifying the mid-stance period from accelerometer and gyroscope signals [111]. In another study, detection of signal local maximums and minimums was combined with a threshold optimization algorithm and a procedure that eliminated the false peaks and interpolated the missing ones [112]. Template-based methods were also applied for the segmentation of walking sequences into individual strides. In the latter case, recorded gait signals are compared to a template or reference signal for finding repeatable patterns and extracting time markers for their segmentation [113]–[115]. Dynamic Time Wrapping was used as a template-based method and applied to the gait data acquired during the short and controlled walking paths [114]. This approach gave a sensitivity of 97.7% and 75.5% for healthy subjects and PD patients, respectively, while allowing a time difference of 100 ms between extracted time markers and correct gait events [114]. Another template-based method was applied to the data recorded with different sensor configurations, including inertial sensors positioned on the heel, low back, and signals acquired with the optoelectronic system [115]. For all three settings, the time difference between the detected markers and the real events was in the range 20-28 ms.

In a pilot study, presented in this Chapter, four different methods for gait segmentation were applied on inertial and force gait data recorded from healthy subjects and patients with PD, and compared for proposing the best segmentation technique [116]. The methods resulted in time markers that were related to specific gait events: heel strike or toe-off, and the results were validated using benchmark data.

4.1. Method

4.1.1. Experiment

Fifteen PD patients (Gender: 9 male/6 female; Age: 62±7 years) and fifteen age- and gender-matched healthy controls (HC) (Gender: 8 male/7 female; Age: 63±7 years) were included in this study. All participants were asked to walk with their natural pace along a 15-meter long and a 3-meter wide hallway. The selected environment provided participants time and space to perform the requested task most naturally. Four trials were recorded per each subject. Few minutes of rest were given between the consecutive trials since fatigue may influence the performance. All participants performed the walking task using their shoes.

Patients were recruited from the Clinic of Neurology, Clinical Centre of Serbia, School of Medicine, University of Belgrade, Belgrade, Serbia, whereas healthy subjects were selected among patients' company or clinic's workers. All testing was performed during one day at the Clinic. The study was carried out under the ethical standards of the Declaration of Helsinki and approved by the Ethical Committee, School of Medicine, University of Belgrade. All subjects provided written consent prior to participation in the study.

4.1.2. Instrumentation

In this study, the custom-made wireless sensor system (SENSY) was used [117]. The system includes two inertial measurements units (IMUs) comprising 3-axial accelerometers (ADXL330, Analog Devices, Norwood, Massachusetts, USA) and 3-axial gyroscopes (LPR530, LPY530, Analog

Devices, Norwood, Massachusetts, USA), as well as two shoe insoles each with five force sensing resistors (FSR) placed under the 1st, 3rd, 5th metatarsal bones, big toe, and heel area. During the experiment, IMUs were positioned laterally on the feet. Shoe insoles were provided in the corresponding sizes for all subjects. Reference time markers were measured using the GAITRite electronic walkway (CIR Systems, Havertown, Pennsylvania, USA) with a 5.5 m long active area. Two systems were synchronized using the GAITRite trigger output, which was connected to an analog-to-digital input of an external sync box. The trigger was generated when the GAITRite recording started and stopped, producing synchronization impulses in the gait data acquired with the SENSY system.

4.1.3. Data processing

Signals were recorded with the sampling frequency $f_s = 100$ Hz. Calibrated data was processed in custom-made scripts written in Matlab 7.6 R2008a (MathWorks, Natick, Massachusetts, USA). The raw force, accelerometer, and gyroscope signals were filtered using a 5-point moving average filter before any further processing. Examples of the recorded and processed signals are given in Figure 4.1.

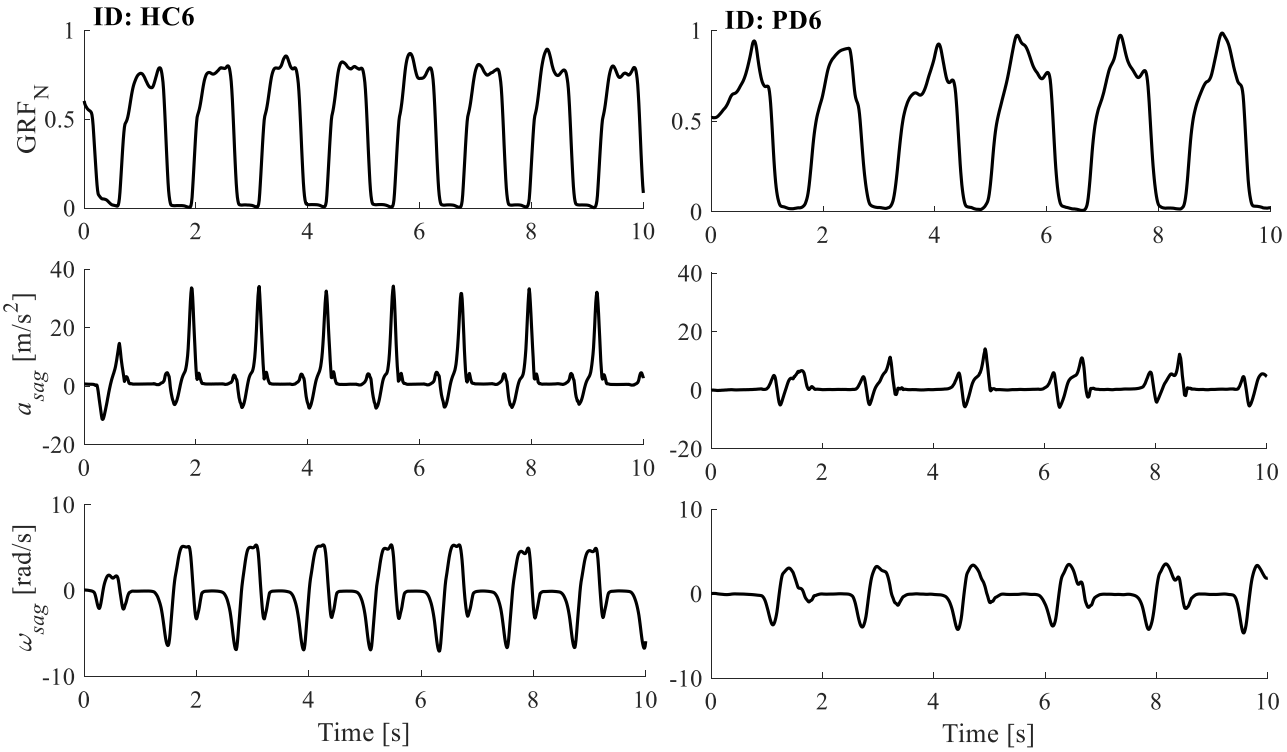

Figure 4.1 Examples of the 10 s long signals for one HC subject (left) and one PD patient (right). On the upper panel, GRF_N sequence is presented, whereas the middle and lower panels show the accelerometer signal measuring anterior-posterior movement in the sagittal plane a_{sag} and the gyroscope signal measuring rotations in the sagittal plane ω_{sag}, respectively.

4.1.3.1. Methods for gait segmentation

4.1.3.1.1. Setting a threshold for FSR signals (M1)

Force sensing resistors provide information about the force that ground exerts on a body during the contact of the foot with the ground, i.e., the ground reaction force (GRF). The typical

profile of the GRF signal for one foot, recorded with force sensors, is presented in Figure 4.2. The presented GRF is normalized with respect to body weight. When foot contacts the ground, the GRF signal begins to rise. The first peak in the signal (referred to as "impact peak") represents the moment when body weight is transferred onto a limb that has just finished swinging forward and contacted the ground ("weight acceptance"). Afterwards, the complete foot is in contact with the ground providing single support (or one limb support) for the body weight. The moment when the foot starts to push and lift off the ground represents the second peak in the GRF signal (referred to as "active peak"). The value of the GRF signal falls to zero when the foot leaves the ground and begins the swing phase. Therefore, GRF provides essential information about the transitions between different gait phases, which makes it suitable for the gait segmentation problem and detection of specific gait events, such as HS and TO events.

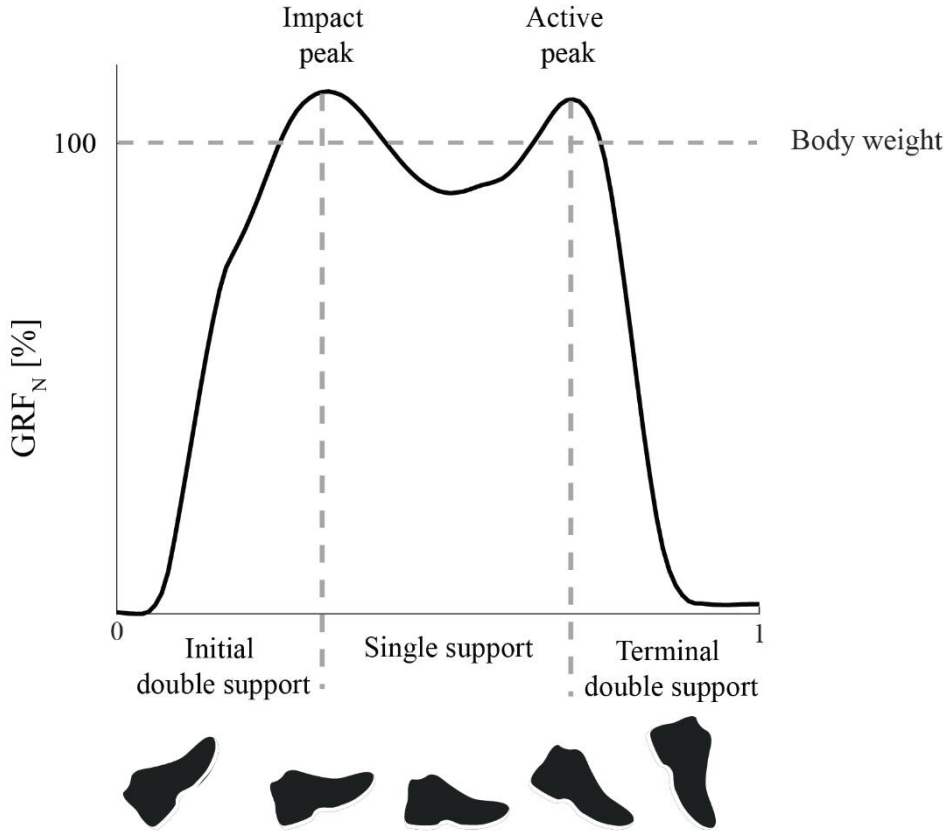

Figure 4.2 Presentation of a typical GRF profile, normalized with respect to a bodyweight (GRF_N [%]). Different positions of a foot are illustrated during the corresponding phases of the GRF profile. The example is given for one HC subject.

Firstly, the FSR signals from heel, toe, and metatarsal areas of one foot were averaged and normalized with respect to the maximum of the averaged signal. The obtained signal represented the normalized ground reaction force (GRF_N).

In order to detect moments that represent HS and TO events in the gait cycle, a threshold TH_{GRF} was applied to the normalized ground reaction force GRF_N. A binary sequence b_{GRF} was obtained. For samples i when GRF_N was valued below the threshold TH_{GRF}, the binary sequence was given the zero value, i.e. $b_{TH}(i) = 0$ (corresponding to the swing phase). Similarly, for samples i when GRF_N was valued above the threshold TH_{GRF}, the binary sequence was assigned with ones, i.e.

$b_{GRF}(i) = 1$ (corresponding to the stance phase). Time markers corresponding to HS and TO events were detected from the calculated binary sequence. The transitions from 0 to 1, i.e., when $b_{GRF}(i) = 0$ and $b_{GRF}(i+1) = 1$ (from the swing to the stance phase) were detected as the HS events (later referred to as the M1a method). Similarly, the transitions from 1 to 0, i.e., when $b_{GRF}(i) = 1$ and $b_{GRF}(i+1) = 0$ (from the stance to the swing phase) were marked as TO events (later referred to as the M1b method).

The threshold value was determined as the lowest value that allowed the detection of all observed gait events. It was established empirically, as the 10% of the maximum value of the normalized ground reaction force GRF_N sequence, i.e. $TH_{GRF} = 0.1$.

In Figure 4.3, an example is provided for this segmentation method. A solid black line shows the calculated normalized ground reaction force GRF_N. A binary sequence b_{GRF} is calculated using the threshold $TH_{GRF} = 0.1$ (marked with a dotted grey line in Figure 4.3). The transitions from the succeeding gait phases were detected as HS and TO events, using the computed binary sequence b_{GRF}.

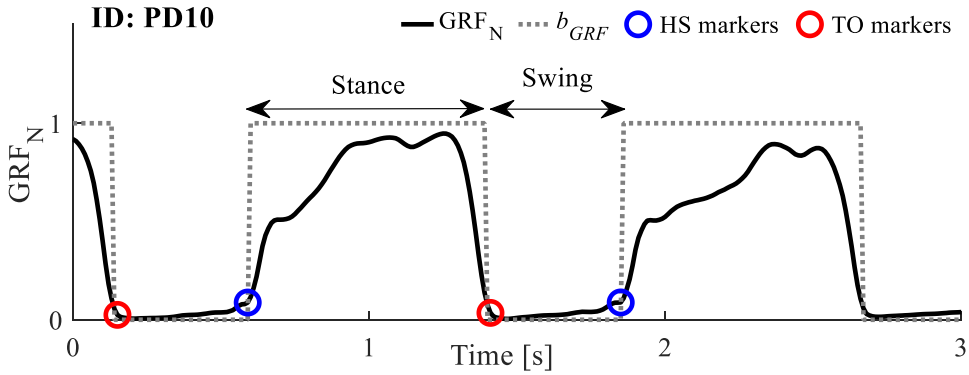

Figure 4.3 Presentation of the GRF_N signal (marked with a solid black line) and the calculated binary function b_{GRF} (represented with a dotted grey line). The detected HS and TO markers are shown with blue and red circles, respectively. An example is given for one PD patient.

4.1.3.1.2. Detection of peaks from accelerometer and gyroscope signals (M2)

The segmentation method based on peak detection was applied to the accelerometer (later referred to as M2a method) and gyroscope signals (later referred to as M2b method). The signals were normalized prior to peak detection. The applied technique is previously introduced in the literature and tested using several datasets [112].

M2a method was applied on the accelerometer signal measuring anterior-posterior motion in the sagittal plane a_{sag}. Prominent positive peaks were detected from the selected accelerometer signal. These peaks could be related to HS events of individual gait cycles. Similarly, M2b method was applied on the gyroscope signal measuring rotation in the sagittal plane ω_{sag}. From the selected signal, deep negative valleys were detected. These valleys could be related to TO events of the individual gait cycles. The orientation of the gyroscope signal was inverted before further processing.

The peaks were detected using a thresholding procedure. All peaks valued above some threshold TH_{peak} were extracted from the signal. In order to find the optimal threshold, the value of the threshold TH_{peak} varied from 0.2 to 0.8 (with a step of 0.01). It was showed that higher threshold

values (closer to 1) allow detection of a fewer number of peaks, whereas very low thresholds (below 0.2) cause the detection of many false peaks [112].

The peak detection procedure was repeated for each threshold value from the selected range. The gait cycle duration was calculated as the difference between the samples at which two succeeding peaks were located. The variance of the gait cycle duration was then calculated for each threshold value. The optimal threshold $\mathrm{TH}_{\mathrm{peak-opt}}$ for detection of peaks was selected as the value that, from the applied range of values, achieved minimal variance of the calculated gait cycle duration (as shown in Figure 4.4).

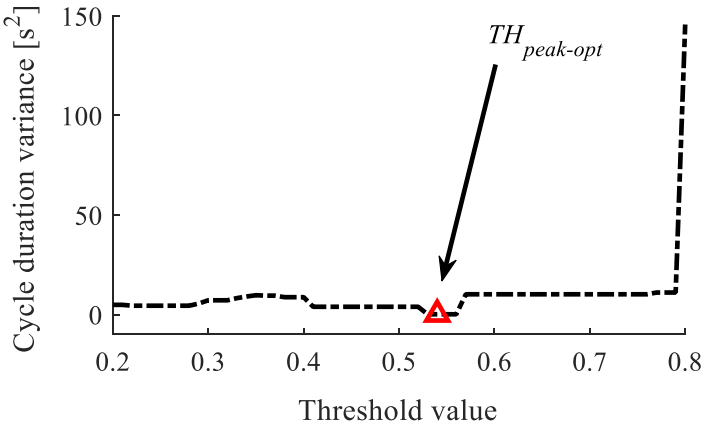

Figure 4.4 Variance of the gait cycle duration as a function of the threshold value. The threshold value achieving minimal variance of the gait cycle duration is selected as an optimal threshold $TH_{peak-opt}$ (marked with a red triangle).

By applying the optimal threshold $TH_{peak-opt}$, peaks were detected from the signal and duration of each individual gait cycle d_i was calculated using the samples representing two consecutive detected peaks. The initial potential cycle (IPC) was found and defined as the cycle that fulfilled the criterium $0.9\bar{d} < length(IPC) < 1.1\bar{d}$, where $\bar{d}$ represented the average duration of the detected gait cycles. This cycle was observed as the correctly detected cycle, and it was used for examination of all other detected peaks. For all other cycles that fulfilled the criterium $0.9\bar{d} < d_i < 1.1\bar{d}$, it was considered that peaks were correctly identified. For $d_i < 0.9\bar{d}$, false peaks were detected, and those peaks were eliminated from further analysis. Similarly, $d_i > 1.1\bar{d}$ indicated that some peaks were missed, and they were linearly interpolated between the detected peaks.

The final sequence of samples at which the detected peaks were located represented the sequence of time markers that were used for gait segmentation. An example of normalized accelerometer and gyroscope signals with detected time markers is presented in Figure 4.5.

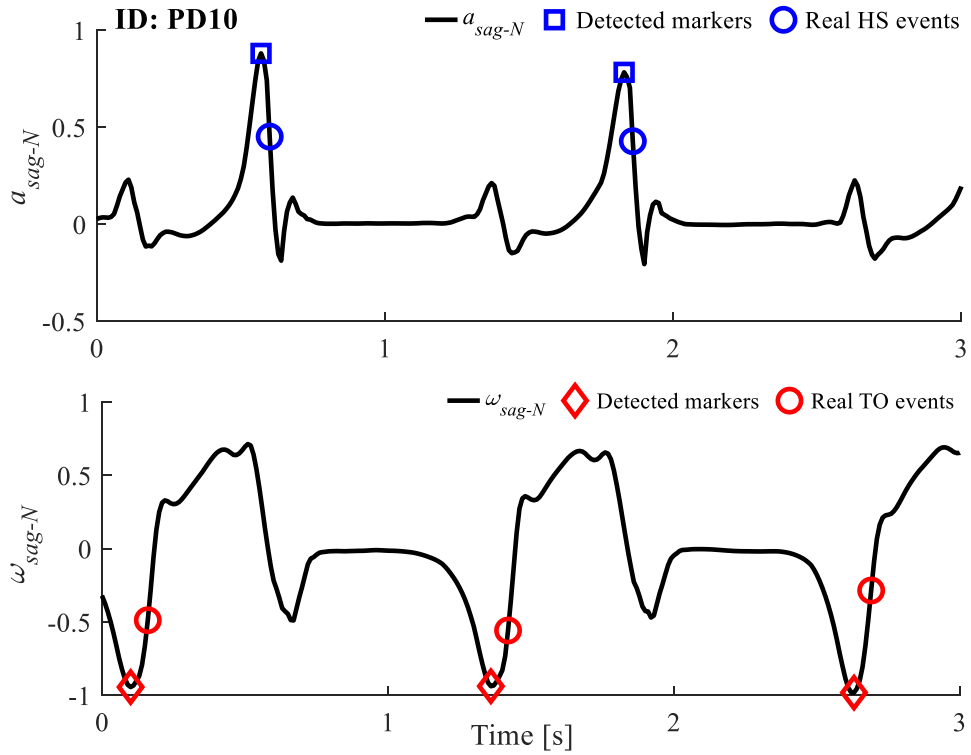

Figure 4.5 Upper panel: Presentation of the normalized accelerometer signal measuring anterior-posterior motion in the sagittal plane a_{sag-N} with detected markers (marked with blue squares) and true HS events (marked with blue circles). Lower panel: Presentation of the normalized gyroscope signal measuring rotation in the sagittal plane ω_{sag-N} with detected markers (marked with red diamonds) and true TO events (marked with red circles). An example is given for one PD patient.

4.1.3.1.1. Template-based method – Recognition of gait patterns from accelerometer signals (M3)

Template-based methods compare walking sequences with a reference (template) signal for finding resembling and repeatable patterns that correspond to individual strides. The method M3 was presented in the literature and applied to the accelerometer signal measuring anterior-posterior movement in the sagittal plane a_{sag} [115].

In order to define a template signal, the autocorrelation function (AC) of the analysed signal was calculated. The AC was then filtered using a 4th order lowpass filter with a cut-off frequency set to twice the value of the AC dominant frequency. The template signal length (TL) was then calculated as the temporal distance between the two most prominent AC peaks valued above 0.5 [115]. A shorter sequence was extracted from the analysed signal – beginning at 115% of TL from the start and ending at 115% of TL before the end of the signal. Within this sequence, peaks (separated for at least 40% of TL samples) were detected and used for the extraction of shorter segments. The template signal was obtained by averaging the obtained segments.

The template signal was slid along the analysed signal and compared with the signal segment with the same length as the template signal. A sliding step was set to one sample. The similarity of these signals was measured using two metrics [115]: 1) standard deviation of the amplitude difference, and 2) correlation coefficients of the template signal and the short window of the observed signal. The ratio of these two calculated sequences was calculated, and it represented a new

characteristic that was used for the detection of time markers (later referred to as "coefficient signal"). Peaks separated for at least 60% of TL distance are detected from the coefficient signal and considered as time markers for the gait segmentation. The obtained time markers were then shifted for 15% of TL and compared with the HS events [115].

An example of the analysed accelerometer signal is presented in Figure 4.6, together with the extracted template signal, coefficient signal, and time markers.

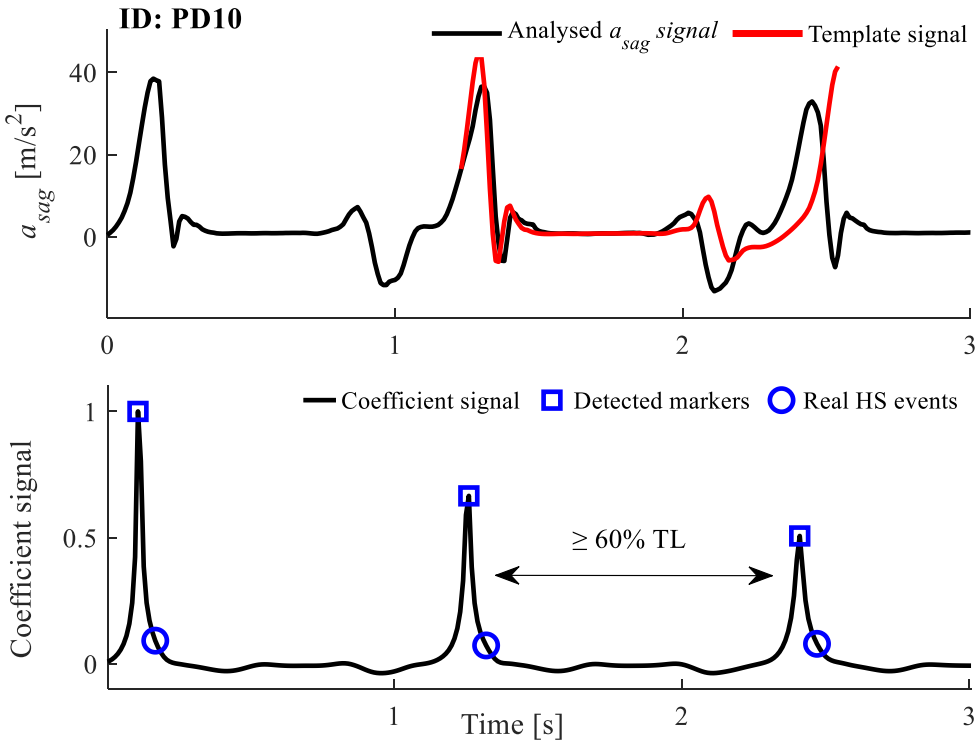

Figure 4.6 Upper panel: Presentation of the analysed accelerometer signal measuring anterior-posterior motion in the sagittal plane a_{sag} with extracted template signal. Lower panel: Presentation of the calculated coefficient signal with detected peaks (marked with blue squared markers) and correct HS events (marked with blue circles). An example is given for one PD patient.

4.1.3.1.2. Pattern recognition from gyroscope signals using Dynamic Time Wrapping (M4)

Dynamic Time Wrapping (DTW) represents a signal analysis method that finds an optimal alignment of different time sequences [118]. DTW provides a measure of similarity between analysed time series by performing "elastic" transformation to find similar patterns within data. In terms of the gait segmentation problem, this analysis method can be implemented as a template-based method, where the analysed signal is compared with a "representative stride" for the identification of individual strides [114].

DTW definition

Let $X = (x_1, x_2, \dots, x_n),\ N \in \mathbb{N}$ and $Y = (y_1, y_2, \dots, y_n),\ M \in \mathbb{N}$ represent time series that are being compared. These time series are sampled at equidistant time steps. Distance matrix (or local cost matrix) $C_l \in \mathbb{R}^{NxM}$ is calculated as the pairwise distances between the analysed time series X and Y [119]:

$$C_l \in \mathbb{R}^{NxM}: c_{ij} = \|x_i - y_j\|, i \in [1:N], j \in [1:M] \tag{4.1}$$

An alignment path (also called warping path) is found through the areas with low cost (distance), i.e., through the valleys of the calculated distance matrix. It defines the correspondence of the elements of the X time series to the elements of the Y time series, following some specified conditions. The formal definition of the warping path is given as [119]:

$$p = (p_1, p_2, \dots, p_n), p_l = (p_i, p_j) \in [1:N] \times [1, M], l \in [1:K] \tag{4.2}$$

and it must satisfy the following criteria [119]:

1. Boundary condition: The first and last points of the warping path must coincide with the first and last elements of the local cost matrix, i.e. $p_1 = (1,1)$ and $p_K = (N, M)$.
2. Monotonicity condition: Time samples of the warping path points must be monotonously aligned: $n_1 \leq n_2 \leq \cdots \leq n_K$ and $m_1 \leq m_2 \leq \cdots \leq m_K$.
3. Step size condition: The warping path is limited to small shifts in time: $p_{l+1} - p_l \in \{(1,0), (0,1), (1,1)\}$.

The distance function (or cost function) can be calculated from the warping path that is computed from the local cost matrix, and it is given as [119]:

$$c_p(X, Y) = \sum_{l=1}^{L} C_l\,(x_{n_1}, y_{m_1}) \tag{4.3}$$

The optimal warping path (later referred to as p^*) is the warping path with a minimal distance or cost related to the alignment. The procedure for finding the optimal warping path is computationally challenging since it requires that all possible warping paths are tested so the optimal one could be found. Because of that, an accumulated cost matrix or global cost matrix D is calculated from all possible warping paths.

The elements in the first row of D are calculated as [119]:

$$D(1, j) = \sum_{k=1}^{j} C_l(x_1, y_k), j \in [1:M] \tag{4.4}$$

The element in the first column of D is computed as [119]:

$$D(i, 1) = \sum_{k=1}^{i} C_l(x_k, y_1), i \in [1:N] \tag{4.5}$$

All other elements in D are found as [119]:

$$D(i, j) = min\{D(i-1, j-1), D(i-1, j), D(i, j-1)\} + C_l\big(x_i, y_j\big), \quad i \in [1:N], j \in [1:M] \tag{4.6}$$

When the accumulated cost matrix is calculated, the distance function is calculated as the optimal warping path by implementing the backtracking procedure from the last element of D $p^* = (1,1)$ to the first element of the D $p^* = (N, M)$.

In this study, DTW was applied for recognition of gait patterns from the gyroscope signal describing rotations in the sagittal plane ω_{sag} [114]. Gyroscope signals from 10 randomly selected subjects were segmented into individual strides using a peak detection algorithm. The extracted strides were then averaged, which provided the pattern of the representative stride. The previously described procedure was applied for finding the accumulated cost matrix and the distance function as the measure of similarity between the analysed signal and the representative stride. Local minima from the calculated distance function were detected using a thresholding technique [114]. The threshold was set to 5% of the function maximum. The extracted local minima defined time markers for the segmentation of gait into individual strides. The obtained time markers were related and compared with TO events.

4.1.3.2. Evaluation of the implemented methods

Extracted time markers were compared with the reference markers that corresponded to the real HS and TO events and that were obtained using the GAITRite platform. In order to have a reliable, consistent, and repeatable pre-processing basis for the stride-based gait analysis, the gait segmentation should be related to some specific event or change in the analysed signal. In the case of the inertial-based gait segmentation methods M2-M4, detected time markers did not represent the exact HS and TO events. Because of that, the efficiency of the segmentation methods was evaluated using the following metrics:

1) Sensitivity:

$$Se = \frac{TP}{TP + FN} \cdot 100\ [\%] \tag{4.7}$$

2) Precision:

$$Pr = \frac{TP}{TP + FP} \cdot 100\ [\%] \tag{4.8}$$

3) Absolute error:

$$Ae = m_{det} - m_{ref}\ [ms] \tag{4.9}$$

where TP, FN, and FP represented the number of true positive, false negative, and false positive events, respectively. If the time difference between the detected and reference time markers laid in the range ±50 ms (for M1) and ±100 ms (for M2-M4), the detected markers were considered as TP events. Lower temporal boundaries were applied to the first method since it was expected (based on the definition of the implemented segmentation techniques) that the M1 method would detect events that were closer (in the context of time) to the real events compared to other methods. FNs represented imprecisely detected or completely missed events. Falsely identified events were considered as FPs. Based on the Equations (4.7) and (4.8), Sensitivity Se gave the percent of precisely detected events

with respect to the total number of actual events, whereas the Precision Pr provided the measure of the share that correctly identified events had in the total number of detected events. In Equation (4.9), m_{det} and m_{ref} represented the detected and reference time markers. Absolute error Ae represented the temporal difference of the identified markers and the real events. It was calculated for each detected event that was marked as true positive. By using this metric, segmentation consistency was examined on the level of each individual gait cycle, which represents a very important term for having an applicable and reliable segmentation method in the stride-based analysis.

4.2. Results

One hundred and twenty recordings from 30 subjects (444 strides in total) were included in the analysis. In Table 4.1, Sensitivity Se and Precision Pr results are presented. The results are shown separately for all four segmentation methods and both PD and HC groups, summarized for both legs and averaged for all subjects in the group. Results for the Absolute error Ae metric are shown in Figure 4.7 using the boxplot representation. The results are presented for all four segmentation methods and both PD and HC groups, separately. Examples of correctly and wrongly detected HS events are shown in Figure 4.8.

The M1 and M3 methods provided comparable results, with the highest values for Sensitivity Se and Precision Pr metrics (for both groups) compared to other methods. The poorest results were obtained for the M4 technique. The methods M2-M4 applied to the inertial data showed lower consistency in the obtained values of the Absolute error Ae evaluation metric, compared to the method M1.

Table 4.1 Segmentation results, presented through descriptive statistics (average±std) of the Se and Pr metrics, for all segmentation methods and both subject groups, separately.

Method	Metrics	PD	HC
M1a	Se [%]	91.1±0.07	99.6±0.01
	Pr [%]	99.6±0.01	99.9±0.02
M1b	Se [%]	91.1±0.07	99.6±0.01
	Pr [%]	99.6±0.01	99.9±0.02
M2a	Se [%]	87.9±0.06	93.3±0.05
	Pr [%]	97.7±0.01	98.8±0.01
M2b	Se [%]	90.2±0.06	91.6±0.09
	Pr [%]	96.5±0.05	99.6±0.02
M3	Se [%]	91.1±0.03	98.6±0.02
	Pr [%]	94.9±0.02	99.8±0.01
M4	Se [%]	85.7±0.05	87.7±0.08
	Pr [%]	95.5±0.05	99.4±0.02

PD – Parkinson's disease patients; HC – Healthy controls; M1a – Gait segmentation method based on force data for detection of HS events; M1b – Gait segmentation method based on force data for detection of TO events; M2a – Peak detection algorithm for detection of HS related peaks; M2b – Peak detection algorithm for detection of TO related peaks; M3 – Template-based detection of HS events; M4 – Template-based detection of TO events; Se – Sensitivity; Pr – Precision.

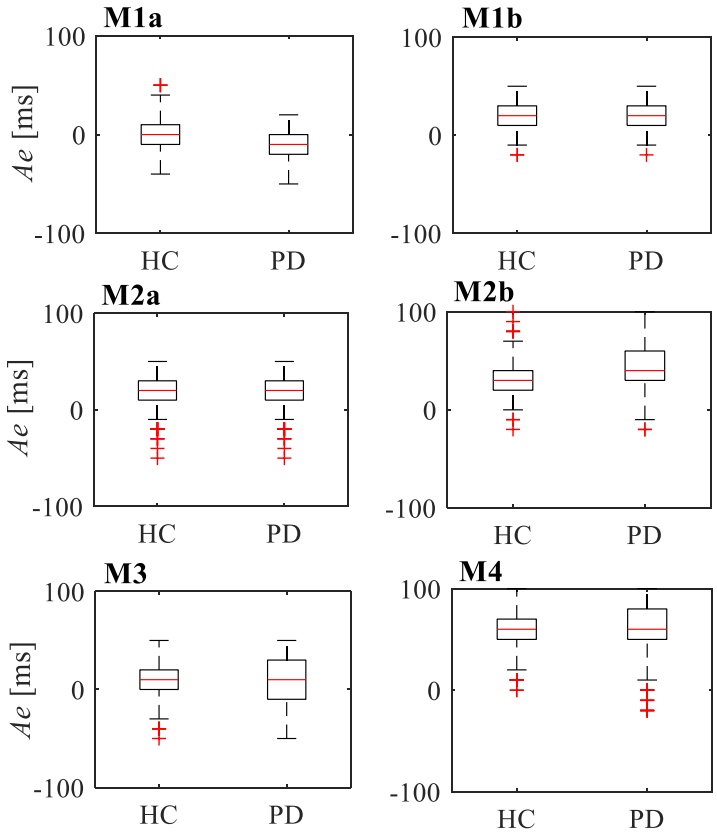

Figure 4.7 Boxplot representations of the Absolute error Ae evaluation metric obtained for all four segmentation methods.

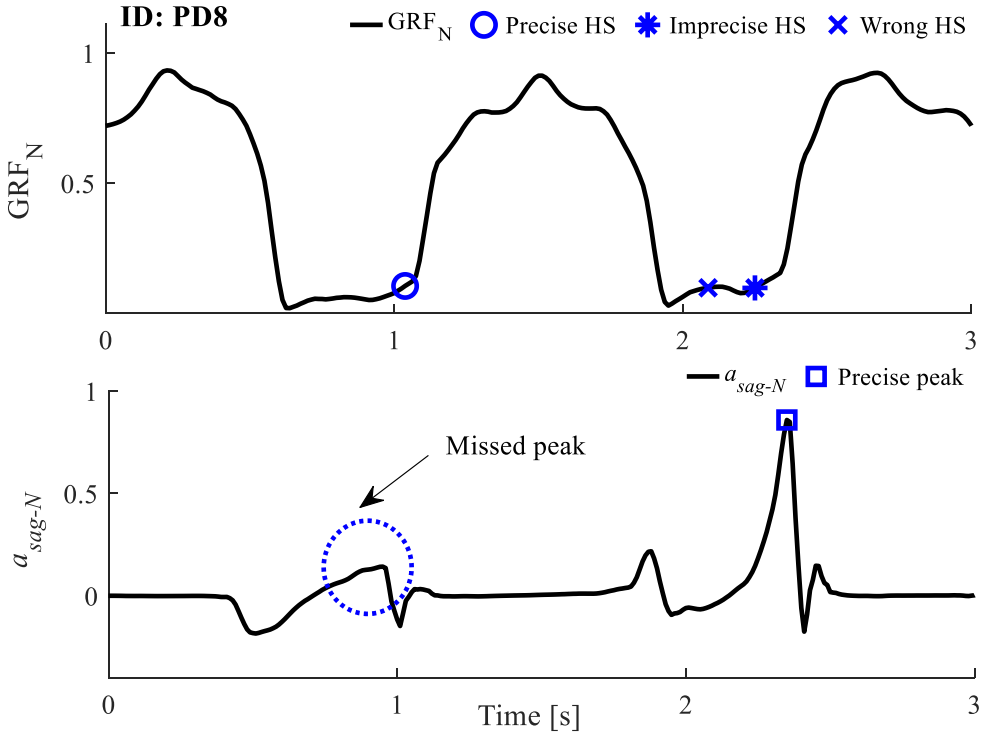

Figure 4.8 Presentation of two strides long GRF_N signal (upper panel) and two strides long normalized accelerometer signal a_{sag-N} (lower panel), with correctly detected HS (marked with a blue circle), one precisely detected peak (marked with a blue square), one imprecisely detected HS (marked with a blue star), and one wrongly detected HS (marked with a blue cross). The area of a missed peak is marked with a dashed blue ellipse. An example is given for one PD patient.

4.3. Discussion

In this pilot study, four methods were applied for segmenting the walking sequences into individual strides. The selected and implemented methods differed in terms of applied analysis (thresholding techniques, peak detection, template-based analysis) and type of analysed signals (signals recorded with force or inertial sensors). The methods were examined and validated on the data acquired from both healthy subjects and PD patients.

The first method was based on FSR signals, and it used thresholding for the detection of HS and TO events. This method provided the best results with the highest values for the Sensitivity Se and Precision Pr metrics compared to the other three methods. It is an expected result since FSR signals are easiest to interpret and transform into characteristic gait phases and events. However, by applying a universal threshold, some gait events can be overlooked or falsely detected (in Figure 4.8, small ridge during the swing phase caused false-positive events), which consequently influences the efficiency of the method.

In order to provide a complete analysis of the gait, FSR sensors must be combined with some other types of sensors (such as inertial sensors), since they can provide only information about the temporal and force gait characteristics. Furthermore, these sensors are sensitive to breaking and temperature (which may cause changes in thresholds as well). New shoe insoles should be provided for each examined patient, and placing individual sensors on shoe insoles can be time-consuming. Besides, patients with impaired motor functions may perform gait patterns differently (e.g., not starting the stance phase with a heel strike), which would consequently reduce the clinical applicability of the introduced gait segmentation method.

On the other hand, inertial sensors are easy to use and apply in clinical settings, providing significant information about kinematic characteristics of the gait. In this study, three segmentation methods were implemented on the signals acquired with inertial sensors. The techniques were selected as the segmentation techniques that had great potential for clinical applications. The template-based method M3 applied to the accelerometer data provided results that were comparable with the method M1. The other two inertial-based methods M2 and M4, provided poorer results with decreased Sensitivity Se and Precision Pr for up to 12%. Furthermore, the methods applied to the inertial data had wider distributions of the Absolute error Ae feature, which was especially visible for PD patients (as shown in Figure 4.7). This result showed that time differences between the detected and actual gait events varied from stride to stride and between different subjects. Therefore, these methods allow the detection of some specific changes in the signals, not concrete gait events, which makes them less reliable than methods based on force data.

Methods using a reference signal for finding repeatable gait patterns among signals, such as template-based methods implemented here, can be applied for both regular and impaired gait patterns, but in that case, the shape of the gait pattern must be uniform without prominent stride to stride variability. These methods would not provide reliable results for patients experiencing gait disturbances with highly expressed intra-variability. Gait patterns showing prominent peaks are suitable for applying peak detection algorithms. However, they are not applicable to the signals describing altered gait patterns that do not have expressed or repeatable peaks.

In order to have a gait segmentation method that is suitable and applicable for clinical settings, the applied technique must provide reliable, reproducible and automatized analysis that requires minimal technical skills for use, and that can be applied for all types of gait disturbances. Therefore, analysed methods must be additionally examined for other types of gait disturbances to exploit their practical capabilities entirely.

5. Deep learning for supporting diagnosis

In the clinical practice, several different tests are simultaneously considered for identifying patients with PD since no test can provide a definitive PD diagnosis. Because of that, it was decided that support should be developed utilizing nonknowledge-based reasoning. For that purpose, DL models were selected, designed and examined. These models allow automatic recognition of patterns in data, which makes them suitable for resolving this kind of problem. The DL models are developed based on data recorded during the walking task with the wireless and wearable sensor system. Walking represents a basic everyday human activity. Furthermore, changes in the normal gait pattern may indicate the presence of a motoric impairment in patients with neurodegenerative disorders. Gait disturbances are also one of the most incapacitant and identifiable signs of parkinsonism. In this Chapter, a new method that utilized DL models for the provision of an objective and automatic recognition of PD patients based on gait data is presented.

5.1. Overview of artificial neural networks

Artificial neural networks (ANNs) represent the core of the DL; therefore, in order to comprehend DL, one should understand the underlying ANN principles first. ANNs represent ML algorithms that are inspired by the biological functions of the human brain. Perceptron is a basic type of the artificial neuron that consists of external inputs, one internal input (also called "bias"), one output, and a step function [120]. The perceptron is fed with an input feature vector $\boldsymbol{x} = (x_1, x_2, \dots, x_n)$, which is multiplied with a set of weights $\boldsymbol{W} = (w_1, w_2, \dots, w_n)$:

$$z = \sum_{i=1}^{n} w_i x_i \tag{5.1}$$

where z represents the weighted sum of the input. Usually, the bias feature ($x_0 = 1$) is added to the network [120]:

$$s = z + b = \sum_{i=1}^{n} w_i x_i + b \tag{5.2}$$

with s representing the state of the perceptron, and b the bias parameter. Usually, the state is represented as $s = \sum_{i=0}^{n} w_i x_i$, where $w_0 = b$.

The resulting state value is compared with the threshold, and the output value is obtained:

$$a = \begin{cases} 1 & \text{if } \sum_{i=o}^{n} w_i x_i > 0 \\ -1 & \text{otherwise} \end{cases} \tag{5.3}$$

The model of the perceptron is presented in Figure 5.1.

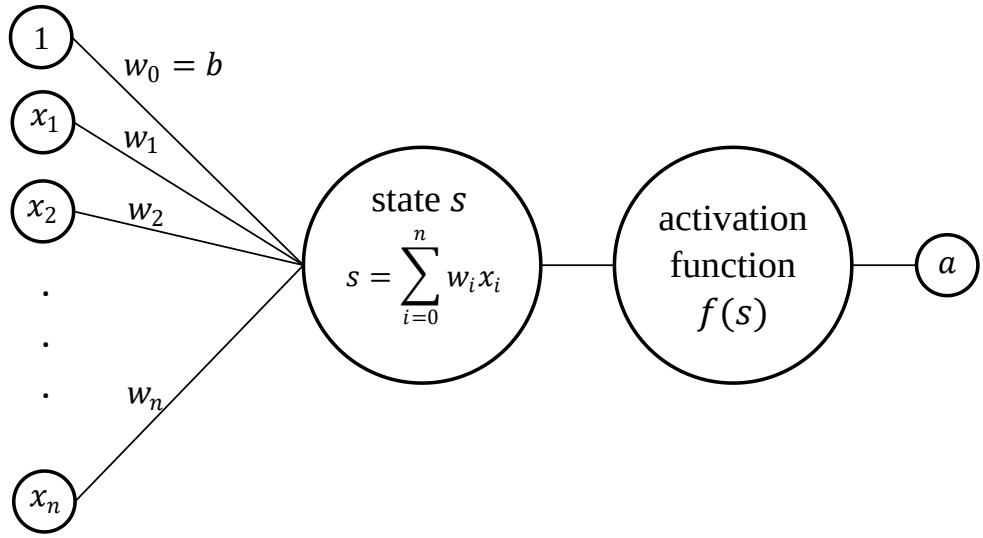

Figure 5.1 The general model of the perceptron.

The values of the weight and bias parameters are learned during the training phase. The perceptron predicts the output for one training sample pair $(\boldsymbol{x}, y)$ at a time where $\boldsymbol{x}$ represents the input vector for that sample, and y corresponds to its label [120]. In order to find the optimum values of the parameters, the perceptron learning rule is applied – for the misclassified samples, the error between the predicted and actual output is calculated, and used for updating the values of the perceptron parameters, as follows:

$$w_i' = w_i + \Delta w_i = w_i + \eta(a - y)x_i \tag{5.4}$$

where w_i represents the weight value from the previous iteration, w_i' is the updated weight value, and η marks the learning rate. The learning rate controls to what extent the parameter values are modified, and usually, it is set as some small value from the range of 0-1. The large values of the learning rate might prevent the algorithm from converging towards the optimal value, whereas too small values might require more training iterations and therefore result in a very slow algorithm. The initial weights are given some random values. The procedure is repeated until the algorithm converges towards the optimum.

Single perceptron with the step activation function can only learn linear patterns, and the algorithm fails to converge if given training examples are not linearly separable. Although stacking multiple perceptrons in layers may help with resolving some more complex tasks, other architectures and neurons are usually applied for finding more complex non-linear patterns among data.

5.1.1. Feed-forward neural networks

Within ANNs, units (or artificial neurons) are usually organized in layers [120]. Typical ANN consists of an input layer, an output layer, and one or more hidden layers. The input layer takes the external information from the environment and passes it to the network, whereas the output layer provides resulting data to the environment [120]. Units of the hidden layers are connected to the units from other layers and do not have connections with the environment. The abovementioned architecture of the network is called a deep feed-forward neural network or just a feed-forward neural network (FFNN). FFNNs are fully connected and do not contain any loops, i.e., all neurons from one layer are connected to all neurons in the succeeding layer, without giving any connections to the neurons from the previous or current layer. Units of the input layer represent features, which can be scalars, vectors, or multidimensional matrices. Input data is often normalized and scaled into some range of values, i.e. [0,1] or [1,1], prior to the development of an ANN model. This procedure usually accelerates the learning process and helps with algorithm converging [15].

In order to represent complex non-linear patterns, non-linear activation functions are applied in artificial neurons. The most common non-linear activation functions are sigmoid, hyperbolic tangent, rectified linear unit, soft-sign, and softmax [15].

The sigmoid (or logistic) function is given as follows [120]:

$$f(s) = \frac{1}{1 + e^{-ms}} \tag{5.5}$$

where s corresponds to the state of the artificial neuron, and m is a constant value that controls the steepness of this activation function. The sigmoid function squashes a large range of input values into a continuous range from 0 to 1. The sigmoid activation function is presented in Figure 5.2, upper left panel.

The hyperbolic tangent function is given as follows [15]:

$$f(s) = \tanh(s) = \frac{e^{2s} - 1}{e^{2s} + 1} \tag{5.6}$$

The output of the hyperbolic tangent function is squashed into the range from -1 to 1 (the S-shape). The function is continuous, monotonous and differentiable. The hyperbolic tangent activation function is presented in Figure 5.2, upper right panel.

The rectified linear unit (later referred to as “ReLU”) is given as follows [15]:

$$f(s) = \max(0, s) \tag{5.7}$$

The function is continuous, but not differentiable for $s = 0$. The ReLU activation function is presented in Figure 5.2, lower left panel.

The soft-sign function is given as follows:

$$f(s) = \frac{s}{|s| + 1} \tag{5.8}$$

The soft-sign function is an alternative and closely related to the hyperbolic tangent function. The difference is that the soft-sign converges polynomially, in contrast to the hyperbolic tangent function, which converges exponentially. The soft-sign activation function is presented in Figure 5.2, lower right panel.

The softmax function is given as follows [15]:

$$f(s) = \frac{e^{s_k}}{\sum_{k=1}^{K} e^{s_k}}, \qquad k = 1, \ldots, K \tag{5.9}$$

where K represents the number of units in the layer. The softmax function is usually applied in the output layer for classification tasks that include multiple target classes, where each neuron outputs the estimated probability of the corresponding class.

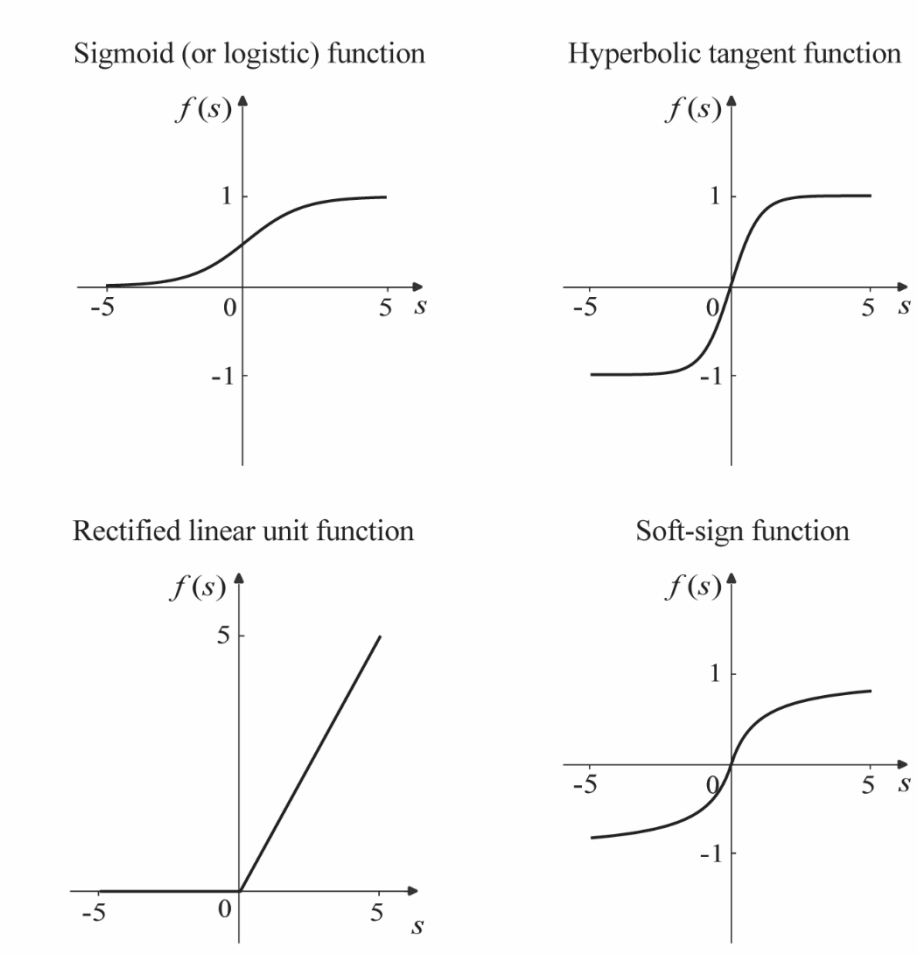

Figure 5.2 Presentation of the most common activation functions that are applied in the neural networks: sigmoid (or logistic) function (upper left panel), hyperbolic tangent function (upper right panel), rectified linear unit function (lower left panel) and soft-sign function (lower right panel).

5.1.2. Backpropagation algorithm

The following denotation is adopted for describing the neural network learning algorithm. The layers in the network are indexed with l, and the total number of layers in the network is represented with L. The number of training examples is denoted with M. One training example is given with $(\boldsymbol{x}, y)$, where $\boldsymbol{x}$ represents the feature vector, and y is the target label of that example. Sometimes, the target is also represented as a vector, where different vector elements correspond to different classification groups. In such case, y takes the value of 1 for the correct classification group and the zero value for the others. A set of parameters connecting layers $l-1$ and l is denoted with $\boldsymbol{W}^{(l-1)}$. The output $\boldsymbol{a}^{(l)}$ of a layer l is given as [121]:

$$\boldsymbol{a}^{(l)} = f^{(l)}(\boldsymbol{s}^{(l)}) = f^{(l)}(\boldsymbol{W}^{(l-1)}\boldsymbol{a}^{(l-1)}) \tag{5.10}$$

where the layer input and state are denoted by $\boldsymbol{a}^{(l-1)}$ and $\boldsymbol{s}^{(l)}$ respectively, and $f^{(l)}$ marks the activation function. The number of units in the output layer is marked with K. The measure of the overall error can be calculated with the loss function (or cost function) as follows:

$$J(W) = -\sum_{k \in K} y_k \log\left(a_k{}^{(L)}\right), \quad k = 1, \ldots, K \tag{5.11}$$

In Equation (5.11), a cross-entropy function is used for calculating the overall classification error; however, depending on the observed task, other functions can be applied as well, including mean absolute error (or L^1 loss), mean square error (or quadratic loss or L^2 loss), mean bias error, hinge loss, and others [15].

Error backpropagation is the most commonly used learning algorithm in ANNs. Initially, network parameters are given some small random values. The input training example is propagated forward through the network, and the output is calculated for that training example as [121]:

$$\boldsymbol{a}^{(L)} = f^{(L)}\left(\boldsymbol{W}^{(L-1)} f^{(L-1)}\left(\boldsymbol{W}^{(L-2)} \ldots f^{(2)}\left(\boldsymbol{W}^{(1)}\boldsymbol{a}^{(1)}\right)\right)\right) \tag{5.12}$$

where $\boldsymbol{a}^{(1)} = \boldsymbol{x}$. The algorithm propagates the error backward, and the error gradient is used for updating the values of the network parameters (weights and biases) for each layer. Because of that, the algorithm is also called "gradient descent". The goal of the algorithm is to obtain the optimum values of the network parameters, so the error of the algorithm is minimized, i.e., to compute $\min_W J(W)$. The derivative of the loss function in terms of the neural network input is given with the following chain rule [121]:

$$\begin{aligned} &\frac{dJ}{da^{(L)}} \cdot \frac{da^{(L)}}{ds^{(L)}} \cdot \frac{ds^{(L)}}{da^{(L-1)}} \cdot \frac{da^{(L-1)}}{ds^{(L-1)}} \cdot \frac{ds^{(L-1)}}{da^{(L-2)}} \cdots \frac{da^{(2)}}{ds^{(2)}} \cdot \frac{\partial s^{(2)}}{\partial a^{(1)}} \\ &\qquad = \frac{dJ}{da^{(L)}} \cdot (f^{(L)})' \cdot \boldsymbol{W}^{(L-1)} \cdot (f^{(L-1)})' \cdot \boldsymbol{W}^{(L-2)} \cdots (f^{(2)})' \cdot \boldsymbol{W}^{(1)} \end{aligned} \tag{5.13}$$

where operator $'$ and $\cdot$ denote derivative and Hadamard product (or element-wise product), respectively. The gradient ∇ represents the transpose of the derivative represented in the Equation

(5.13). Therefore, although the entries are the same, the order of multiplication is reversed, and matrices are transposed [121]:

$$\nabla_x J = (\boldsymbol{W}^{(1)})^T \cdot (f^{(2)})' \cdots (\boldsymbol{W}^{(L-2)})^T \cdot (f^{(L-1)})' \cdot (\boldsymbol{W}^{(L-1)})^T \cdot (f^{(L)})' \nabla_{a^{(L)}} J \tag{5.14}$$

The new quantity can be introduced and defined as the gradient of the input at the level of the layer l [121]:

$$\boldsymbol{\delta}^{(l)} = \left(f^{(l)}\right)' \cdot (\boldsymbol{W}^{(l)})^T \cdot \left(f^{(l+1)}\right)' \cdots (\boldsymbol{W}^{(L-2)})^T \cdot \left(f^{(L-1)}\right)' \cdot (\boldsymbol{W}^{(L-1)})^T \cdot \left(f^{(L)}\right)' \cdot \nabla_{a^{(L)}} J \tag{5.15}$$

It can also be interpreted as the error at the level of the layer l. The delta is a vector with a length that equals the number of units in that layer. This quantity can be calculated recursively as [121]:

$$\boldsymbol{\delta}^{(l)} = \left(f^{(l)}\right)' \cdot (\boldsymbol{W}^{(l)})^T \cdot \boldsymbol{\delta}^{(l+1)} \tag{5.16}$$

The gradient of the parameters connecting the layers l and $l+1$ [121]:

$$\nabla_{W^{(l)}} J = \boldsymbol{\delta}^{(l+1)} (\boldsymbol{a}^{(l)})^T \tag{5.17}$$

The gradient $\nabla_{W^{(l)}} J$ is influenced by the factor $\boldsymbol{a}^{(l)}$ since the parameters $\boldsymbol{W}^{(l)}$ connect units from the layers l and $l+1$ and affect the layer $l+1$ proportionally to its input $\boldsymbol{a}^{(l)}$. The parameters connecting the layers l and $l+1$ are updated according to the following formula [121]:

$$\boldsymbol{W}^{(l)} = \boldsymbol{W}^{(l)} - \eta \nabla_{W^{(l)}} J \tag{5.18}$$

where η represents the learning rate. The weights are updated for the specified number of repetitions (also called iterations) until the network reaches the best solution for the output values, or until it reaches its final iteration. The backpropagation algorithm is illustrated on the example of one simple FFNN with one hidden layer in Figure 5.3.

When parameter updating is performed after each training example, the algorithm is called "stochastic gradient descent". Sometimes, the input data is divided into batches prior to the learning process. A batch size represents a number of input examples that have been fed to the network before updating the network parameters. The error is calculated for each example in the batch. After feeding all batch examples, the gradient of the cumulative error is applied for updating the network parameters. The batch size is observed as a hyperparameter. Batch gradient descent is an algorithm that uses all training samples at once. The mini-batch gradient descent represents the version of this algorithm that uses smaller portions of the input examples (the number of examples in one batch can take a value between 1 and the total number of examples in the input set). Division of data to batches causes an algorithm to have one more hyperparameter: an epoch. The epoch is an interval during which the algorithm has processed all training examples to update the model parameters.

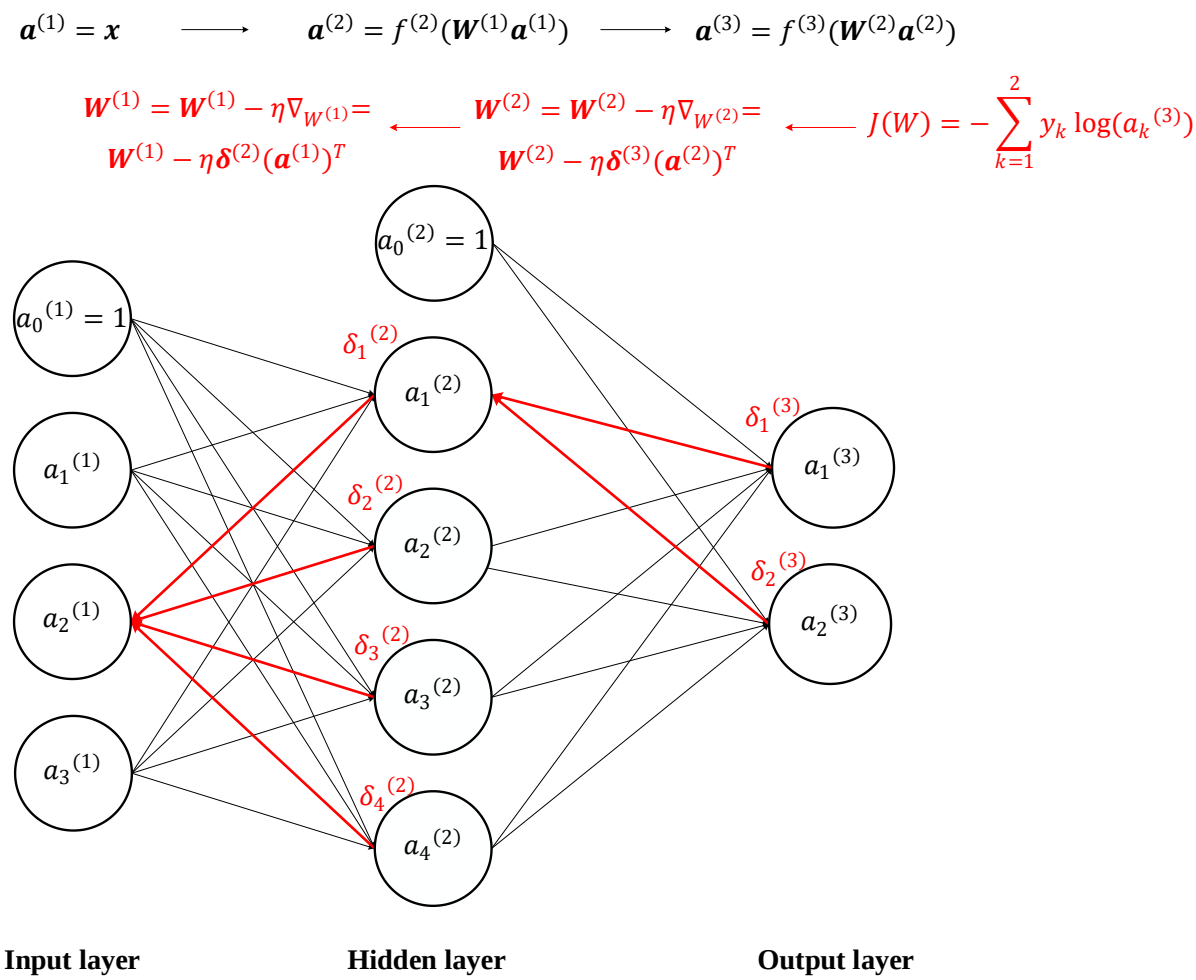

Figure 5.3 Illustration of the backpropagation algorithm on the example of one simple feed-forward neural network with an input layer, one hidden layer, and an output layer.

5.1.3. Performance evaluation

Generalization represents the central problem in ML, and it is defined as the ability of algorithms to perform well on previously unseen data [15]. Because of that, prior to the learning process, input data is divided into training data, used for fitting the model, and test data, used for examining the performance of the designed model and its ability to generalize [15]. When dividing data to training and test sets results with a too-small test set (implying statistical uncertainty in test results), then alternative strategies can be applied to provide a more accurate estimation of the model performance. The most common approach includes dividing original input data to k randomly selected non-overlapping splits, also referred to as the k-fold cross-validation. In each trial, one data split is used for testing the model, whereas the other $k-1$ folds are applied for training. The procedure is repeated until every split or fold is used as the test set precisely one time. The performance is measured on test data and then averaged for all trials.

In the literature, different performance measures are introduced and applied. Binary classification tasks are usually evaluated using the following metrics [16]:

1) Accuracy:

$$Ac = \frac{TP + TN}{TP + TN + FP + FN} \cdot 100\ [\%] \tag{5.19}$$

2) Sensitivity:

$$Se = \frac{TP}{TP + FN} \cdot 100\ [\%] \tag{5.20}$$

3) Specificity:

$$Sp = \frac{TN}{TN + FP} \cdot 100\ [\%] \tag{5.21}$$

In these Equations, TP, TN, FP, and FN represent the number of examples that were classified as true positives, true negatives, false positives, and false negatives, respectively. Sometimes, precision, F1-score, and area under the curve are used as well.

5.1.4. Regularization

As shown in the example of the FFNNs, during the learning process, training error is computed, and the algorithm tries to minimize the error. However, for the model to generalize well, it is also necessary for a test error (error calculated on test data) to be small, and that a gap between the training and test errors is minimized [15]. Two problems can emerge during the learning process: underfitting and overfitting. Underfitting represents the inability of the model to obtain a low training error. The big gap between the two errors implies that the model is overfitting.

There are different techniques for preventing algorithms from underfitting or overfitting. Underfitting usually suggests that the model is too simple for the observed task. Increasing the complexity of the model or number of iterations can help with the underfitting problem. However, overfitting represents a more complex problem, and it expresses the inability of the model to generalize well. Regularization represents a set of techniques that are being applied to mitigate the overfitting problem [15]. In further sections, there will be a more detailed explanation of the regularization techniques that have been used in this thesis.

5.1.4.1. Parameter Norm Penalties

The most common regularization strategy includes adding a norm penalty $\Omega(W)$ to the loss function, as follows [15]:

$$\tilde{J}(W) = J(W) + \lambda\Omega(W) \tag{5.22}$$

where $\tilde{J}(W)$ is a regularized loss function, and $\lambda \in [0, \infty)$ is the hyperparameter controlling the contribution of the norm penalty. Smaller values of the λ hyperparameter cause model to be less regularized and vice versa. By minimizing the loss function $\tilde{J}(W)$, the algorithm also minimizes the norm penalty function, which consequently shrinks the weight vector at each iteration before performing the gradient update and prevents the weights from achieving high values [15]. Typically, the norm penalty is chosen as the function that penalizes the weight parameters. The most common is the L^2 norm penalty or weight decay:

$$\Omega(W) = \frac{1}{2}\sum_{l=1}^{L-1}\left\|\boldsymbol{W}^{(l)}\right\|_2^2 \tag{5.23}$$

Other functions can be applied as the norm penalty, including L^1 or a combination of L^1 and L^2 norm penalties [15].

5.1.4.2. Dropout

Dropout represents a computationally inexpensive but powerful regularization technique. It randomly removes some portion of layer units [122]. The most effective manner of removing a unit from the network includes multiplying it with a zero. The architecture of the network changes from iteration to iteration, and an ensemble of all subnetworks that are formed in this manner is trained [122]. The models share the parameters – the parameters learned in the previous iteration are transferred to a new subnetwork. By applying dropout, the layer cannot rely on only a few input features since they are not always present during the training. In this way, the layer learns to use all inputs, which prevents the network from overfitting [122]. Dropout is usually used together with a mini-batch gradient algorithm. With every new training example, a binary mask is applied to the layer units [15]. The probability of removing the layer units is a hyperparameter that needs to be selected before the training. Typically, a probability of 0.5 is used for hidden layers.

5.1.4.3. Dataset Augmentation

One of the best strategies to prevent a network from overfitting is to feed it with a larger amount of data [15]. When collecting more data requires many resources, data augmentation can be a useful tool for creating bigger datasets. For two-dimensional data, data augmentation techniques often imply to some transformation of the original images (image rotations, adding some noise, and others). In the case of one-dimensional time-series data, augmentation strategies applied in the literature typically include cropping data to shorter time-series.

5.1.4.4. Batch normalization

During the training process, the layer parameters change, which consequently alters the distribution of the next layer inputs as well. Because of that, a lower learning rate and cautious initialization of the network parameters are required, which consequently slows down the learning process. This phenomenon is called “internal covariate shift,” and it can be resolved by normalizing the layer inputs [123]. The normalization becomes the part of the network model – it is performed for each batch of data during the training. The use of batch normalization allows a less strict selection of learning rate and network parameter values.

In general, batch normalization is not considered as a regularization technique; however, it was shown that it could act as the regularization strategy and improve the generalization abilities of the network.

5.1.5. Long short-term memory network

A recurrent neural network (RNN) represents a dynamic system that is capable of processing time series [15]. RNNs have a looping mechanism (connections) that propagate data from earlier time steps to the current. For each time step, the information is preserved within the unit's internal state.

The standard RNNs suffer from a problem called "short-term memory", i.e., they cannot carry information for more than approximately ten time steps [120]. With every time step, a backpropagated error tends to grow or shrink, and with a sufficiently large number of time steps, it explodes or vanishes. Exploding gradients cause network weights to oscillate, whereas, with vanishing gradients, the network takes a lot of time for training or it does not train at all. One possible way for solving this problem is a gradient-based method called a long short-term memory neural network [120].

Long short-term memory (LSTM) network represents a special type of RNN, capable of learning relationships for more than a thousand time samples [124]. One LSTM unit consists of a memory cell, input gate, forget gate, and output gate. The memory cell captures the information for different time steps, whereas the gates control the information flow through the memory cell.

The parameters (weight and biases) of the forget gate regulate the amount of information that is discarded from the cell. The forget gate activation vector is computed as [120]:

$$\boldsymbol{a_f} = f(\boldsymbol{W_f x_t} + \boldsymbol{u_f h_{t-1}}) \tag{5.24}$$

where $\boldsymbol{W_f}$ and $\boldsymbol{u_f}$ represent the weight vector of the input and recurrent connections of the forget gate, respectively. The input feature vector for a time step t is denoted with $\boldsymbol{x_t}$, whereas the $\boldsymbol{h_{t-1}}$ represents a hidden state vector obtained as a result of that LSTM unit from the previous time step. The activation function is marked with f.

The input gate controls the flow of new information to the memory cell. Firstly, the input gate activations vector is computed as [120]:

$$\boldsymbol{a_i} = f(\boldsymbol{W_i x_t} + \boldsymbol{u_i h_{t-1}}) \tag{5.25}$$

where $\boldsymbol{W_i}$ and $\boldsymbol{u_i}$ represent the weight vector of the input and recurrent connections of the input gate, respectively. In this way, the LSTM unit decides what values are updated. Afterwards, new candidates for a cell state vector values are found by calculating a cell input activation vector [120]:

$$\widetilde{\boldsymbol{c_t}} = f(\boldsymbol{W_c x_t} + \boldsymbol{u_c h_{t-1}}) \tag{5.26}$$

where $\boldsymbol{W_i}$ and $\boldsymbol{u_i}$ represent the weight vector of the input and recurrent connections of the cell input, respectively. Afterwards, the cell state vector is updated as follows [120]:

$$\boldsymbol{c_t} = \boldsymbol{a_f} \cdot \boldsymbol{c_{t-1}} + \boldsymbol{a_i} \cdot \widetilde{\boldsymbol{c_t}} \tag{5.27}$$

where $\boldsymbol{c_{t-1}}$ represents the cell state vector from the previous time step, and the operator $\cdot$ denotes the Hadamard product (or element-wise product). The output gate regulates the amount of information used for calculating the output activation of the LSTM unit. The activation vector of the output gate is computed as [120]:

$$\boldsymbol{a_o} = f(\boldsymbol{W_o x_t} + \boldsymbol{u_o h_{t-1}}) \tag{5.28}$$

where $\boldsymbol{W_o}$ and $\boldsymbol{u_o}$ represent the weight vector of the input and recurrent connections of the output gate, respectively. The output vector of the LSTM unit or hidden state vector represents the final output of the LSTM unit at the time step t, and it is computed as:

$$\boldsymbol{h_t} = \boldsymbol{a_o} \cdot f(\boldsymbol{c_t}) \tag{5.29}$$

The learning algorithm applied in the LSTM networks represents the combination of two algorithms, backpropagation through time and real-time recurrent learning [120].

5.1.6. Convolutional neural network

The convolutional neural network (CNN) represents a special type of FFNNs that can process raw data with a grid-like topology, including both a 1-dimensional grid of time samples (or time-series) and a 2-dimensional grid of pixels (or images) [15].

In general, convolution is an operation defined with the following formula [15]:

$$s(t) = (x * y)(t) = \int x(a)\omega(t-a)da \tag{5.30}$$

In Equation (5.30), any two functions of a real-valued argument can be used. The first argument (the function x in the abovementioned Equation) is typically referred to as the "input". The second argument (the function ω in the abovementioned Equation) is denoted as the "kernel" or "filter". Sometimes, the output of the convolution operation is called the "feature map". The discrete convolution is defined as [15]:

$$s(t) = (x * y)(t) = \sum_{a=-\infty}^{\infty} x(a) \cdot \omega(t-a) \tag{5.31}$$

where functions x and ω are defined on some finite number of t, and operator $\cdot$ represents the Hadamard product (or element-wise product). Discrete convolution over more than one axis is defined as [15]:

$$\begin{aligned} S(i,j) = (I * K)(i,j) &= \sum_m \sum_n I(m,n) \cdot K(i-m, j-n) \\ &= \sum_m \sum_n I(i-m, j-n) \cdot K(m,n) \end{aligned} \tag{5.32}$$

where I and K represent 2-dimensional input and kernel, respectively.

Within CNNs, kernels are organized within convolutional layers, and they are defined by their height H_K, width W_K and stride S_K (observed as network hyperparameters). The height and width determine the size of the filter, whereas the stride represents the size of a step for crossing the input both vertically and horizontally. The output of one convolutional layer represents a feature map. Sometimes a padding technique is applied to pixels/samples near the input edges: the original input is extended with the additional pixels/samples P so the resulting feature map can take some specific size. The size of the resulting feature map is defined as:

$$W_s = \frac{W_I - W_K + 2P}{S_K} + 1 \tag{5.33}$$

$$H_s = \frac{H_I - H_K + 2P}{S_K} + 1 \tag{5.34}$$

where W_I and H_I represents the width and height of the input. The number of kernels that are applied within one convolutional layer defines the number of channels (or depth) of the resulting feature map. In these Equations, stride values used for traversing the input horizontally and vertically can differ. In the case of 1-dimensional input, the resulting feature map has a size of $1xW_s$, where W_s is calculated using the same formula (5.33), and the depth of the feature map is defined by the number of applied kernels. The illustration of the CNN learning process in the case of 1-dimensional input data is given in Figure 5.4.

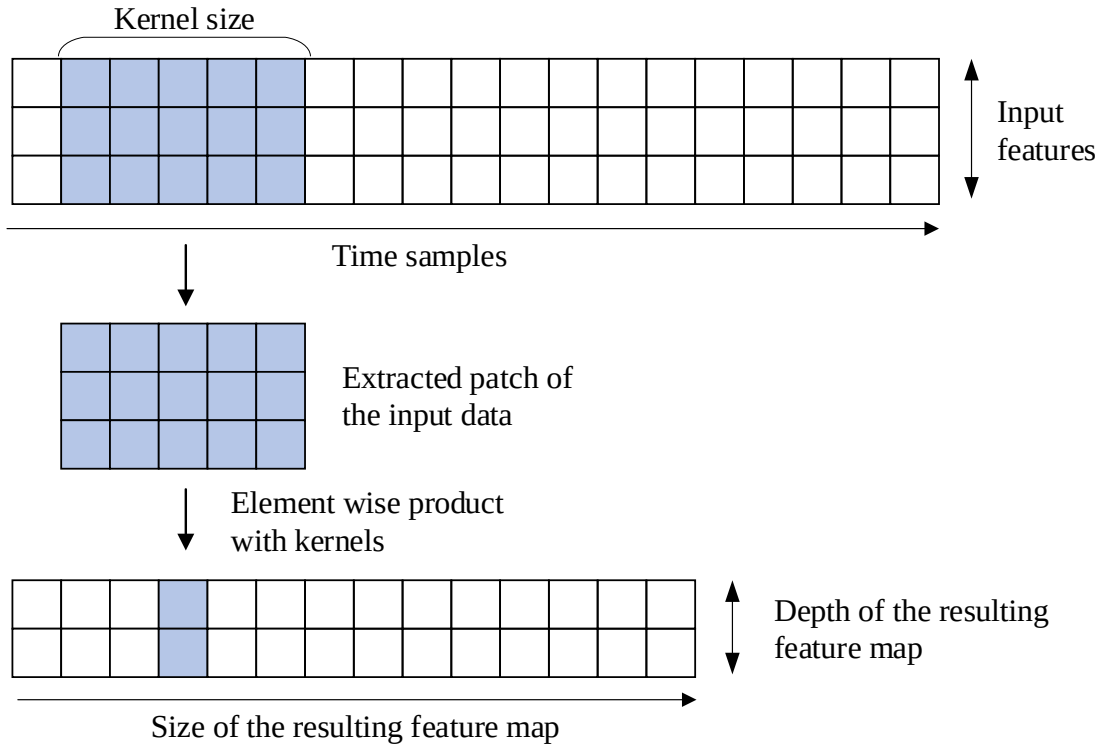

Figure 5.4 Illustration of the CNN learning process in the case of 1-dimensional input data.

Other important properties of the CNNs include [15]:

1. Sparse connectivity or sparse weights – This property arises from the fact that the kernel is usually much smaller than the input, e.g., the input can have thousands of elements (pixels or time samples), but small features can occupy only a few dozens of elements. In this way, a smaller number of parameters needs to be stored and trained, which reduces the number of required operations and memory requirements, and improves the statistical efficiency of the network.
2. Parameter sharing – Each pixel/sample of the kernel is used at every or almost every position of the input (depending on the selected values for the stride S_K and padding P). This means that one set of parameters is learned at different positions of the input.
3. Equivariant representations – This property refers to the equivariance to translation, causing the output to change in the same manner as the input. When 1-dimensional input is processed,

convolution gives a "timeline," showing when different features emerge in the input. If some features are moved later in the input, the same features will emerge later in the output as well.

Within multilayer convolutional neural networks, the output feature map of one layer is fed to the next layer as the input. A typical convolutional neural network consists of three layers: a convolutional layer, a non-linear layer, and a max-pooling layer [15]. The convolutional layer produces a set of linear activations, which then runs through a non-linear activation function (usually ReLU). In the end, a pooling layer is used to merge similar features. The result of the pooling is computed as the summary statistics of a local patch of the feature maps' pixels/samples. The most common pooling layer calculates the maximum value of nearby outputs, and it is called the max-pooling. Other commonly used statistics include average, weighted average or L^2 norm of a neighbouring local patch [15]. The pooling layer makes the output invariant to a small translation of the input, which is useful for the cases when the existence of a feature is essential, but not its precise location. The size of the output of the max-pooling layer can be calculated using the same Equations (5.33) and (5.34).

5.2. Method

5.2.1. Experiment

The study comprised forty-eight subjects in total: thirty-three patients with PD (Gender: 17 female/16 male; Age: 64.3±7.9 years) and fifteen age- and gender-matched HC subjects (Gender: 7 female/8 male; Age: 62.5±6.9 years). The patients were initially recruited at the Clinic of Neurology, Clinical Centre of Serbia, School of Medicine, University of Belgrade, Belgrade, Serbia, in 2015. Healthy controls were selected among healthy staff members or persons accompanying the patients at the Clinic of Neurology. Neurologists (specialists for movement disorders) diagnosed PD patients using the UK Parkinson's Disease Society Brain Bank criteria [38]. Parkinsonism signs were assessed with the UPDRS scale [42]. The H&Y scale was applied for the evaluation of disease severity [35]. The performed assessment showed that all PD patients were in an early or mild stage of disease development. The criteria for H&Y scores (H&Y≤2) and disease duration (<5 years) were applied for distinguishing patients in the early stage of PD development. Fifteen out of thirty-three PD patients (Gender: 9 female/6 male; Age: 62.0±9.8 years) met the set criteria, and they were also observed as patients in the early stage of PD development (later referred to as "PDearly"). The clinical data of both PD and PDearly patient groups are presented in Table 5.1.

The clinical diagnosis of PD has lower reliability, especially if it is given in the early stage of disease development [125]. For that reason, diagnostic follow-up was performed by two neurology specialists (with more than ten years of experience) in 2020, 5 years after the initial inclusion of PD patients. The physicians confirmed the diagnosis that was given before or at the beginning of the study for all observed patients (Table 5.1, last row), increasing the reliability of the labels for classification tasks. All thirty-three PD patients were included in further analysis.

Table 5.1 Clinical features of PD patients presented through descriptive statistics (average±std, median), with separately presented information for patients in the early stage of PD.

Clinical features	Statistics	PD	PDearly
H&Y	Average±std	2.0±0.8	1.5±0.5
	Median	2.5	1.5
Disease duration (years)	Average±std	9.2±6.5	3.4±1.3
	Median	7	3.25
UPDRS Total	Average±std	78.9±33.0	43.8±16.9
	Median	85	40
UPDRS III	Average±std	40.5±16.2	24.4±8.4
	Median	39	23
UPDRS gait	Average±std	1.5±0.9	1.0±0.8
	Median	2	1
Confirmed diagnosis	No. of cases	33/33	15/15

PD – Parkinson's disease patients; PDearly – Patients in the early stage of Parkinson's disease development; H&Y – Hoehn and Yahr scale; UPDRS – Unified Parkinson's disease rating scale; UPDRS III – Unified Parkinson's disease rating scale, Part III – Motor examination; UPDRS gait – Unified Parkinson's disease rating scale, scores given for the evaluation of the severity of gait disturbances.

The participants were asked to complete a walking task, which was captured and analysed under four different conditions [126]:

1. Regular or baseline walking (later referred to as "BASE") – walking along a straight path with a regular, usual rhythm.
2. Motor dual-task (later referred to as "MOTOR") – walking along a straight path with a regular, usual rhythm while carrying a glass of water, trying not to spill it.
3. Cognitive dual-task (later referred to as "COGNITIVE") – walking along a straight path with a regular, usual rhythm while performing a mathematical task – serial subtractions of the number "7" from the number "100". The mathematical task was given by the examiners, who took care that the participants provided the correct answers.
4. Combined dual-task (later referred to as "COMBINED") – walking along a straight path with a regular, usual rhythm, while carrying the glass of water and performing the described mathematical task, in parallel.

For all subjects, four walking sequences were captured per each walking condition with few minutes of break between the successive trials. The exception was one PD patient who performed only two walking sequences per each condition because of particularly evidenced fatigue during the experiment. The subjects performed the walking task in their shoes.

The included patients did not experience any freezing of gait or fall episodes during the experiment. The measurements were conducted in a 15-meter long and 3-meter wide hallway that did not contain any obstacles, narrow passages, or floor patterns that could affect the walking of patients. In that manner, the participants were provided with a clear space and time to walk at their natural pace.

For all subjects, the measurements were conducted during one day at the Clinic of Neurology, Clinical Centre of Serbia, School of Medicine, University of Belgrade, Belgrade, Serbia. The study was performed following the ethical standards of the Declaration of Helsinki and approved by the Ethical Committee, School of Medicine, University of Belgrade. All participants gave their written informed consent to participation in the study.

5.2.2. Instrumentation

In this study, the wireless sensor system SENSY was applied for recording the walking task [117]. The system comprises two IMUs, and two shoe insoles, each with three force sensing resistors (FSR) positioned below the area of the 2nd and 4th metatarsal bones and heel area, respectively (illustrated with gray circles on Figure 5.5). The IMUs incorporated a 3-axial analog accelerometer (ADXL330, Analog Devices, Norwood, Massachusetts, USA) and a 3-axial gyroscope sensor (LPR530, LPY530, Analog Devices, Norwood, Massachusetts, USA). During the experiment, IMUs were placed laterally on the subject's feet (illustrated with a gray rectangle in Figure 5.5). Shoe insoles were provided in a corresponding size for each participant and positioned in their shoes during the measurements. The sensors were connected to their central units, which collected and wirelessly sent signals to a remote computer (proprietary communication protocol based on IEEE 802.15.4 standard). The data was acquired with a sampling frequency $f_s = 100$ Hz, using a custom-made software developed in LabWindows/CVI 9.0 (National Instruments, Austin, Texas, USA).

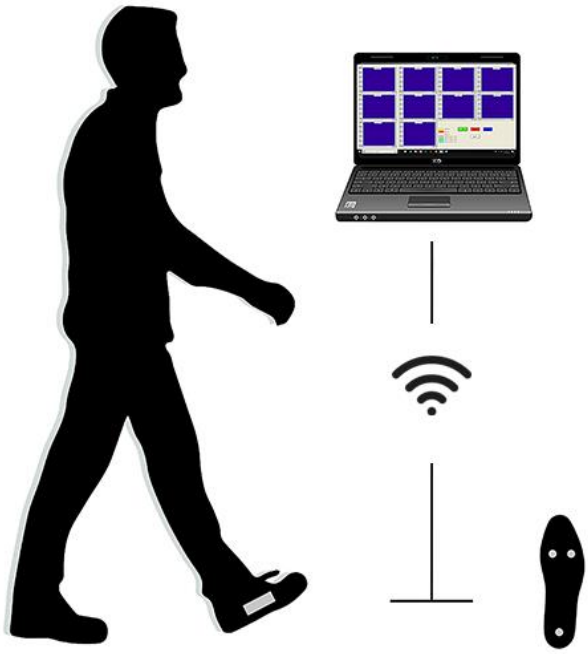

Figure 5.5 Illustration of the used SENSY system and its position during the experiment, with the program for data acquisition running on the remote computer.

5.2.3. Data processing

Data processing was executed in custom-made scripts written in Matlab 9.6 R2019a (MathWorks, Natick, Massachusetts, USA). A single GPU, Cuda device, GeForce GTX 1050 Ti (Nvidia Corporation, Santa Clara, California, USA) was used for training and testing of developed models.

All recorded signals were initially filtered using the same 5-point moving average filter for all subjects. The normalized ground reaction force GRF_N was calculated from the recorded and filtered FSR signals, using the same procedure described in Chapter 4.

An example of the pre-processed force, accelerometer, and gyroscope signals is presented in Figure 5.6. The example is provided for one PD patient in the early stage of disease development (H&Y=2, diseased for two years). The presented signals are recorded from the more affected (right) leg during the BASE task.

The analysed walking sequences had 14 feature dimensions that represented the normalized ground reaction force GRF_N, three accelerometer axes $a_{x,y,z}$ and three gyroscope axes $\omega_{x,y,z}$ from both legs. The initial dataset which consisted of the whole non-cropped and pre-processed 14-dimensional walking sequences (later referred to as "ORIGINAL") was used as an input for further data processing.

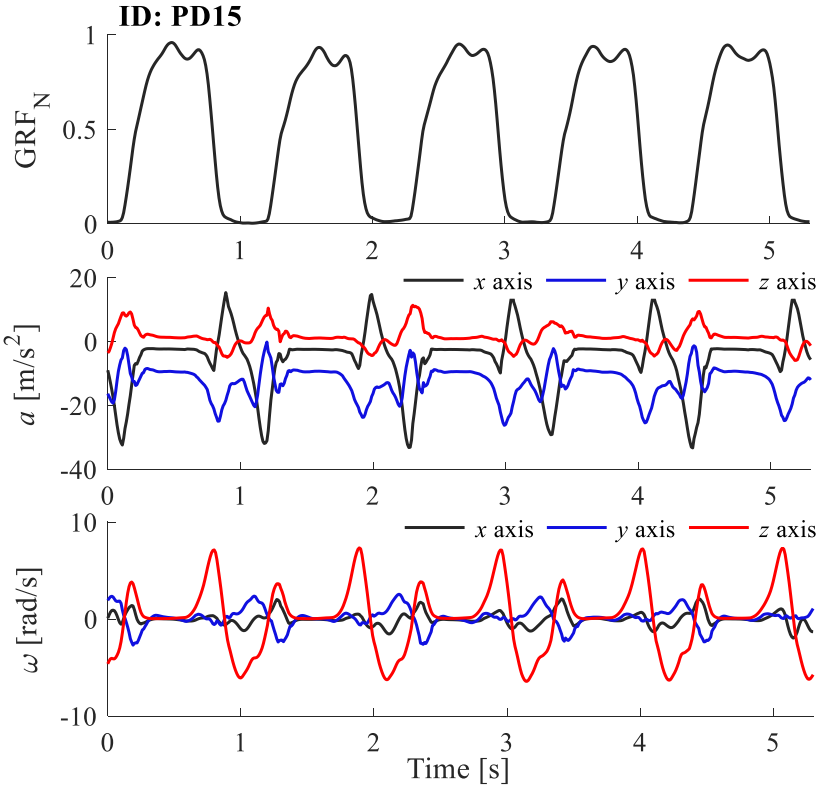

Figure 5.6 Presentation of the pre-processed signals: the normalized ground reaction force GRF_N (upper panel), three accelerometer axes $a_{x,y,z}$ (middle panel) and three gyroscope axes $\omega_{x,y,z}$ (bottom panel) from the more affected leg. The example is given for one PD patient in the early stage of disease development.

5.2.3.1. Gait segmentation

Segmentation of walking sequences was performed using the gait segmentation method M1b that was already presented in Chapter 4. This method was applied to the calculated normalized ground reaction force GRF_N. The moments representing toe-off events from the left leg were detected and used in further analysis as the time markers for segmenting the gait into individual strides.

5.2.3.2. Data augmentation problem

In this study, two strategies were developed and applied: stride-based and time-based data augmentation. These techniques were applied to the ORIGINAL dataset. In addition to providing more data for training and testing, the introduced augmentation techniques allowed examination of the influence that a length of the walking sequences might have on the performance of the developed models.

5.2.3.2.1. Stride-based data augmentation

The extracted time markers were applied to the ORIGINAL dataset for providing shorter 14-dimensional walking sequences. The data augmentation was executed along the following lines:

1) Cropping to 14-dimensional walking segments that include eight successive strides (later referred to as "STRIDE-8"). The neighbouring walking segments were shifted by a length of one stride.
2) Cropping to 14-dimensional walking segments that include five successive strides (later referred to as "STRIDE-5"). The neighbouring walking segments were shifted by a length of one stride.
3) Cropping to 14-dimensional walking segments that include two successive strides (later referred to as "STRIDE-2"). The neighbouring walking segments were shifted by a length of one stride.

Based on the detailed analysis of the ORIGINAL database, it was established that the shortest recorded walking sequence comprised nine strides; therefore, the upper limit for data augmentation was set to eight strides, which provided no less than two cropped segments per any recorded walking sequence.

The increased intra-variability (sometimes referred to as a stride-to-stride variability) represents one of the most notable characteristics of the parkinsonian gait [125]. In order to observe these essential gait characteristics, at least two successive strides should be contained within one cropped walking segment, which was selected as a lower limit for segmenting the original walking sequences.

5.2.3.2.2. Time-based data augmentation

In the case of time-based data augmentation, data was cropped on a time level. The data augmentation was executed along the following lines:

1) Cropping to 8 s long 14-dimensional walking segments (later referred to as "TIME-8"). The neighbouring walking segments were shifted by a length of 1 s.
2) Cropping to 5 s long 14-dimensional walking segments (later referred to as "TIME-5"). The neighbouring walking segments were shifted by a length of 1 s.
3) Cropping to 2 s long 14-dimensional walking segments (later referred to as "TIME-2"). The neighbouring walking segments were shifted by a length of 1 s.

The selection of cropping limits was performed using the same principle as for the previous augmentation strategy. The shortest walking sequence within the ORIGINAL database was 9.25 s long; therefore, the upper limit for data augmentation was set to 8 s, which provided no less than two cropped segments per any recorded walking sequence. The lower limit for cropping the walking

sequences was set based on the value of the typical gait frequency of 1 Hz [126]. For a typical gait and sampling frequency of 100 Hz, two strides should be comprised in a 2 s long walking sequence, which was set as a lower limit for gait augmentation.

By using both augmentation strategies, seven datasets were developed and fed to the designed deep learning models in total: ORIGINAL, STRIDE-8, STRIDE-5, STRIDE-2, TIME-8, TIME-5, and TIME-2.

5.2.3.3. Classification of PD patients and healthy controls

Two classification tasks were observed and analysed in this study:

1) classification of all patients with PD and HC subjects (later referred to as "PD-HC");
2) classification of PDearly patients and HC subjects (later referred to as "PDearly-HC").

For this purpose, two deep learning models were designed and validated using the developed datasets: long short-term memory network and convolutional neural network.

5.2.3.3.1. Long short-term memory network

Different architectures of the LSTM network were tested to find a network topology that provides the best results for the observed classification tasks. The architecture of the final designed network is shown in Figure 5.7.

The designed network had one LSTM layer with 100 hidden neurons, one fully connected (FC) layer with 100 hidden neurons, and a softmax layer. The Xavier initialization scheme was applied for the initialization of values of both input and recurrent weights [129]. For the gates, the sigmoid activation function was used, while the soft-sign function was applied as the activation function for updating the memory cell and hidden states. A dropout layer was applied after both the LSTM and FC layers to prevent the LSTM network from overfitting, with the probability of dropping out the hidden units of 0.5.

The Adaptive moment estimation (ADAM) solver was applied for training. The cross-entropy was used as a loss function. The network was trained for 30 epochs, with a mini-batch size of 128. For the case when stride-based datasets were used for training, one mini-batch could contain walking segments of different lengths. Because of that, the input data was sorted in an ascending order prior to any model training and testing. During the training and testing process, the walking segments belonging to one mini-batch were cropped to the length of the shortest walking segment from the corresponding mini-batch. The L_2 norm penalty, with regularization parameter $\lambda = 0.05$, was added to the loss function so the complex models could be penalized. The learning rate was given the initial value $\eta = 0.001$; after every five epochs, the learning rate was decreased for a factor of 0.2. Furthermore, a limitation of value 1 was applied to the gradient values, to prevent the gradients from exploding/vanishing. In this study, input data was not normalized, since it was shown that data normalization reduced the performance of the LSTM network, indicating that the amplitude of the input data carried crucial information that contributed to more precise recognition of gait disturbances.

The LSTM network was trained and tested on all developed datasets: ORIGINAL, STRIDE-8, STRIDE-5, STRIDE-2, TIME-8, TIME-5, and TIME-2.

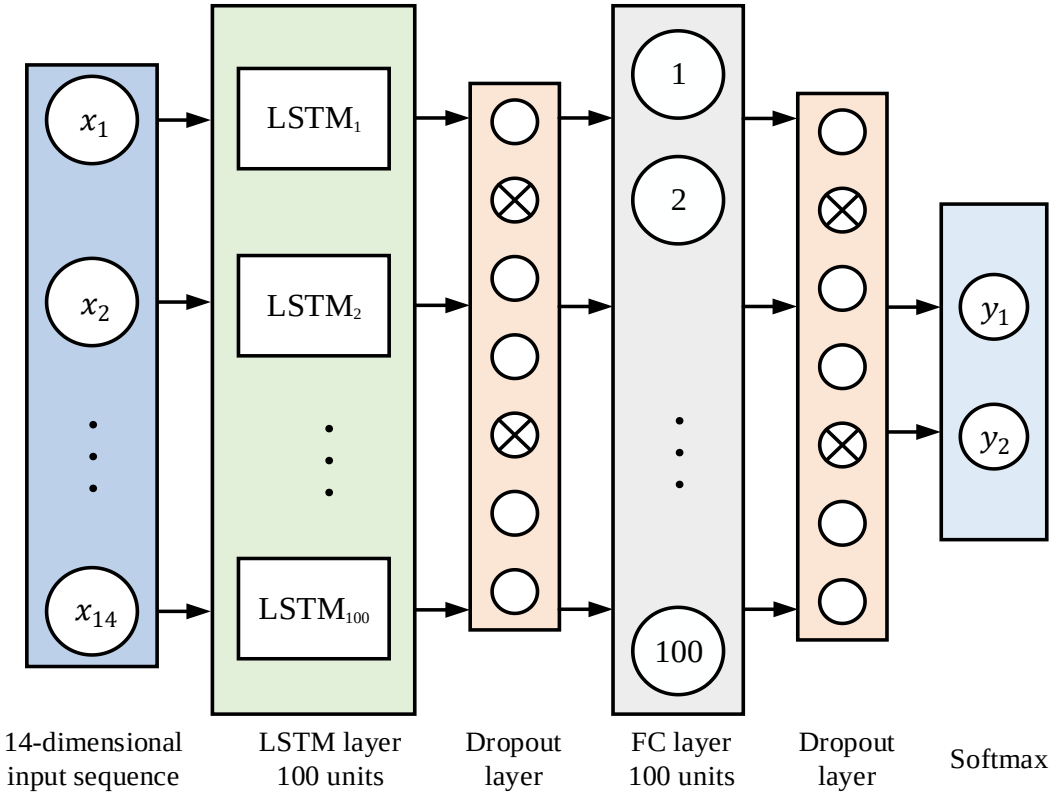

Figure 5.7 The topology of the developed LSTM network. Marks $x_1, x_2, \ldots, x_{14}$ represented 14 input feature dimensions, namely GRF_N, $a_{x,y,z}$ and $\omega_{x,y,z}$ signals from both legs. Labels y_1 and y_2 corresponded to two groups being classified.

5.2.3.3.2. Convolutional neural network

The second DL model was designed using the CNN model. The final network consisted of 14 convolutional blocks of the same architecture, marked as $C_1, C_2, \ldots C_{14}$. The convolutional blocks were fed with the individual dimensions of the 14-dimensional input data, corresponding to the normalized ground reaction force GRF_N, three accelerometer axes $a_{x,y,z}$ and three gyroscope axes $\omega_{x,y,z}$ from both legs. Each convolutional block comprised two parts:

1) convolutional layer (CONV-1) with 16 filters size of 1x10 samples; followed by a batch normalization layer, ReLU activation function layer, and a max-pooling layer (POOL-1) with a pooling patch size of 1x2 samples;
2) convolutional layer (CONV-2) with 32 filters size of 1x10 samples, followed by a batch normalization layer, ReLU activation function layer, and a max-pooling layer (POOL-2) with a pooling patch size of 1x2 samples.

The features learned by the convolutional blocks were merged and fed as the input to the FC layer with 100 hidden neurons. A dropout layer with a probability of 0.5 for dropping out the hidden units was put after the FC layer, and followed by a softmax function layer. The topology of the designed CNN network is presented in Figure 5.8. The batch normalization layer and ReLU activation function layers were not illustrated in this Figure to simplify the illustration.

The same hyperparameters were used, as in the case of the LSTM network. The data was not normalized prior to network training and testing. The CNN network was trained and tested on three time-based datasets: TIME-8, TIME-5, and TIME-2.

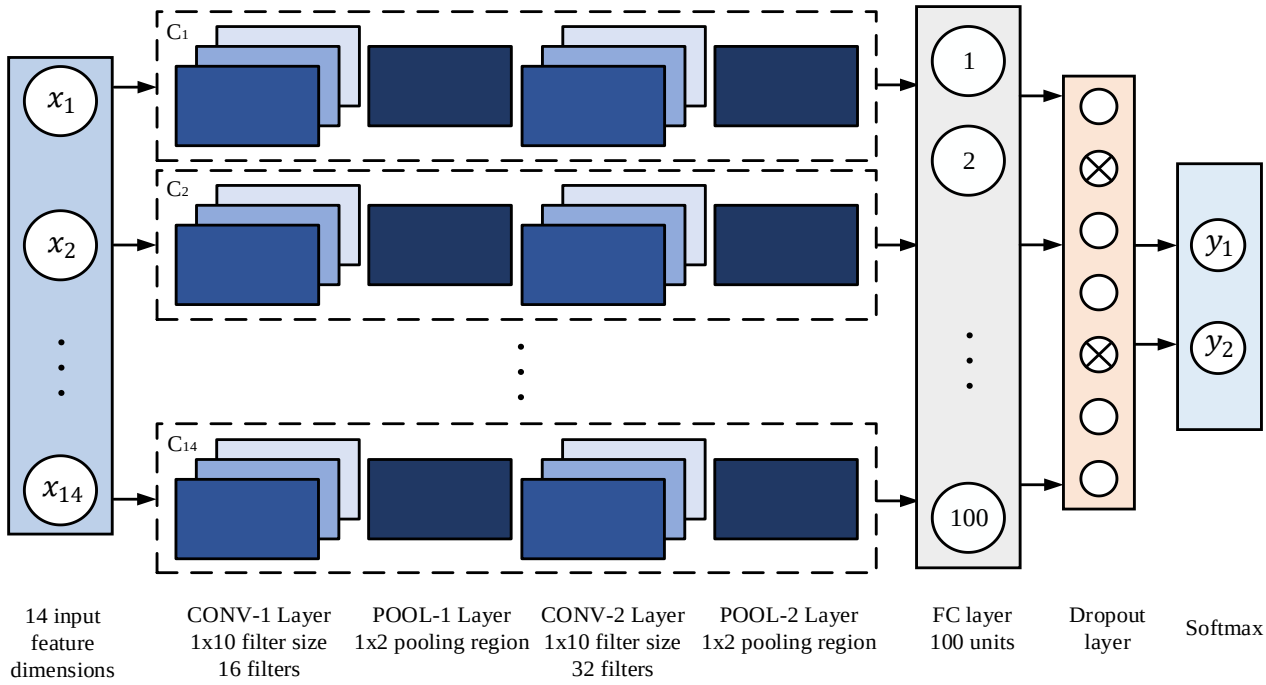

Figure 5.8 The topology of the developed CNN network. Marks $x_1, x_2, \dots, x_{14}$ represented 14 input feature dimensions, namely GRF_N, $a_{x,y,z}$ and $\omega_{x,y,z}$ signals from both legs. Labels y_1 and y_2 corresponded to two groups being classified. Marks $C_1, C_2, \dots, C_{14}$ represented the convolutional blocks, which were fed with a corresponding input feature dimension.

5.2.3.4. Evaluation

A 5-fold stratified subject-wise cross-validation was used to evaluate the performance of the developed models. Firstly, participants from each subject group were randomly split into five folds, as equally as possible. This manner of data partitioning assured that data was divided on a subject level and that data from one subject was always placed in the same fold. Furthermore, in this way, all folds contained data from both subject groups that were observed for a specific classification task.

The standard k-fold cross-validation procedure was applied for validating the models. One fold (out of 5 folds) was used for testing, whereas the other four folds were applied for training. The procedure was rerun five times, each time with a different fold used for testing the models. The results obtained for five repetitions were averaged to provide final quantification of the model performance.

The performance of the developed DL models was evaluated using the Accuracy Ac, Sensitivity Se, and Specificity Sp metrics, which were calculated following the formulas (5.19)-(5.21). The Accuracy represented the percentage of the correctly classified walking segments with respect to the total number of the observed segments. The Sensitivity measured the proportion of the accurately categorized walking segments belonging to the diseased individuals. In contrast, the Specificity represented the percentage of the walking segments of the healthy participants that were correctly recognized.

5.3. Results

5.3.1. Data augmentation

The ORIGINAL dataset comprised 760 non-cropped walking sequences in total, each sequence had 14 feature dimensions representing the normalized ground reaction force GRF_N, three accelerometer axes $a_{x,y,z}$ and three gyroscope axes $\omega_{x,y,z}$ from both legs. The initial dataset was augmented using two approaches: stride-based and time-based augmentation, which resulted in 6 new datasets. The results of the performed augmentation are presented in Table 5.2, separately for different datasets and different subject groups.

Table 5.2 The size of the developed datasets expressed as the number of analysed walking segments, and presented for each subject group separately, and in total.

Dataset	PD [# of segments]	PDearly [# of segments]	HC [# of segments]	Total [# of segments]
ORIGINAL	520	240	240	760
STRIDE-8	5,571	2,150	1,113	6,684
STRIDE-5	7,131	2,870	1,833	8,964
STRIDE-2	8,691	3,590	2,553	11,244
TIME-8	8,693	3,542	1,646	10,339
TIME-5	10,523	4,262	2,366	12,889
TIME-2	12,083	4,982	3,086	15,169

PD – Parkinson's disease patients; PDearly - Patients in the early stage of Parkinson's disease development; HC – Healthy controls; ORIGINAL – Dataset with original non-cropped walking segments; STRIDE-8 – Dataset with 8 strides long walking segments; STRIDE-5 – Dataset with 5 strides long walking segments; STRIDE-2 – Dataset with 2 strides long walking segments; TIME-8 – Dataset with 8 s long walking segments; TIME-5 – Dataset with 5 s long walking segments; TIME-2 – Dataset with 2 s long walking segments.

In the case of the stride-based datasets, the number of observed strides was uniform for all subjects; however, the duration of the walking segments varied between the participants. In the STRIDE-8, STRIDE-5, and STRIDE-2 datasets, the shortest segments were 6.7 s, 4.1 s, and 1.6 s long, respectively, whereas the longest duration among all walking segments was 24.3 s, 16.9 s, and 12 s, respectively. Furthermore, the average duration of the walking segments was 9.8 s, 6.1 s, and 2.4 s, respectively, for these three datasets. In contrast, for the time-based datasets, the duration of walking segments was uniform for all subjects, but the number of observed strides varied between the subjects. With this augmentation technique, 6.25, 3.9, and 1.6 strides were on average included within one walking segment from the TIME-8, TIME-5, and TIME-2 datasets, respectively.

5.3.2. Model complexity

The developed CNN model, with 5,362,848 parameters in total, was more complex compared to the LSTM network, which required training of only 56,301 parameters.

5.3.3. Model performance

The results obtained for the LSTM network are presented in Table 5.3. All datasets gave comparable results for the recognition of all PD patients. The accuracy varied for just a few percent, with slightly better results in favour of the time-based datasets compared to the stride-based datasets. The ORIGINAL dataset gave the worst results, showing that a lower number of walking segments for training and testing had a significant impact on the model performance. The TIME-8 dataset provided the best results, with Ac, Se, and Sp of 91.63%, 94.58%, and 75.15%, respectively (shown in the grey-shaded cells in Table 5.3, third column).

Table 5.3 Classification results for the LSTM network, presented through Ac, Se, and Sp metrics for all developed datasets.

Dataset	Metric	PD-HC	PDearly-HC
ORIGINAL	Ac [%]	85.26	80.00
	Se [%]	89.39	77.50
	Sp [%]	76.25	82.50
STRIDE-8	Ac [%]	88.28	71.84
	Se [%]	90.19	68.56
	Sp [%]	75.75	78.38
STRIDE-5	Ac [%]	89.55	66.04
	Se [%]	91.63	59.11
	Sp [%]	79.05	74.58
STRIDE-2	Ac [%]	87.20	67.04
	Se [%]	91.30	59.10
	Sp [%]	72.65	76.66
TIME-8	Ac [%]	91.63	74.29
	Se [%]	94.58	71.77
	Sp [%]	75.15	79.59
TIME-5	Ac [%]	91.20	73.94
	Se [%]	92.51	66.53
	Sp [%]	76.57	88.53
TIME-2	Ac [%]	87.60	71.46
	Se [%]	90.67	66.84
	Sp [%]	76.69	76.20

PD-HC – Classification of all Parkinson's disease patients and healthy controls; PDearly-HC – Classification of patients in the early stage of Parkinson's disease development and healthy controls; ORIGINAL – Dataset with original non-cropped walking segments; STRIDE-8 – Dataset with 8 strides long walking segments; STRIDE-5 – Dataset with 5 strides long walking segments; STRIDE-2 – Dataset with 2 strides long walking segments; TIME-8 – Dataset with 8 s long walking segments; TIME-5 – Dataset with 5 s long walking segments; TIME-2 – Dataset with 2 s long walking segments; Ac – Accuracy; Se – Sensitivity; Sp – Specificity.

The early PD recognition confirmed that the time-based datasets outperformed the stride-based datasets. Furthermore, longer walking segments contributed to a more accurate classification

of two subject groups. Contrary to the result obtained for the first classification task, the ORIGINAL dataset provided the best results, with Ac, Se, and Sp of 80.00%, 77.50%, and 82.50%, respectively (shown in the grey-shaded cells in Table 5.3, last column). This result indicated that the length of the walking segment had a significant impact on the performance of the model, even though in the latter case, the notably smaller number of walking segments was used for training and testing.

Furthermore, the ratio of the calculated Se and Sp parameters differed for the two classification tasks. In the case of PD-HC classification, higher sensitivity and lower specificity were achieved. On the other hand, early PD recognition resulted in higher specificity and lower sensitivity.

For the PD-HC classification task, the CNN model gave the best result in the case of the TIME-8 dataset with Ac, Se, and Sp of 92.49%, 94.15%, and 83.93%, respectively, followed by the TIME-5 dataset with Ac, Se, and Sp of 91.21%, 95.50%, and 74.16%, respectively, and the TIME-2 dataset with Ac, Se, and Sp of 88.47%, 94.23%, and 65.25%, respectively. Similar results were obtained for the PDearly-HC classification - the TIME-8 dataset provided the best results with Ac, Se, and Sp of 83.26%, 85.18%, and 75.65%, respectively, followed by the TIME-5 dataset with Ac, Se, and Sp of 80.27%, 85.01%, and 77.67%, respectively, and the TIME-2 dataset with Ac, Se, and Sp of 77.43%, 81.29%, and 76.98%, respectively.

The best classification results of the two models are compared in Table 5.4. For both classification tasks, CNN gave better results compared to the LSTM network (shown in the grey-shaded cells in Table 5.4).

Furthermore, the analysis of the obtained results showed that the models did not perform poorly for individual subjects but for different walking segments (no matter to whom they belonged), indicating that no subject influenced the performance of the networks.

Table 5.4 The best classification results for the LSTM and CNN models, presented through Ac, Se, and Sp metrics.

Metric	**PD-HC**		**PDearly-HC**	
	LSTM	**CNN**	**LSTM**	**CNN**
$\boldsymbol{Ac}$ [%]	91.63	92.49	80.00	83.26
$\boldsymbol{Se}$ [%]	94.58	94.15	77.50	85.18
$\boldsymbol{Sp}$ [%]	75.15	83.93	82.50	75.65

PD-HC – Classification of all Parkinson's disease patients and healthy controls; PDearly-HC – Classification of patients in the early stage of Parkinson's disease development and healthy controls; LSTM – Long short-term memory network; CNN – Convolutional neural network; Ac – Accuracy; Se – Sensitivity; Sp – Specificity.

5.3.4. Influence of walking conditions on networks' performance

The influence of the walking conditions on the performance of the developed deep networks was also explored. It was evaluated as the percent of walking segments that were correctly classified with regard to the total number of walking segments that were observed for each walking condition. The results are shown in Figure 5.9, for both classification tasks, both models, and three time-based datasets.

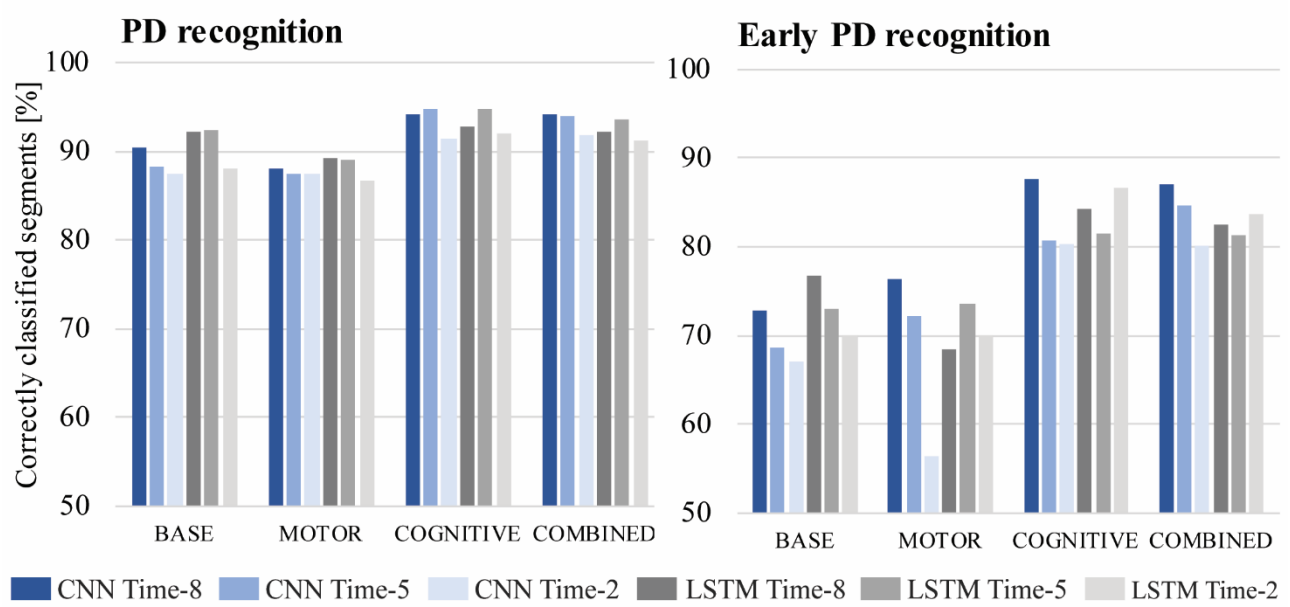

Figure 5.9 The influence of the walking conditions on the performance of the developed DL models for PD recognition (left) and early PD recognition (right), expressed as a percent of accurately classified walking segments per each walking condition.

The walking segments recorded during the COGNITIVE and COMBINED tasks were in larger percent correctly classified compared to the BASE and MOTOR tasks. These results were confirmed for both classification tasks and all three datasets. The differences between the tasks were less expressed for the PD-HC classification task. In contrast, this discrepancy was up to 15% for the classification of healthy subjects and early PD patients. For most of the observed cases, the walking segments recorded during the MOTOR task were in a smaller percent accurately classified compared to other tasks.

5.4. Discussion

In this Chapter, a new method was developed and presented for providing objective and automatic recognition of Parkinson's disease patients. The particular focus was given to the recognition of PD in the early stage of disease development. The developed support utilized nonknowledge-based reasoning. For that purpose, DL models, more specifically long short-term memory network and convolutional neural network, were designed and fed with gait data. The networks were developed and evaluated for two classification tasks, including classification of all PD patients and healthy controls, and classification of early PD patients and healthy subjects. It was also examined how the duration of the walking segments, augmentation strategy, and walking conditions influenced the performance of these models.

Gait data was recorded with a wearable wireless inertial and force sensor system. The used sensors are lightweight, small, affordable, and can be applied at any time and place. These important properties make them appropriate for clinical practice that requires a fast and accurate diagnostic assessment of a large number of patients, but also for applications in the everyday environment and patients' self-management.

The processed gait data had 14 feature dimensions: the normalized ground reaction force GRF_N, three accelerometer axes $a_{x,y,z}$ and three gyroscope axes $\omega_{x,y,z}$ from both legs. Two

augmentation strategies were applied to the original walking sequences: the stride and time-based augmentation techniques. Six new datasets were developed, and together with the dataset comprising the original walking sequences, were fed to the designed deep learning models.

LSTM network represents a special type of recurrent neural network that can find long term dependencies in time-series data. In this study, a LSTM model was developed and validated using all seven datasets. In the case of recognition of all PD patients, time-based datasets provided slightly better results compared to the ORIGINAL and stride-based datasets. The TIME-8 dataset provided the best results with Ac, Se, and Sp of 91.63%, 94.58%, and 75.15%, respectively (shown in the third column, the grey-shaded cells in Table 5.3). Although walking segments were sorted by their length prior to the model training and testing, the LSTM network required that data comprised in one mini-batch was equalized in its length during the learning process. In the case of stride-based datasets, this could cause some information loss and, therefore poorer performance of models that were developed using these datasets. In contrast, recognition of the early-stage PD was more affected by the length of the walking segments. The results showed increased accuracy using longer walking segments for training and testing. Among the seven datasets, the best result was obtained for the ORIGINAL dataset (shown in the last column, grey cells in Table 5.3) with Ac, Se, and Sp of 80.00%, 77.50%, and 82.50%, respectively. This dataset comprised the whole non-cropped walking segments, and therefore the fewest samples for training and testing (as shown in Table 5.2). Furthermore, the ratio between the sensitivity and specificity parameters showed some discrepancy between the two classification tasks, with lower sensitivity and higher specificity for the early PD recognition. In the latter case, some patients had less prominent or almost undeveloped gait disturbances, which could cause their walking segments to be confused with those belonging to healthy individuals.

A deep learning model based on convolutional neural networks was also designed. CNN represents a powerful technique for the extraction of meaningful representations from two- or one-dimensional data. Three time-based datasets were fed to the CNN model. The CNN model outperformed the LSTM model for both classification tasks. The best result was obtained for the TIME-8 dataset (shown in grey cells in Table 5.4) with Ac, Se, and Sp of 92.49%, 94.15%, and 83.93%, respectively for the PD-HC classification task, and Ac, Se, and Sp of 83.26%, 85.18%, and 75.65%, respectively for the PDearly-HC classification task. These results show the high applicability of CNN models for PD recognition.

The gait disturbances represent one of the most incapacitant PD signs; however, this symptom is less prominent in the early stage of the disease development. This fact was supported by the results obtained in this study, showing that a larger number of strides or longer walking sequences should be analysed in order to capture early changes in the gait pattern caused by PD. The CNN network would probably provide even better results with data acquired from a larger number of patients due to its complexity and ability to process big data. On the other hand, the LSTM network is much simpler, and it would probably benefit from longer walking segments, especially for the early PD recognition.

The influence of the dual-task paradigm was also examined on the ability of the designed models to recognize PD. In the literature, the dual-task paradigm is usually applied to examine the interplay between gait and cognition [130]. It was shown that it could influence and alter gait patterns even in healthy subjects [131], [132]. This effect is even more prominent for PD patients, significantly increasing the variability of their gait pattern. The presented results showed that COGNITIVE and COMBINED tasks contributed to an accurate recognition of PD in larger percent compared to the

BASE and MOTOR walking. In the case of the identification of all PD patients, the differences were smaller, indicating that in advanced stages, walking of PD patients is disturbed to the same extent regardless of the condition under which the gait was recorded. In contrast, classification of early PD patients and healthy controls was influenced a lot more by the dual-task paradigm, showing that tasks including some mental occupation while walking (i.e., COGNITIVE and COMBINED) contribute to a more accurate early PD recognition (with differences up to 15%). In contrast, walking segments recorded during the MOTOR task were accurately classified with the smallest percent, which indicated that motor occupation probably altered the gait pattern of both early PD patients and healthy individuals.

Since a small number of subjects were included in the study, a 5-fold stratified subject-wise cross-validation was applied for the evaluation of models' performance to provide meaningful interpretations of the obtained results. Subject-wise cross-validation indicated that all data from one subject was put in the same fold. Therefore, during the testing phase, the predictions were made for data belonging to a subject that was previously unseen by the models. This type of evaluation is especially important since deep learning models can pick up some complex predictors, which in the case of a record-wise validation, could capture a relationship between the data and identity of the subjects and provide high but unrealistic accuracy [133].

Other gait databases were also applied in the literature for recognizing PD using deep learning algorithms. Some systems showed high accuracy results in this field [63], [95]; however, none of these studies considered early PD identification, and to the knowledge of the author, there are no other available results for the early PD recognition using deep learning models and gait data recorded with wearable, wireless sensors. Furthermore, both developed models outperformed deep learning solutions that are using other types of data for recognizing PD in the early stage [68].

6. Amplitude analysis of repetitive movements using wearable sensors

In clinical practice, several motor tests (defined within the UPDRS scale) are applied for assessing the severity of bradykinesia symptom, including finger-tapping, hand opening/closing, hand pronation/supination, and toe-tapping (or foot-tapping) [41], [42]. As part of the test, patients are instructed to perform a specified movement with the biggest amplitude and, as fast as possible, for some number of repetitions, e.g., ten times [59], [60], or for some short time interval, typically 10-15 s [58], [72], [81], depending on the version of the UPDRS scale that is followed. Afterwards, these movements are evaluated with a score that is given based on the specifically defined instructions. The evaluation criteria are the same for these four movements: neurologists observe the amplitude, speed, amplitude decrement, and the number of occasional interruptions that may occur during the test. The only difference in the evaluation process between these four tests relates to the way the amplitude of these movements is observed. Therefore, in order to provide an objective analysis and quantification of these movements, firstly, the amplitude of these movements should be determined.

In this Chapter, the method for capturing and calculating the amplitude of the abovementioned hand and leg movements is defined and presented for each movement separately. The method is demonstrated on the example of one subject.

6.1. Measurement protocol

Subjects are told to sit comfortably in the chair, with their back put against the chair back. They are instructed to perform four motor tasks as following.

Finger-tapping (FT) test: Subject's hand is placed in front of the subject's body, flexed, and supported at the elbow. Each recording contains a sequence of two tasks: 1) fingers are firmly closed and perform a 3D circular or zig-zag movement in the duration of 3-5 s, which is later used for auto-calibration; 2) finger-tapping movement in the duration of 15 s or for 10 repetitions. Finger-tapping movement starts and ends with fingers closed in a "zero" position. The subject is instructed to tap his/her index finger and thumb as fast as with the largest amplitude possible. One cycle of the movement is presented in Figure 6.1.

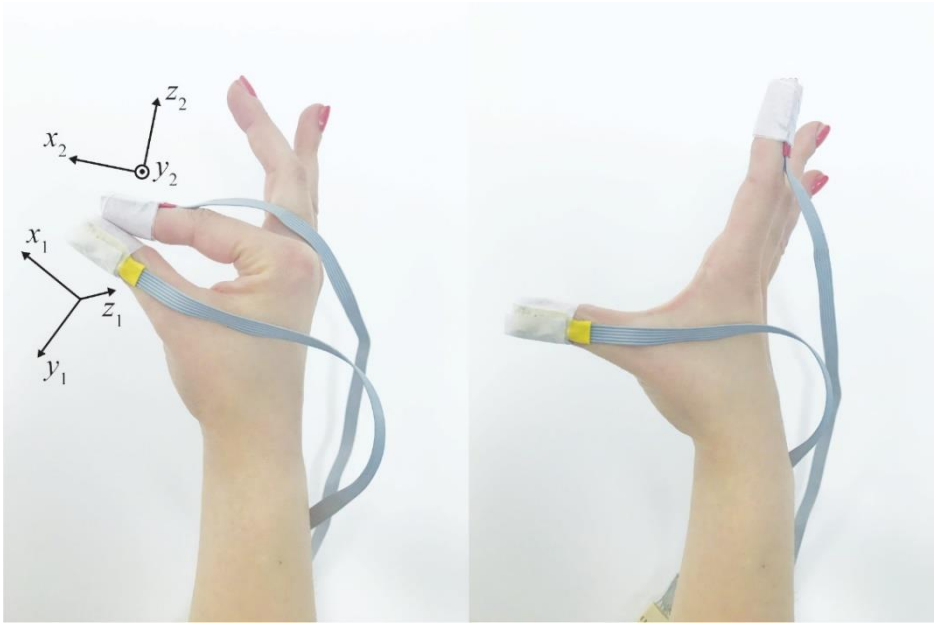

Figure 6.1 Presentation of the repetitive finger-tapping test: the fingers are closed in a "zero" position (left), and the fingers are opened with the highest possible aperture (right).

Hand opening-closing (HOC) test: Subject's hand is placed in front of the subject's body, flexed and supported at the elbow, so the palm faces the examiner. Each recording contains a sequence of two tasks: 1) palm is firmly closed and performs a 3D circular or zig-zag movement in the duration of 3-5 s, which is later used for auto-calibration; 2) hand opening-closing movement in the duration of 15 s or for 10 repetitions. HOC movement starts and ends with the hand closed in a fist (in a "zero position"). The subject is instructed to open and close his/her hand as fast as possible, with the largest possible amplitude. One cycle of the movement is presented in Figure 6.2.

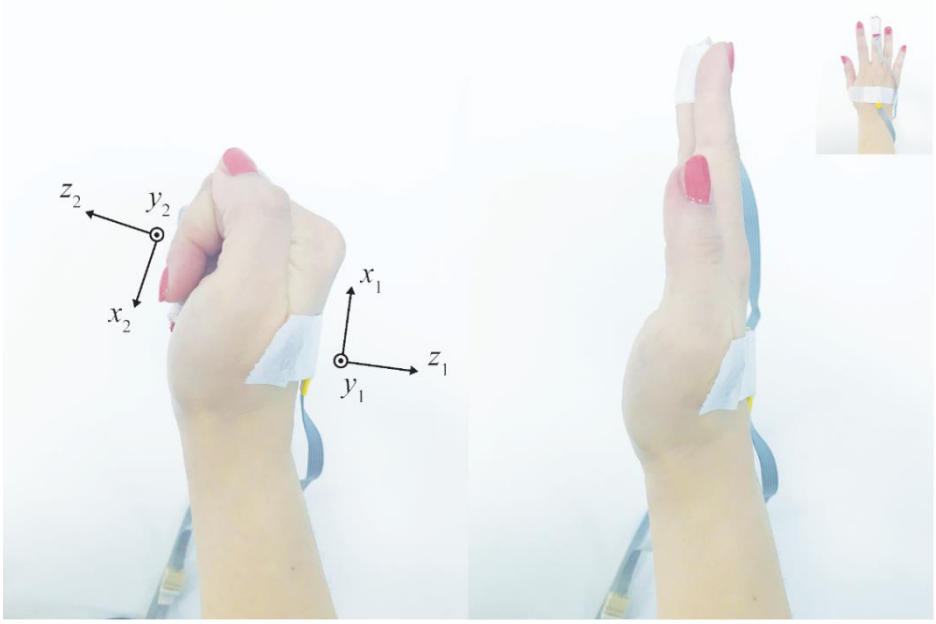

Figure 6.2 Presentation of the repetitive hand opening/closing test: the hand is closed in a "zero" position (left), and the hand is opened with the highest possible aperture (right).

Hand pronation-supination (HPS) test: Subject's hand is placed in front of the subject's body, extended with a palm down at the initial position. Each recording contains a sequence of hand

pronation-supination movements in the duration of 15 s or for 10 repetitions. HPS movement starts and ends with palm oriented down at full supination. The subject is instructed to rotate palm up and down alternatively, as fast and as fully as possible. One cycle of the movement is presented in Figure 6.3.

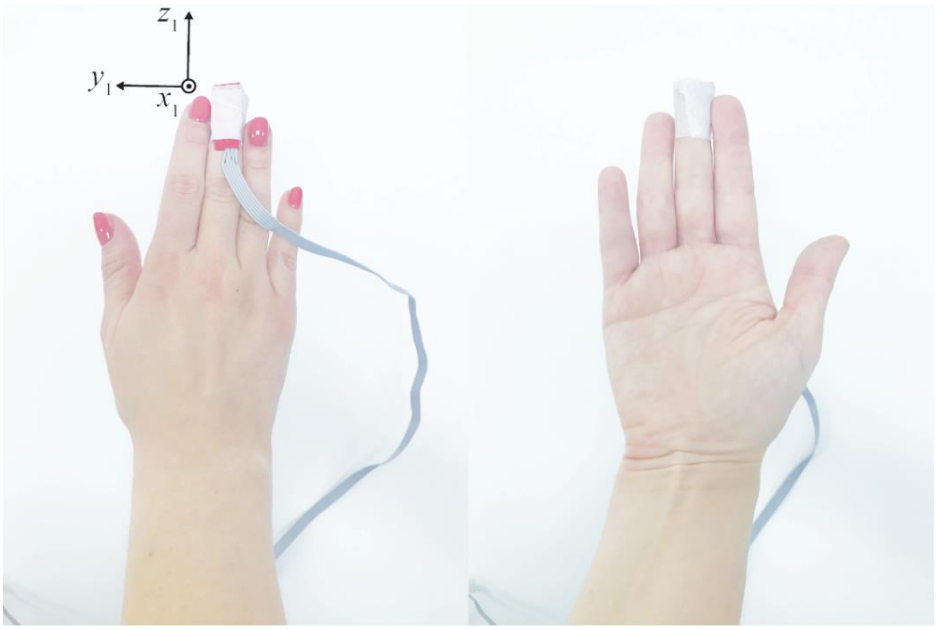

Figure 6.3 Presentation of the repetitive hand pronation/supination test: the hand is rotated to full supination (left), and a hand is rotated to full pronation (right).

Toe-tapping (TT) test: Subject's feet are placed in front of the subject's body, slightly bent at the knee with the heel placed on the ground, while sitting in a straight-back chair. Each recording contains a sequence of toe-tapping movement in the duration of 15 s or for 10 repetitions. TT movement starts and ends with the complete foot on the ground (both toes and heel are placed on the ground). The subject is instructed to tap his/her toes as fast as with the largest amplitude possible, while holding the heel on the ground. One cycle of the movement is presented in Figure 6.4.

Figure 6.4 Presentation of the repetitive toe-tapping test: the foot is entirely placed on the ground (left), and the toes are lifted as high as possible while holding the heel on the ground (right).

6.2. Measurement system

A wireless inertial sensor system is used for recording the four repetitive hand and leg movements. The system comprises two IMUs, each with a 3-axial gyroscope L3G4200 (STMicroelectronics, Geneva, Switzerland) [75]. IMUs are connected to their sensor-control units (SCUs), placed on subjects' forearm during the experiment. SCUs acquire and wirelessly transmit data to a remote computer. A custom-made software, developed in LabWindows/CVI 9.0 (National Instruments, Austin, Texas, USA) controls data acquisition. The position of the IMUs depends on the performed test, and it is organized in the following way:

1) FT test: IMUs are positioned over the fingernails of the index finger and thumb. The adopted orientation of the local coordinate systems of the sensors is presented in Figure 6.1.
2) HOC test: One IMU is positioned over the fingernail of the middle finger, whereas the other IMU is mounted on the same hand, placed over the middle of the 3rd metacarpal bone. The adopted orientation of the local coordinate systems of the sensors is presented in Figure 6.2.
3) HPS test: One IMU is positioned over the fingernail of the middle finger. The adopted orientation of the local coordinate system of the sensor is presented in Figure 6.3.
4) TT test: One IMU is positioned over the footbridge. The adopted orientation of the local coordinate system of the sensor is presented in Figure 6.4.

IMUs are miniature (10x12mm) and lightweight (10 g), which allows subjects to perform the specified movements in a natural manner.

6.3. Calculation of movement amplitude

The method for calculating the amplitude of the repetitive movements is described for each movement individually in the following sections.

6.3.1. Finger-tapping test

The FT movement amplitude is defined as the aperture of the fingers during the repetitive finger-tapping. It is expressed as the angle of the relative rotation of the thumb and index finger. This movement is very complex, and although the precise instructions are provided within the clinical scale, patients may perform it with large inter-variability (rotations and translations of different finger joints) [134]. Their poor understanding of the given instructions and expressed disease symptoms can influence their ability to execute this movement correctly. Because of that, the FT movement is observed and analysed in a simplified manner: it is approximated as the scissor-like movement and observed only in terms of rotations of whole fingers (ignoring the movements of the finger joints) [134]. This approximation is in compliance with other suggested solutions in the literature [135].

6.3.1.1. The angle of the relative rotation of fingers

The approach for calculating the angle of the fingers' relative rotation is introduced and described in [134]. The gyroscope sensors positioned on the fingers provide a measure of angular velocities in 3-dimensional space with respect to their local Cartesian coordinate systems. The local x-axis of the sensors is directed along the axis of the corresponding finger, whereas the y-axis and z-

axis were directed transversally and perpendicular to the surface of the nail, respectively (as shown in Figure 6.1).

By placing the two sensors on the thumb and index finger, their local Cartesian coordinate systems are relatively rotated to one another (Figure 6.1). In order to calculate the relative movement of the fingers, it is necessary to determine the mutual position of the sensors upon their placement on the fingers. Due to that fact, the auto-calibration sequence is performed at the beginning of each recording sequence [134]. During the short auto-calibration, fingers are firmly pressed against each other while performing fast circular or zig-zag movements in 3-dimensional space. In this way, a short sequence with very small or no relative motion between the fingers is obtained. Angular velocity vectors of two sensors are equal during the auto-calibration sequence [134]:

$$\overrightarrow{\omega_1} = \overrightarrow{\omega_2} = \vec{\omega} \tag{6.1}$$

where $\overrightarrow{\omega_1}$ and $\overrightarrow{\omega_2}$ represent vectors of the angular velocity of the thumb and index finger sensors, respectively. Since the Cartesian axes of these two sensors are not parallel, components of the angular velocity differ between the two sensors [134].

The relative movement is observed from the index finger coordinate system since the index finger performed significantly larger swings than the thumb. In addition, it is shown that in such cases, signal processing is more numerically stable [134]. In order to transform components of the angular velocity of the thumb into the index finger coordinate system, a rotational matrix $[\boldsymbol{R}]$ was introduced [136]:

$$\begin{bmatrix} \omega_{2x} \\ \omega_{2y} \\ \omega_{2z} \end{bmatrix} = \begin{bmatrix} r_{11} & r_{12} & r_{13} \\ r_{21} & r_{22} & r_{23} \\ r_{31} & r_{32} & r_{33} \end{bmatrix} \begin{bmatrix} \omega_{1x} \\ \omega_{1y} \\ \omega_{1z} \end{bmatrix} \tag{6.2}$$

where $(\omega_{2x}, \omega_{2y}, \omega_{2z})$ and $(\omega_{1x}, \omega_{1y}, \omega_{1z})$ represent components of the angular rotation of the thumb and index finger sensors, respectively, whereas $r_{ij},\ i,j = 1,2,3$ represent elements of the rotational matrix $[\boldsymbol{R}]$. The matrix should be time-invariant during the calibration process. For each time step, connections between the components of $\overrightarrow{\omega_1}$ and $\overrightarrow{\omega_2}$ are described with three relations, each involving three elements of the rotational matrix $[\boldsymbol{R}]$. The goal of the auto-calibration is to estimate the elements of the rotational matrix and approximate the initial relative rotation of these two local coordinate systems. By taking the components of $\overrightarrow{\omega_1}$ and $\overrightarrow{\omega_2}$ at three different time steps, a system of three linear equations can be formed and used for computation of the matrix elements [134]. Unfortunately, there are several problems with this approach. Firstly, these equations could be ill-conditioned. Besides, the obtained matrix may not be orthonormal because of the sensor imperfections, which would require additional processing [134].

There are several alternative solutions to this problem. This method implements the procedure based on the Euler angles since it represents a more physically understandable and intuitive approach compared to quaternions [134]. Transformation of one Cartesian coordinate system to another can be performed by three subsequent rotations [136], as shown in Figure 6.5. The angles of these three rotations represent the Euler angles.

The transformation of the coordinate system $(x_1, y_{1,} z_1)$ to the other coordinated system $(x_2, y_{2,} z_2)$ starts with a counter-clockwise rotation about the z_1-axes for an angle ϕ. The resulting coordinate system is marked with (x_1', y_1', z_1'). Afterwards, the new coordinate system is rotated counterclockwise about the x_1'-axes for an angle θ, which again results with another coordinate system, later referred to as (x_1'', y_1'', z_1''). In the last rotation, the second intermediate coordinate system is rotated counterclockwise about the z_1''-axes for the angle ψ. With this final rotation, a desired coordinate system $(x_2, y_{2,} z_2)$ is obtained. Therefore, the Euler angles completely describe the rotation of the coordinate system $(x_2, y_{2,} z_2)$ with respect to the coordinate system $(x_1, y_{1,} z_1)$ [136].

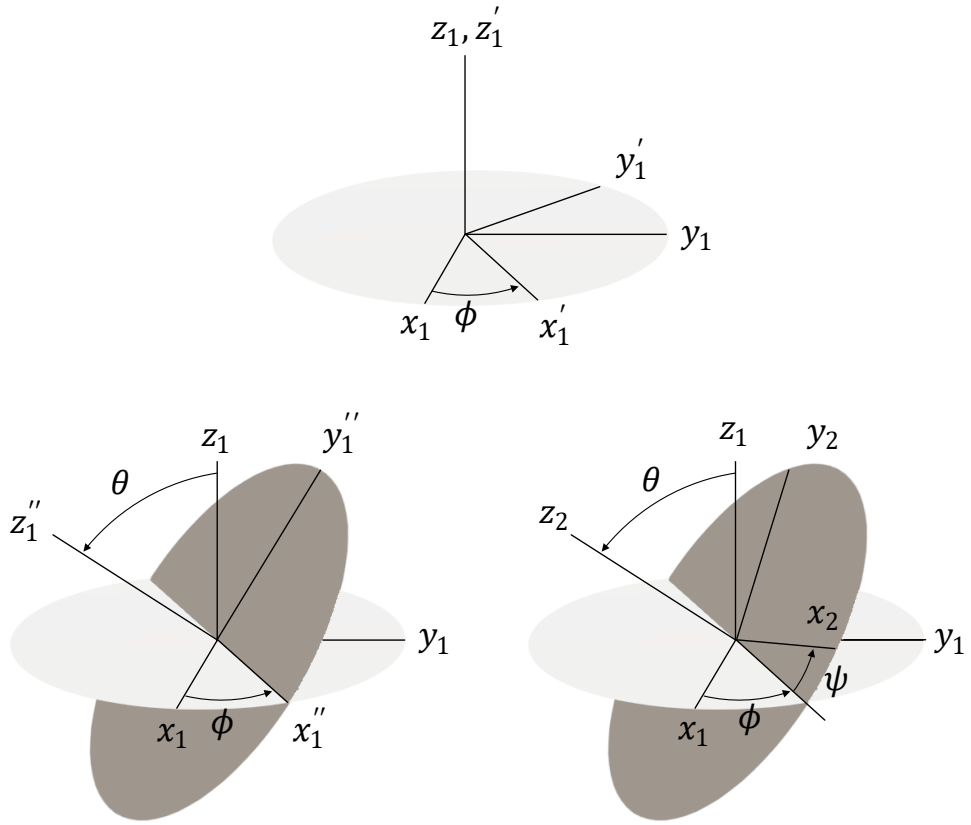

Figure 6.5 Rotations that are defining the Euler angles.

In further annotation, the matrix describing the complete transformation of the coordinate system will be marked with $[\boldsymbol{R}]$. The matrix $[\boldsymbol{R}]$ is equal to the product of three matrices, which correspond to the three rotations. The first rotation is described by [136]:

$$[\boldsymbol{x_1'}] = \left[\boldsymbol{R_\phi}\right][\boldsymbol{x_1}] \tag{6.3}$$

where $\boldsymbol{x_1'}$ and $\boldsymbol{x_1}$ represent the column matrices. Similarly, it is performed for the other two rotations [136]:

$$[\boldsymbol{x_1''}] = [\boldsymbol{R_\theta}][\boldsymbol{x_1'}] \tag{6.4}$$

and

$$[\boldsymbol{x_2}] = \left[\boldsymbol{R_\phi}\right][\boldsymbol{x_1''}] \tag{6.5}$$

The complete transformation is described with the following equation [136]:

$$[\boldsymbol{x_2}] = [\boldsymbol{R}][\boldsymbol{x_1}] = \left[\boldsymbol{R_\phi}\right][\boldsymbol{R_\theta}]\left[\boldsymbol{R_\phi}\right][\boldsymbol{x_1}] \tag{6.6}$$

The matrices $\left[\boldsymbol{R_\phi}\right]$, $[\boldsymbol{R_\theta}]$ and $\left[\boldsymbol{R_\phi}\right]$ have the form described in the Equations (6.7)-(6.9) [136]:

$$\left[\boldsymbol{R_\phi}\right] = \begin{bmatrix} \cos\phi & \sin\phi & 0 \\ -\sin\phi & \cos\phi & 0 \\ 0 & 0 & 1 \end{bmatrix} \tag{6.7}$$

$$[\boldsymbol{R_\theta}] = \begin{bmatrix} 1 & 0 & 0 \\ 0 & \cos\theta & \sin\theta \\ 0 & -\sin\theta & \cos\theta \end{bmatrix} \tag{6.8}$$

$$\left[\boldsymbol{R_\psi}\right] = \begin{bmatrix} \cos\psi & \sin\psi & 0 \\ -\sin\psi & \cos\psi & 0 \\ 0 & 0 & 1 \end{bmatrix} \tag{6.9}$$

Based on the Equations (6.7)-(6.9), the complete transformation matrix equal to [136]:

$$[\boldsymbol{R}] = \begin{bmatrix} \cos\psi\cos\phi - \cos\theta\sin\psi\sin\phi & \cos\psi\sin\psi + \cos\theta\cos\psi\sin\phi & \sin\psi\sin\theta \\ -\sin\phi\cos\phi - \cos\theta\sin\psi\cos\phi & -\sin\psi\sin\psi + \cos\theta\cos\psi\cos\psi & \cos\psi\sin\theta \\ \sin\theta\sin\phi & -\sin\theta\cos\psi & \cos\theta \end{bmatrix} \tag{6.10}$$

This matrix is automatically orthonormal. In order to calculate angles ϕ, θ, and ψ, based on the Equations (6.2) and (6.10), an optimization function is obtained [134]:

$$\begin{aligned} f(\phi,\theta,\psi) = {} & \left(\omega_{2x} - (r_{11}\omega_{1x} + r_{12}\omega_{1y} + r_{13}\omega_{1z})\right)^2 \\ & + \left(\omega_{2y} - (r_{21}\omega_{1x} + r_{22}\omega_{1y} + r_{23}\omega_{1z})\right)^2 \\ & + \left(\omega_{2z} - (r_{31}\omega_{1x} + r_{32}\omega_{1y} + r_{33}\omega_{1z})\right)^2 \end{aligned} \tag{6.11}$$

This function is minimized using an algorithm that implements the Nelder-Mead simplex (direct search) method [137]. In this way, the estimation of the angles ϕ, θ, and ψ is performed and afterwards, the initial rotational matrix is calculated.

As already mentioned, each trial begins with the auto-calibration sequence, which is recorded prior to the finger-tapping sequence. Therefore, the initial rotational matrix is calculated for each recording individually and then applied for the finger-tapping sequence, which is captured immediately after the auto-calibration sequence.

The relative rotation of the thumb with respect to the index finger is calculated as [134]:

$$\overrightarrow{\omega_r} = \overrightarrow{\omega_1} - \overrightarrow{\omega_2} \tag{6.12}$$

By observing the Equations (6.2) and (6.12), the relative rotation $\overrightarrow{\omega_r}$ is given as [134]:

$$\begin{bmatrix} \omega_{rx} \\ \omega_{ry} \\ \omega_{rz} \end{bmatrix} = \begin{bmatrix} r_{11} & r_{12} & r_{13} \\ r_{21} & r_{22} & r_{23} \\ r_{31} & r_{32} & r_{33} \end{bmatrix} \begin{bmatrix} \omega_{1x} \\ \omega_{1y} \\ \omega_{1z} \end{bmatrix} - \begin{bmatrix} \omega_{2x} \\ \omega_{2y} \\ \omega_{2z} \end{bmatrix} \tag{6.13}$$

Since, two local coordinate systems additionally rotate relative one to another during the FT movement, the rotational matrix $[\boldsymbol{R}]$ is updated for each time step, as follows [134]:

$$[\boldsymbol{R_n}] = \begin{bmatrix} \cos\Delta\phi & -\sin\Delta\phi & 0 \\ \sin\Delta\phi & \cos\Delta\phi & 0 \\ 0 & 0 & 1 \end{bmatrix} \begin{bmatrix} \cos\Delta\theta & 0 & \sin\Delta\theta \\ 0 & 1 & 0 \\ -\sin\Delta\theta & 0 & \cos\Delta\theta \end{bmatrix} \begin{bmatrix} 1 & 0 & 0 \\ 0 & \cos\Delta\psi & -\sin\Delta\psi \\ 0 & \sin\Delta\psi & \cos\Delta\psi \end{bmatrix} [\boldsymbol{R_{n-1}}] \quad (6.14)$$

where $[\boldsymbol{R_{n-1}}]$ represents the rotational matrix at the previous time step, and $\Delta\phi = \omega_{rx}\Delta t$, $\Delta\theta = \omega_{ry}\Delta t$ and $\Delta\psi=\omega_{rz}\Delta t$ represent the instantaneous rotations about the three axes of the index finger coordinate system. As shown in the Equation (6.14), relative rotation of the fingers is described with the rotations about three axes of the index finger coordinate system. However, in order to provide a simpler and more understandable representation, the FT amplitude is defined as the most dominant rotation of the relative motion of the fingers ω_{rd} [134]. For most cases, it is expected that the dominant rotation is about the y_2 axis of the index finger coordinate system. Otherwise, the coordinate system is rotated, so the dominant rotation is about a new y_2 axis. The angle of the relative rotation α is calculated by integrating the dominant component of the relative angular velocity ω_{rd} in a time-stepping procedure [134].

In some cases, the drift caused by integration is too big, which requires the approximation of the angle using some other approach. In the literature, it is shown that the elements in the second row of the matrix $[\boldsymbol{R}]$ remain almost constant for all time steps [134]. Hence, in order to find the relative rotation of the fingers, it is enough to use the initial rotation matrix and to project the $\overrightarrow{\omega_1}$ on the y_2 axis:

$$\omega_{rd} \approx r_{21}\omega_{1x} + r_{22}\omega_{1y} + r_{23}\omega_{1z} \quad (6.15)$$

Once again, the angle of the relative rotation α is calculated by integrating the angular velocity ω_{rd} in a time-stepping procedure. This method implements the second approach for the cases where drift exceeds the value of 40 degrees.

By integrating the dominant component of the angular velocity ω_{rd}, a drift occurs regardless of the approach that is used for calculating the relative rotation of the fingers. The procedure for drift removal is described in the next section.

6.3.1.2. Segmentation of movements to individual cycles

In order to remove the drift from the calculated angle sequence, it is necessary to detect moments when fingers are closed, i.e., when the angle between fingers equals to "zero." Because of that, the segmentation of the finger-tapping movement is performed.

One finger-tapping cycle (or tap) consists of two phases: fingers opening and fingers closing. During the opening phase, fingers are moving away from each other. This phase ends when fingers form the highest aperture for that cycle. Afterwards, the closing phase begins, and the fingers are moving towards each other. The closing phase ends with fingers closed in a "zero posture."

Ideally, the dominant component of the relative angular velocity ω_{rd} of the finger-tapping movement would look like a periodic sine wave. The ω_{rd} signal passes through a "zero" value two times per each cycle: when fingers are closed in a "zero posture," and when fingers briefly stop after

forming the highest aperture, so they could start moving in the opposite direction. Based on the adopted orientation of the index-finger coordinate system (as shown in Figure 6.1), the peaks correspond to maximum closing angular velocity, whereas the signal valleys represent the maximum angular velocity during the opening phase. In an ideal movement, fingers are opening and closing with the same angular velocity, and the movement is smooth. However, the real finger-tapping movement is different.

An example of the dominant component of the relative angular velocity ω_{rd} (with marked finger-tapping phases) is presented in Figure 6.6. As shown, the maximum opening and closing angular velocities may differ. The rising edge of the signal is smooth, and there are no setbacks around zero, which means that fingers smoothly pass from the opening to the closing phase after achieving the maximum aperture for that cycle. On the other hand, during the closing phase, there is a short period when the signal stays around the "zero" value or stays in the "zero posture" (marked with a red ellipse in Figure 6.6). During that short period, fingers are closed, and they may slightly slip over one another. This effect is more visible for faster movements when subjects tap their fingers very fast and make a significant impact when closing. Although this movement pattern may be altered to some smaller or larger extent from subject to subject (slower and less smooth movements, longer or shorter "zero posture" segments, and others), this division into phases is maintained for all people.

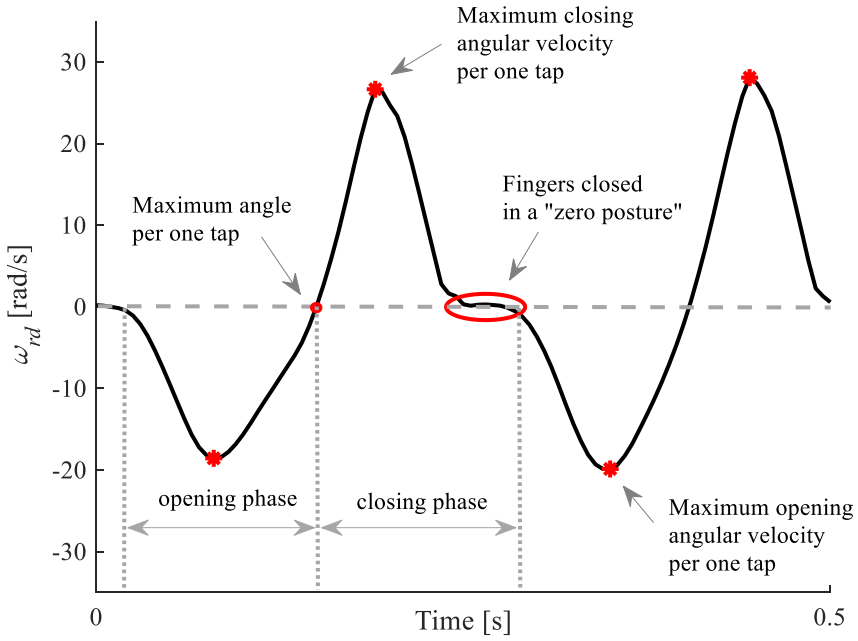

Figure 6.6 Presentation of the short ω_{rd} sequence describing the finger-tapping movement, with marked movement phases. Samples corresponding to maximum closing and opening angular velocities (per one tap) are labelled with red stars. The red dot marks a moment when fingers achieve maximum angle or aperture during one tapping cycle, and red ellipse shows a short period during one cycle when fingers are closed in a "zero posture."

In order to provide automatized segmentation of signals, the observed signal is smoothed using a moving average filter with an adaptive span [138]. The span is calculated as $(f_s/f_0)/2$, where f_s represented the sampling frequency, and f_0 frequency is the basic tapping frequency extracted from the frequency spectrum. In this way, every signal is smoothed based on its intrinsic properties. The smoothed angular velocity is then normalized with respect to its maximum value and later referred to as $\omega_{rd-smooth-N}$ (an example is shown in Figure 6.7). Two thresholds are applied to the normalized

filtered signal, valued at 0.1 and -0.1, respectively. All samples valued above 0.1 are declared as the areas where signal peaks should be located. A local maximum within one interconnected area is extracted from the original signal. The time marker indicating the maximum closing angular velocity (per one tap) is defined as the index of the sample at which this local maximum value is detected (red circles in Figure 6.7). The procedure is repeated for all interconnected areas.

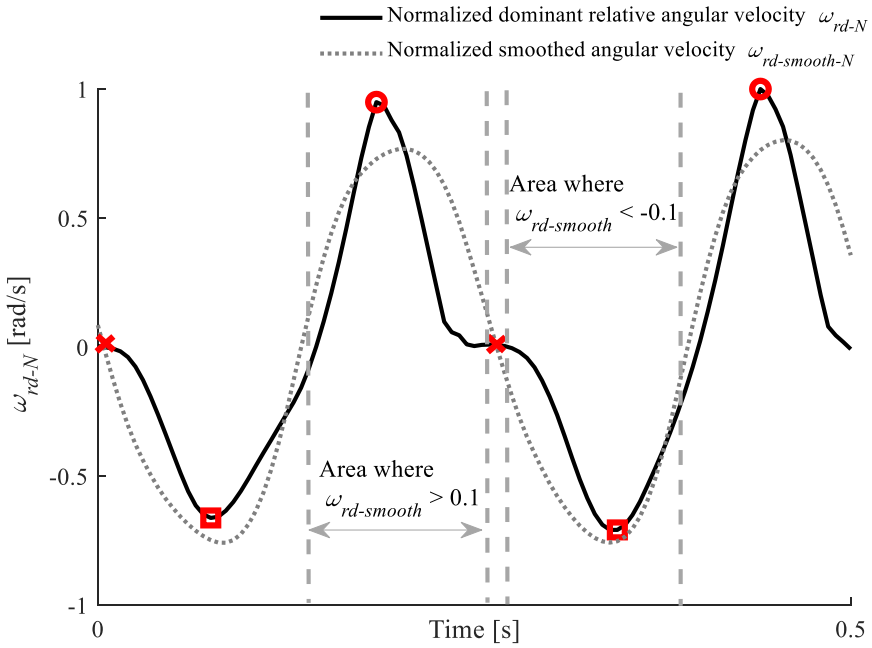

Figure 6.7 Detection of markers indicating the maximum opening and closing angular velocity and "zero posture" moments per one tap. The dominant component of the relative angular velocity ω_{rd} is normalized for the sake of the presentation and shown with a solid black line. The normalized smoothed angular velocity $\omega_{rd-smooth-N}$ is represented with dark grey dashed line. Light grey dashed vertical lines mark areas where smoothed angular velocity takes values below -0.1 or above 0.1 value. Red circles and squares mark moments where angular velocity achieves its maximum value during the closing and opening phase, respectively. Red crosses represent "zero posture" markers.

Time markers representing the maximum closing angular velocity (per one tap) are extracted using the same procedure, by finding a local minimum within each interconnected area where the normalized smoothed angular velocity $\omega_{rd-smooth-N}$ is below the -0.1 threshold (red squares in Figure 6.7). "Zero posture" markers (indicating moments when fingers are closed) are extracted using the maximum closing and opening angular velocity time markers. They are defined in the samples at which the normalized smoothed angular velocity $\omega_{rd-smooth-N}$ passes through a "zero" value for the first time between each two succeeding maximum closing and opening angular velocity time markers (red crosses in Figure 6.7). The sequence of extracted "zero posture" time markers is complemented with two samples representing the beginning and end of the movement sequence.

Time markers representing "zero posture" moments are applied for the drift removal. Polynomial approximation of the third order is fitted through the obtained time markers and subtracted from the drifted angle sequence.

6.3.2. Hand opening/closing test

The HOC movement amplitude is defined as the aperture of the hand during the repetitive hand opening-closing. It is expressed as the angle of the relative rotation of the fingers and palm. This movement is even more complex than the FT movement. Hand opening-closing requires movement of all fingers, including rotations and translation of different joints. Besides, fingers may open and close inconsistently. Because of that, the following simplification of the movement is performed: all fingers are moving together and in the same manner, and HOC movements are observed only in terms of rotations of palm and whole fingers (ignoring the movements of the finger joints).

6.3.2.1. The angle of the relative rotation of fingers and palm

The same procedure for calculating the relative motion of the sensors is applied, as in the case of the FT test. The relative motion is observed from the middle-finger coordinate system since fingers perform much larger swings than a palm.

The initial relative position of the sensors (upon their placement) is determined using the auto-calibration sequence, which is recorded at the beginning of each HOC trial. The calculations are the same as for the FT test. The relative angular velocity of the palm with respect to the middle finger is observed:

$$\overrightarrow{\omega_r} = \overrightarrow{\omega_1} - \overrightarrow{\omega_2} \tag{6.16}$$

where $\overrightarrow{\omega_1}$ and $\overrightarrow{\omega_2}$ represent the angular velocity vectors of the palm and middle-finger sensor, respectively. The dominant component of the relative angular velocity ω_{rd} is automatically detected about the y_2 axis of the index-finger coordinate system and used for further analysis. By integrating the ω_{rd}, the angle between the hand and the finger α is obtained.

6.3.2.2. Segmentation of movements to individual cycles

One hand opening-closing cycle consists of two phases: hand opening and hand closing. The cycle starts with the hand closed in a fist (or a "zero posture"). Afterwards, the hand opening phase starts – the palm and fingers are moving away from each other. Although fingers perform significantly larger swing than a palm, there can be some small backward movement of the palm. The opening phase ends with an outstretched hand forming the highest aperture for that cycle. Afterwards, the closing phase begins – palm and fingers are moving towards each other. The closing phase ends with the hand closed in a fist or "zero posture."

The dominant component of the relative angular velocity ω_{rd} of the ideal hand opening-closing movement would look like a periodic sine wave. The ω_{rd} signal passes through a "zero" value two times per each cycle: when the hand is closed in "zero posture" and when hand briefly stops after forming the highest aperture, so it could start moving in the opposite direction. Based on the adopted orientation of the middle-finger coordinate system (as shown in Figure 6.2), the peaks correspond to maximum angular velocity during the closing phase, whereas the signal valleys represent the maximum opening angular velocity. In an ideal movement, the hand is opening and closing with the same angular velocity, and the movement is smooth. However, the real hand opening-closing movement is different.

An example of the dominant component of the relative angular velocity ω_{rd} with marked movement phases is presented in Figure 6.8. The signal has a similar shape with the signal representing the finger-tapping movement. The maximum opening and closing angular velocities may differ. In the presented case, the rate of change of the angle is larger for the opening phase than for the closing phase. The rising edge of the signal is smooth, and there are no setbacks around zero, which means that hand smoothly passes from the opening to the closing phase after achieving the maximum aperture for that cycle. In contrast, during the closing phase, there is a short period when the signal stays around the "zero" value or stays in the "zero posture" (marked with a red ellipse in Figure 6.8). During that short period, the hand is closed in a fist. This effect is even more expressed than in the case of the finger-tapping movement and more prominent for faster movements, when subjects open and close their hand very fast and make a significant impact when closing. Although this movement pattern may be altered to some smaller or larger extent from subject to subject (slower and less smooth movements, longer or shorter "zero posture" segments, and others), this division into phases is maintained for all people.

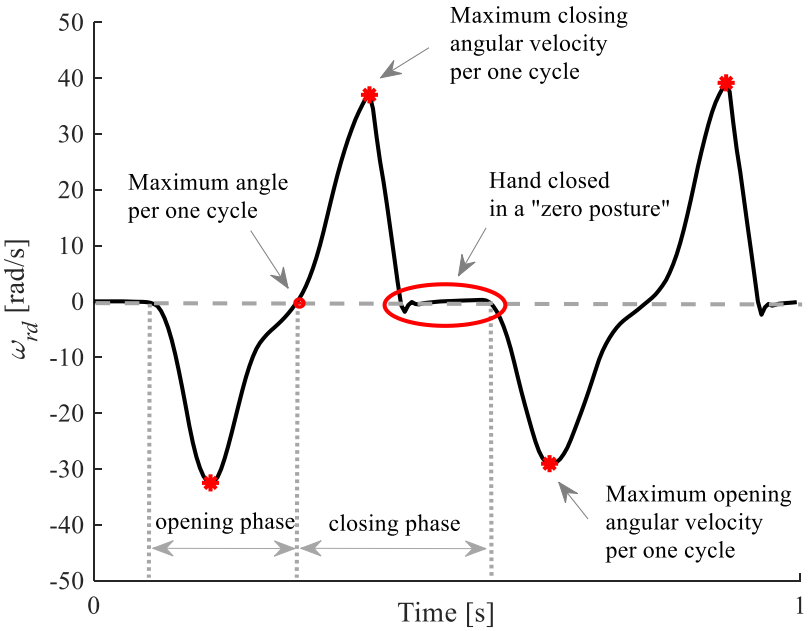

Figure 6.8 Presentation of the short ω_{rd} sequence describing the hand opening-closing movement, with marked movement phases. Samples corresponding to maximum closing and opening angular velocities (per one cycle) are labelled with red stars. The red dot marks a moment when hand achieves maximum angle or aperture during one cycle, and red ellipse shows a period during one cycle when the hand is closed in a "zero posture."

Segmentation is performed in the same manner as for the finger-tapping movement [138]: firstly, the signal is smoothed using a span calculated based on the subject's opening/closing frequency. Afterwards, areas with signal peak and valleys are detected. Based on the adopted orientation, these peaks and valleys correspond to maximum closing and opening angular velocities (per individual cycles), respectively, and the samples at which they are located are extracted as their markers. These markers are then used for finding the moments in which hand is closed in "zero posture." These moments are then saved as time markers for movement segmentation or drift removal. The third-order polynomial fit is calculated through the extracted markers and removed from the drifted angle sequence.

6.3.3. Hand pronation/supination test

The amplitude of the HPS movement is defined as the angle of rotation during the consecutive hand pronation and supination movements. It is expressed as the angle of the dominant rotation of the hand.

6.3.3.1. The angle of the hand rotation

The dominant component of the angular velocity ω_{1d} is automatically detected from the obtained vector of the angular velocity $\overrightarrow{\omega_1}$ and used for further analysis. The dominant axis is about the z_1 axis of the middle-finger sensor. The selected ω_{1d} is integrated for calculating the angle of the hand rotation α.

6.3.3.2. Segmentation of movements to individual cycles

One hand pronation-supination cycle consists of two phases: hand pronation and hand supination. The cycle starts with the hand rotated in full supination. Afterwards, the hand pronation phase starts – the hand is rotating around the axis oriented along the hand. The pronation phase ends with the hand rotated at the highest possible pronation. Afterwards, the supination phase begins and ends with hand rotated at full supination.

The dominant component of the hand angular velocity ω_{1d} of the ideal hand pronation-supination movement would look like a periodic sine wave. The ω_{1d} signal passes through a "zero" value two times per each cycle: when the hand is rotated at full supination and when the hand is rotated at full pronation. Based on the adopted orientation of the middle-finger coordinate system (as shown in Figure 6.3), the peaks and valleys correspond to maximum angular velocity during the supination and pronation phases, respectively. In an ideal movement, the hand is rotating with the same angular velocity in both directions, and the movement is smooth. However, the real repetitive hand pronation-supination movement is different.

An example of the dominant component of the hand angular velocity ω_{1d} with marked movement phases is presented in Figure 6.9. The maximum angular velocities (marked with red star markers in Figure 6.9) may differ while rotating in two opposite directions. When hand stops with rotating at full supination or pronation, the hand may pause briefly and even perform a slight shake due to its inability to perform instant and smooth change of movement direction (shown with red circles in Figure 6.9). Although this movement pattern may be altered to a smaller or larger extent from subject to subject (slower and less smooth movements, longer or shorter stops while changing the direction of the movements, and others), this division into phases is maintained for all people.

Segmentation is performed in the same manner as for the previous movements [138]: firstly, the signal is smoothed using a span calculated based on the subject's pronation/supination frequency. Afterwards, areas with signal peak and valleys are detected. These peaks and valleys correspond to maximum angular velocities during supination and pronation (per individual cycles), respectively, and the samples at which they are located represent their markers. These markers are then used for finding the moments when the hand is rotated in full supination, which represents the beginning point of each HPS movement cycle. These moments are then saved as the time markers for movement

segmentation and drift removal. The third-order polynomial fit was calculated through the extracted markers and removed from the drifted angle sequence.

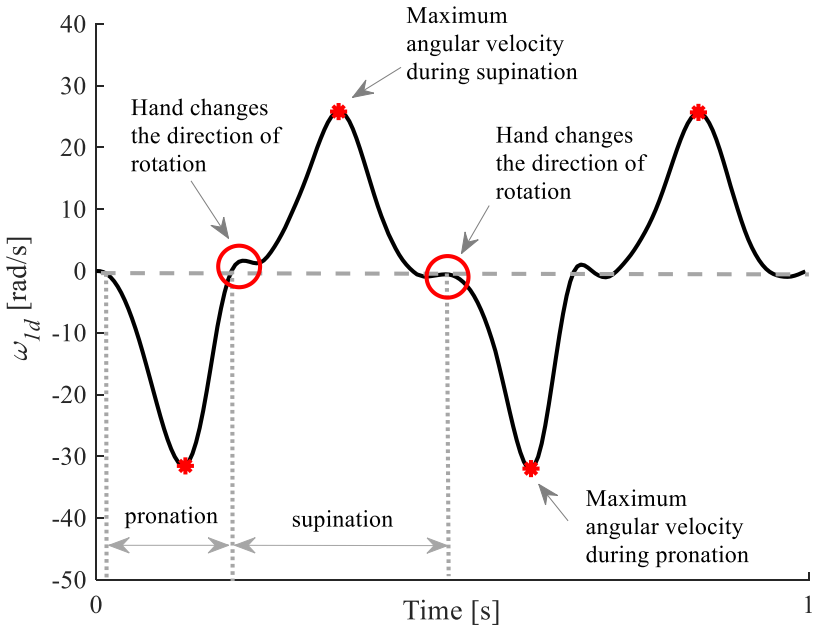

Figure 6.9 Presentation of the short ω_{1d} sequence describing the hand pronation-supination movement, with marked movement phases. Samples corresponding to maximum pronation and supination angular velocities (per one cycle) are labelled with red stars. Red circles mark moments when the hand achieves maximum rotation in one direction.

6.3.4. Toe-tapping test

The TT movement amplitude is defined as the angle that foot forms with the ground while holding the heel on the ground and tapping the toes. It is expressed as the angle of the dominant rotation of the foot.

6.3.4.1. The angle of the foot rotation

The dominant component of the angular velocity ω_{1d} is automatically detected from the obtained vector of the angular velocity $\overrightarrow{\omega_1}$ and used for further analysis. The dominant axis is about the y_1 axis of the foot sensor. The selected ω_{1d} is integrated for calculating the toe-tapping angle α.

6.3.4.2. Segmentation of movements to individual cycles

One toe-tapping cycle (or tap) consists of two phases: toe lifting and toe lowering. The cycle starts with the foot placed entirely on the ground. Afterwards, the toe lifting phases begins – the toes are lifted as high as possible while maintaining the heel on the ground. This phase ends with the toes lifted as high as possible, forming the highest angle with the ground. Afterwards, the toe lowering phase begins and ends when the foot makes full contact with the ground.

The dominant component of the foot angular velocity ω_{1d} of the ideal toe-tapping movement would look like a periodic sine wave. The ω_{1d} signal passes through a "zero" value two times per each tapping cycle: when toes are lifted as high as possible and when the foot makes full contact with the ground. Based on the adopted orientation of the foot coordinate system (as shown in Figure 6.4),

the peaks and valleys correspond to maximum angular velocity during the toe lowering and lifting phases, respectively. In an ideal movement, toes are tapped with the same angular velocity during both cycles, and the movement is smooth. However, the real repetitive toe-tapping movement is different.

An example of the dominant component of the relative angular velocity ω_{1d} with marked movement phases is presented in Figure 6.10. The maximum angular velocities while toe lifting and lowering phases (marked with red star markers in Figure 6.10) may differ. The foot smoothly changes the movement direction (shown with red dots in Figure 6.10). Although this shape may be altered to some smaller or larger extent from subject to subject (slower and less smooth movements, visible stop while the foot is in the full contact with the ground, and others), this division into phases is maintained for all people.

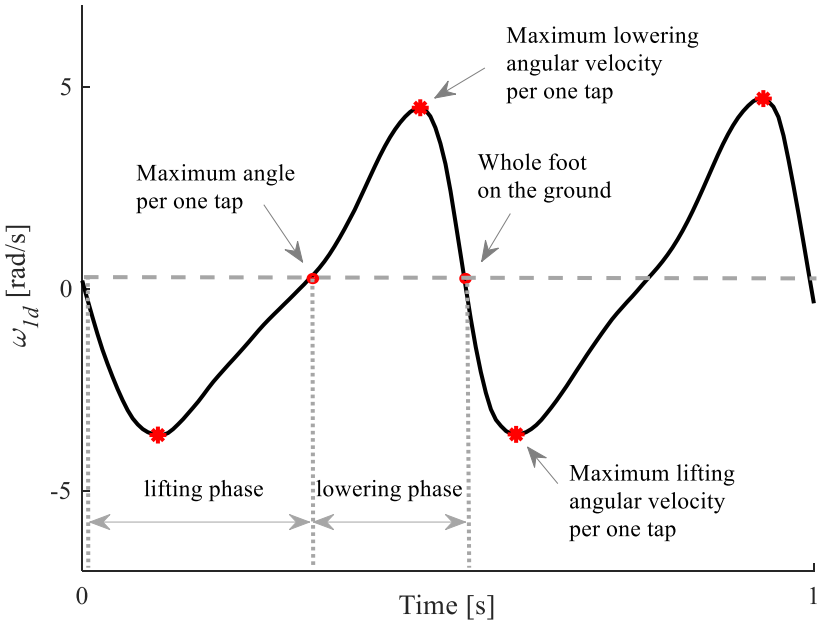

Figure 6.10 Presentation of the short ω_{1d} sequence describing the toe-tapping movement, with marked movement phases. Samples corresponding to maximum toe lowering and lifting angular velocities (per one cycle) are labelled with red stars. The red dots mark moments when foot achieves maximum angle during one cycle or when the whole foot is on the ground.

Segmentation is performed in the same manner as for the previous movements [138]. Firstly, the signal is smoothed using a span calculated based on the subject's toe-tapping frequency. Afterwards, areas with signal peaks and valleys are detected. These peaks and valleys correspond to maximum angular velocities while the foot is lowering to the ground or lifting to the air (per individual cycles), respectively, and the samples at which they are located are extracted as their markers. These markers are then used for finding the moments when the foot is entirely placed on the ground, which represents the beginning point of each TT movement cycle. These moments are then saved as the time markers for movement segmentation and drift removal. The third-order polynomial fit was calculated through the extracted markers and removed from the drifted angle sequence.

6.4. Demonstration of the method on the example of one subject

6.4.1. Method

6.4.1.1. Experiment

The method for measuring and calculating the amplitude of the repetitive hand and leg movements is demonstrated on the example of one healthy subject (Gender: Female, Age: 24). By following the previously introduced experimental setup and protocol, four repetitive movements were recorded: finger tapping, hand opening/closing, hand pronation/supination, and toe-tapping. In addition to regular movements (performed as fast as possible and with the biggest amplitude possible), the participant was requested to simulate different bradykinesia related motion characteristics that could be seen in patients with PD and related disorders. The simulation scenarios included: 1) performing as fast as possible and with the biggest amplitude possible (which corresponded to normal movement), 2) performing with smaller amplitudes and/or speed; 3) performing with decrementing amplitude; 4) performing with occasional hesitations and/or freezes.

The participant was introduced to the simulation scenarios and practiced the endangered movements a few times before the recording. The tasks were performed in duration of 15 s to obtain longer movement sequences for analysis. Four trials were recorded for each hand and each movement. Few minutes of rest were given between the consecutive trials.

6.4.1.2. Instrumentation

The movements were recorded using the previously described wireless inertial sensor system. In addition, the OptiTrack motion capture system (MOCAP) with passive markers (NaturalPoint, Inc., Planar Systems, Beaverton, Oregon, USA) was used as the reference system. This system can track motions in a 3-dimensional space with a high precision, which makes it suitable for providing benchmark data.

The applied configuration consisted of five Prime x22 cameras (distance resolution: ±0.15mm). Marker clusters comprising three markers were designed and positioned over the IMUs. The local coordinate systems of two recording systems were aligned by placing sensors. The used marker clusters were small (bounding box around the marker clusters was 4x6 cm) and lightweight (3-4g), so they did not disturb the subject's performance. The MOCAP system provided the measure of movement amplitude, which was expressed as the rotations of the local coordinate system about the corresponding axes of the adopted global coordinate system (the laboratory). The rotations were described with Euler angles. The obtained measurements were used for comparison with the results of the presented method for calculation of the movement amplitude.

The testing was performed during one day in the Laboratory for eHealth and Biomedical Engineering of the Innovation Center, School of Electrical Engineering in Belgrade, following the ethical standards of the Declaration of Helsinki. The subject provided written informed consent prior to participation in the experiment.

6.4.1.3. Data processing

The inertial sensor and MOCAP system recorded data with a sampling frequency $f_s = 200$ Hz. Calibrated data was then processed in Matlab 9.6 R2019a (MathWorks, Natick, Massachusetts, USA).

6.4.1.3.1. Comparison of two systems

The amplitude of four repetitive movements was calculated based on the gyroscope measurements recorded with the inertial sensor system, using the previously described procedure. The calculated movement amplitude was marked as α. In the case of the MOCAP system, the dominant rotation was found for each movement. The angle of the dominant rotation was used for further processing (later referred to as α_{MOCAP}).

Two systems were synchronized using the cross-correlation function. The lag with the maximum cross-correlation was found and used for shifting the two angle sequences. The similarity of the two angle sequences was measured with the root-mean-square error (RMSE):

$$RMSE = \sqrt{\sum_{n=1}^{N} \frac{(\alpha - \alpha_{MOCAP})^2}{N}} \tag{6.17}$$

where N represents the length of the observed angle sequences.

6.4.2. Results

The examples of the recorded angle sequences describing the amplitude of repetitive movements are presented in Figures 6.11-6.14. The results are presented for both sensor systems and for all four movements.

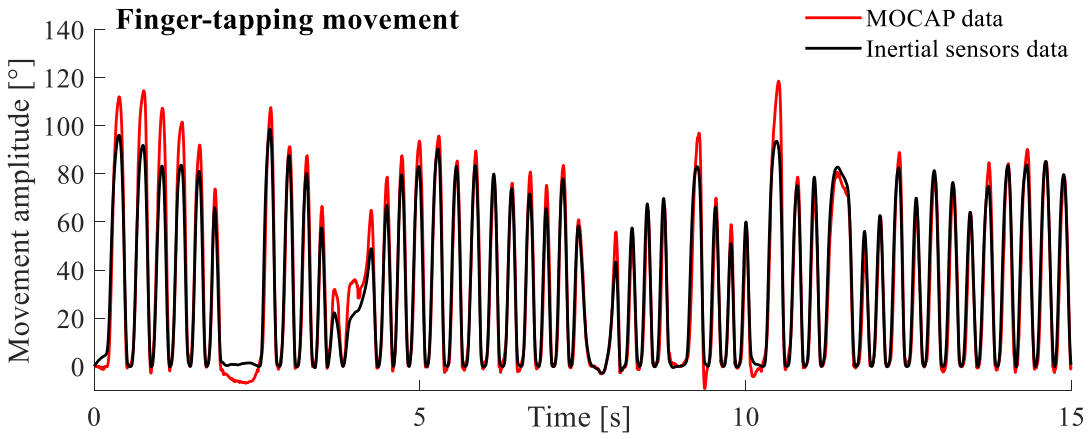

Figure 6.11 An example of the finger-tapping movement amplitude calculated using the inertial sensor system (marked with a black line) and the MOCAP system (marked with a red line).

The example in Figure 6.11 shows a fast finger-tapping movement with changeable tapping amplitude and speed, with occasional “breaks” in the rhythmic performance.

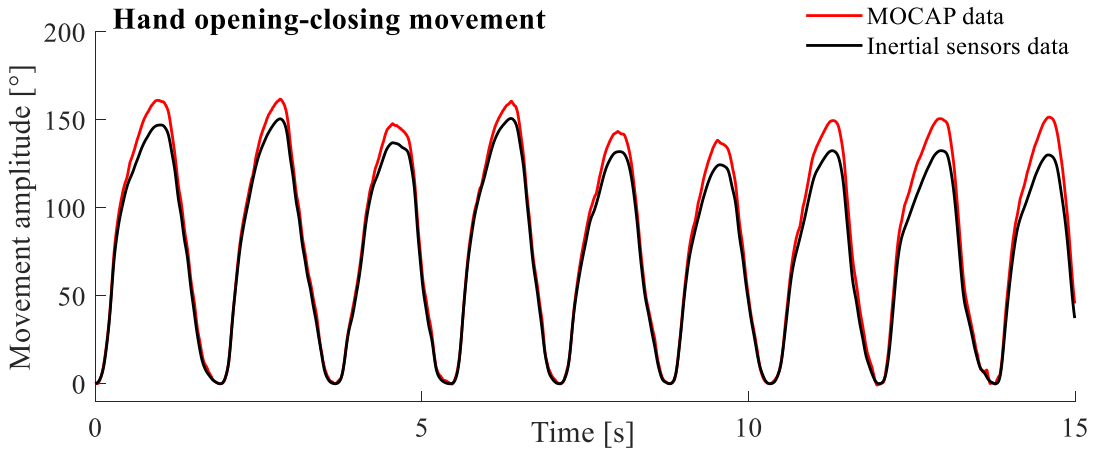

Figure 6.12 An example of the hand opening-closing movement amplitude calculated using the inertial sensor system (marked with a black line) and the MOCAP system (marked with a red line).

A hand opening-closing movement presented in Figure 6.12 is characterized by slow rhythm and high amplitude, with a slight decrease over time.

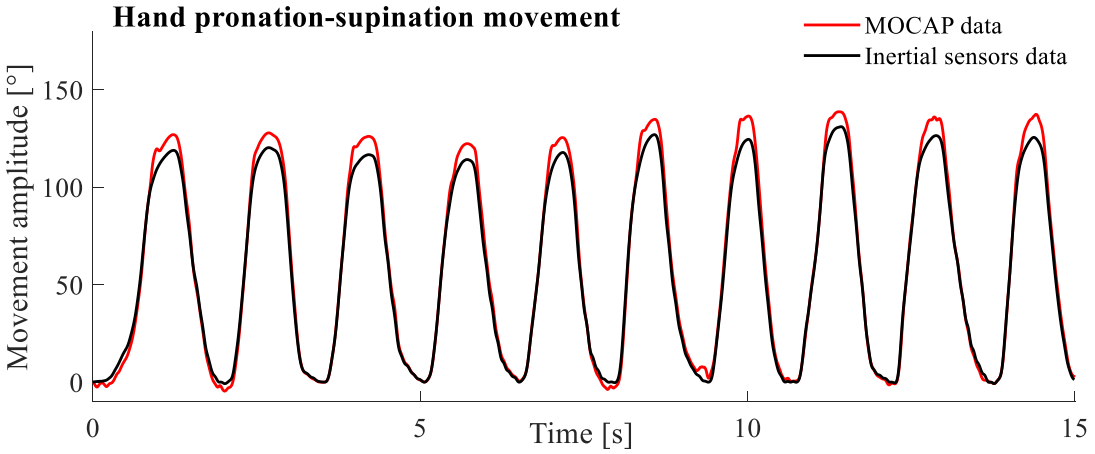

Figure 6.13 The example of the hand pronation-supination movement amplitude calculated using the inertial sensor system (marked with a black line) and the MOCAP system (marked with a red line).

The hand pronation-supination movement presented in Figure 6.13 is characterized by lower speed and high and uniform amplitude.

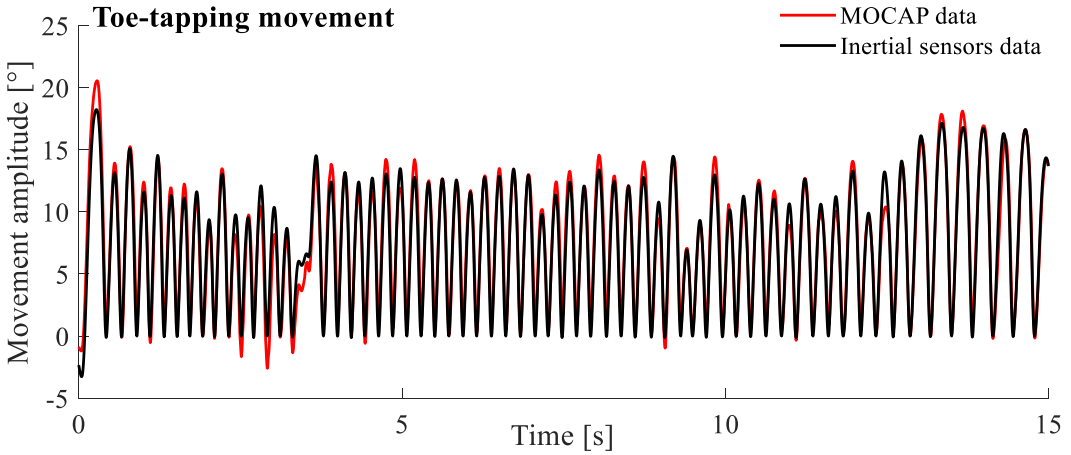

Figure 6.14 An example of the foot-tapping amplitude calculated using the inertial sensor system (marked with a black line) and the MOCAP system (marked with a red line).

The example in Figure 6.14 shows a fast toe-tapping movement with a changeable amplitude and constant tapping speed, with one "break" in the rhythmic performance around the 4th second.

The average RMSE was 4.87º, for all four movements and all recording conditions. The difference between the obtained results originated from the inability to align local coordinate systems of two measurement systems perfectly.

6.5. Discussion

This Chapter presents an objective and automatic method for capturing and calculating the amplitude of the bradykinesia-related repetitive hand and leg movements. The method utilizes a miniature and lightweight inertial sensor system for recording movements, which does not require a lot of time nor skills to be mounted on the patient's hand or leg. The established measurement procedure is simple, easy to apply, and it follows the rules of the standardized clinical testing protocols. The method also comprises an algorithm for calculating the movement amplitude for each movement individually. The algorithm was previously defined and validated for the finger-tapping movement solely [134]. In this thesis, it is extended to other bradykinesia movements as well (hand opening-closing, hand pronation-supination, and toe-tapping). Furthermore, a new algorithm for the segmentation of movements to individual cycles is also presented, together with the detailed inspection and understanding of the observed movement patterns.

The applicability of the proposed method was demonstrated on the example of one healthy subject. The participant performed all four movements following the designed measurement procedure. In addition to the normal performance (repeating the movements fast with the biggest amplitude), the subject imitated movement properties, which are characterizing the presence of bradykinesia in patients with neurodegenerative disorders. The results of the proposed method were compared with the reference data provided by the motion capture system. The systems showed high agreement, with an average root mean square error of $RMSE = 4.87º$, confirming the high applicability of the proposed method. The introduced method represents the basis for further and more detailed analysis of these movements, which will be discussed in the next Chapter.

7. Evaluation of bradykinesia severity based on new metrics and an expert system

As already mentioned, the severity of the bradykinesia symptom is assessed using the repetitive hand or leg motor tests. A patient's performance is visually observed and evaluated with a score from 0 to 4. The UPDRS evaluation criteria includes specifications on how patients should perform the movement, characteristics of the movements which should be observed, and decision rules defining how scores should be given. This information was determined by the experts in movement disorders and carefully selected for providing full insight into the development of the patient's symptom and disease progression. In the case of bradykinesia related repetitive movements, finger-tapping, hand opening-closing, hand pronation-supination, and toe-tapping, the movements are evaluated in terms of the amplitude, amplitude decrement, speed, and number of hesitations and freezes that may appear during the performance. The score is given based on the patient's ability to perform these repetitive movements as fast and as widely as possible, in which part of the movement sequence its amplitude starts to drop, and how many hesitations and freezes patients experience during the performance. The lowest scores are given for normal movements, whereas the higher values represent severe bradykinesia. Although the instructions given in the UPDRS clinical scale defined the scoring process, the evaluation outcome is severely depended on the examiner's experience and knowledge.

In order to provide an objective and detailed assessment of the bradykinesia symptom, a new method for evaluation of bradykinesia is presented in this Chapter [138]. The method for calculating the amplitude of these repetitive movements is defined and presented in Chapter 6. The method observes and focuses on crucial biomechanical movement properties, which can provide significant insight into patients' state and severity of developed symptoms. New metrics for quantification of movement characteristics were obtained as a result of the conducted analysis. The developed parametrization was then used as the input to the expert system, which is implemented as a knowledge-based decision support tool for prediction of scores and evaluation of the bradykinesia severity in patients with parkinsonism. Expert system was designed to match the standardized clinical knowledge and evaluation criteria.

The developed metrics and expert system were validated on the example of the finger-tapping movement that was recorded for several groups of subjects, including patients with different neurodegenerative diseases.

7.1. Method

7.1.1. Experiment

In this study, fifty-six subjects were included, including 13 patients (Gender: 7 male/6 female; Age: 62.23±10.79 years) with idiopathic PD, 17 patients (Gender: 5 male/12 female; Age: 58.41±6.41 years) with MSA, 14 patients (Gender: 11 male/3 female; Age: 65.71±9.33 years) with PSP, and 12 HC controls (Gender: 4 male/8 female; Age: 58.40±7.78 years). The patients were recruited at the Clinic of Neurology, Clinical Centre of Serbia, School of Medicine, University of Belgrade, Belgrade, Serbia. Healthy controls were enlisted among healthy staff members or persons accompanying the patients at the Clinic of Neurology.

Descriptive statistics of clinical data for the included patient groups are provided in Table 7.1. The signs of parkinsonism were assessed using the UPDRS scale [42], whereas the severity of the disease was evaluated using the H&Y scores [35].

Table 7.1 Clinical features presented through descriptive statistics (average±std, median), for each included patient group separately.

Data	Statistics	Group		
		PD	**MSA**	**PSP**
Age (years)	Average±std	62.23±10.79	58.41±6.41	65.71±9.33
	Median	61	58	66.5
H&Y	Average±std	1.80±0.79	3.18±0.75	3.45±0.93
	Median	2	3	4
UPDRS Total	Average±std	42.60±16.93	77.73±13.70	74.45±20.08
	Median	36	79	79
UPDRS III	Average±std	24.60±9.07	46.64±9.08	42.91±13.14
	Median	19.5	45	45

PD – Parkinson's disease patients; MSA – Multiple system atrophy patients; PSP – Progressive supranuclear palsy patients; HC – Healthy controls; H&Y – Hoehn and Yahr scale; UPDRS – Unified Parkinson's disease rating scale; UPDRS III – Unified Parkinson's disease rating scale, Part III – Motor examination.

The testing was performed following the measurement protocol that was presented in the previous Chapter. The participants were asked to sit comfortably in the chair with their back put against the chair back. During the experiment, their hands were placed in front, with arms flexed and supported at the elbow. All subjects were instructed to perform the finger-tapping test – to tap a thumb and index finger as quickly and as widely as possible for 15 s. At the beginning of each trial, a short auto-calibration sequence was recorded. Although the newest version of the UPDRS scale state that the finger-tapping test should be repeated precisely ten times [42], for this study, longer sequences were recorded to obtain enough data for analysis. Several trials were recorded per each hand and each subject, so that subjects could familiarize themselves with the instrumentation and measurement protocol. One minute of rest was given between the consecutive trials since fatigue might influence subjects' performance.

All trials were also captured with a commercial video camera that recorded hand in a close-up view. For each subject and each hand, neurologists selected one representative trial for further

analysis. The selection criteria comprised participants' understanding of the given instructions and duration of the finger-tapping sequence.

For each subject, the testing was performed during one day at the Clinic of Neurology. The study was conducted following the ethical standards of the Declaration of Helsinki and approved by the Ethical Committee, School of Medicine, University of Belgrade. All subjects provided written informed consent prior to entering the study.

7.1.2. Instrumentation

In this study, the previously described measurement system was applied. The used wireless inertial sensor system consisted of two IMUs, each comprising a 3-axial gyroscope [75]. IMUs were placed over the fingernails of the thumb and index finger and connected to their SCUs (Figure 7.1). SCUs were positioned on the lower arm and acquired and wirelessly transmitted data to a remote computer. IMUs were lightweight and miniature, which allowed subjects to perform the requested task most naturally.

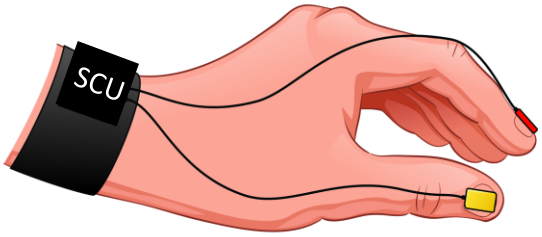

Figure 7.1 Illustration of two small and lightweight inertial measurement units positioned over the fingernails of the thumb and index finger.

7.1.3. Scoring by neurologists

Recorded video files were visually examined and analysed by two neurology specialists that had more than ten years of experience working with movement disorders. The neurologists evaluated each recording with a score from 0 to 4. The scores were given based on their experience and knowledge, following the instructions that were provided in the UPDRS test, Part III–Motor examination, task 3.4 Finger tapping [42]. The scores were given separately for the right and left hand. The videos showed participants' hands in a close-up view, which assured that specialists are blinded to the identity of the subjects during the evaluation.

7.1.4. Data processing

The data was recorded with a sampling frequency $f_s = 200$ Hz. Calibrated data was processed and analysed in a custom-made script, written in Matlab 9.0 R2016a (MathWorks, Natick, Massachusetts, USA).

The angular velocities from the thumb and index finger sensors were processed and transformed using the procedure described in Chapter 6. The relative rotation of the fingers was analysed from the index-finger coordinate system [134]. The relative angular velocity of the thumb with respect to the index finger was computed using the Equation (6.13). The dominant component of the relative angular velocity ω_{rd} was automatically selected and used as the input to further

analysis of the finger-tapping movement. An example of the dominant component of the relative angular velocity ω_{rd} is presented in Figure 7.2.

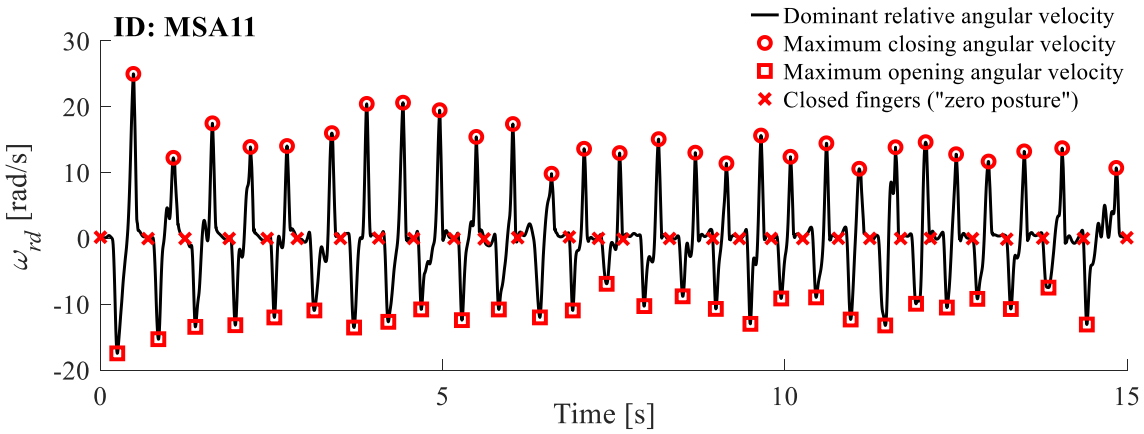

Figure 7.2 Presentation of the dominant component of the relative angular velocity ω_{rd} with extracted time markers indicating maximum closing angular velocity (shown with red circles), maximum opening angular velocity (marked with red squares), and moments when fingers are closed in a "zero posture" (represented with red crosses). An example is given for one MSA patient.

The analysis of the finger-tapping movement consisted of segmentation to individual cycles or taps and calculation of relevant movement properties (as defined in the UPDRS test), including amplitude, amplitude decrement, speed, and the number of hesitations and freezes. In addition, smoothness and intra-subject (or tap-to-tap) variability were calculated for providing a more detailed analysis of the finger-tapping movement.

7.1.4.1. Individual taps

Characteristics of the finger-tapping movement were quantified and evaluated on the level of individual taps. Because of that, the segmentation of the finger-tapping movement sequence was performed using the dominant axis of the relative angular velocity ω_{rd}. The previously introduced segmentation technique was applied, as described in Chapter 6. The signal was smoothed using a moving average filter, with span $(f_s/f_0)/2$, with f_s representing the sampling frequency, and f_0 being the basic finger-tapping frequency automatically calculated from the frequency spectrum. Time markers representing maximum closing and opening angular velocities were extracted from the smoothed signal. Time markers identifying moments when fingers were closed in a "zero posture" were detected between succeeding maximum closing angular velocity and maximum opening velocity markers. The detected "zero posture" markers were complemented with two additional markers identifying the first and last sample of the finger-tapping sequence (as shown with red crosses in Figure 7.2). The final sequence of time markers was then used for drift removal and segmentation of the finger-tapping movement sequence into individual taps.

7.1.4.2. Amplitude

The amplitude of the finger-tapping movement represents very important clinical criteria for the evaluation of the bradykinesia. The procedure for calculating the amplitude of the finger-tapping movement was described in detail in Chapter 6. The amplitude was defined as the angle of the relative rotation of the fingers. The angle was computed by integrating the dominant component of the relative

angular velocity ω_{rd} in a time-stepping procedure [134]. The drift was removed using a third-order polynomial approximation, fitted through the extracted "zero posture" time markers. In these moments, the angle should be equal to zero, as shown with red crosses in Figure 7.2 and Figure 7.3. After removing the drift, the angle sequence α was segmented into individual cycles/taps using the same time markers. For each individual tap, the maximum angle was found, and it was expressed in degrees. The extracted maximum angles were averaged over all cycles of the 15 s long finger-tapping sequence. The obtained average angle was marked with α_{av} [°] and provided as the final parametric result.

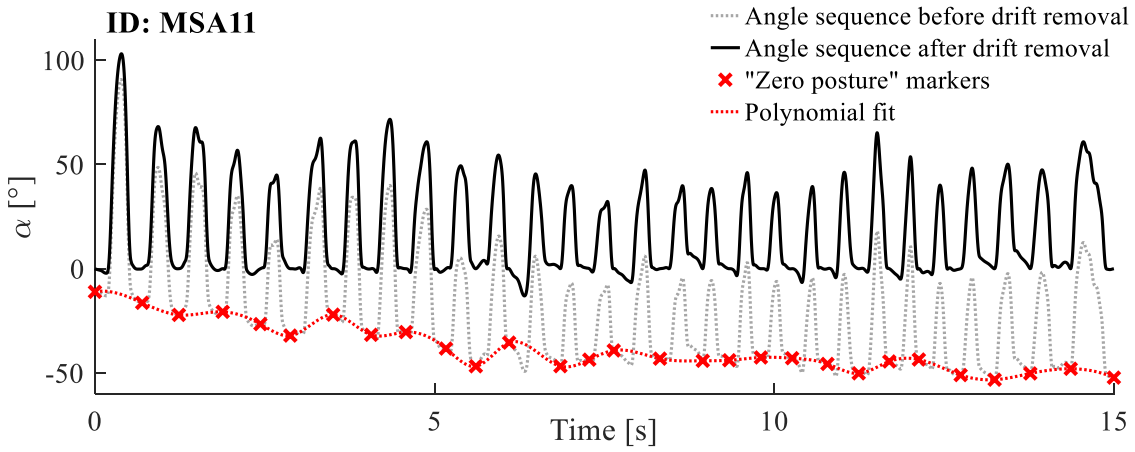

Figure 7.3 Presentation of the angle estimation procedure. The drifted angle sequence is represented with a dotted grey line, whereas a solid black line shows angle sequence after drift removal. Red crosses mark "zero posture" time markers, whereas the dotted red line represents polynomial fit applied for drift removal. An example is given for one MSA patient.

7.1.4.3. Amplitude decrement

Amplitude decrement is evaluated as the movement cycle at which the amplitude begins to decrease. In order to quantify amplitude decrement, inter-tap changes of the calculated tapping angles $\alpha(i)$ were observed. The maximum angle per each individual tap was compared with a threshold TH_α: if the angle was lower than the threshold value then this tap was considered as the tap with significant amplitude decrement. Indices of the first tap that fulfilled this criterion were selected as the parametric result and marked as i_{dec}.

The threshold was given the value of $TH_\alpha = 75\%$ of the maximum angle among all taps that preceded the tap being analysed. This threshold value was heuristically established through extensive search and analysis of the used signal database. A range of threshold values was examined: from 50% to 90%, with a step of 5%. The selected threshold provided the best results among all tested values. The lower threshold values caused detection of the amplitude decrement later in the finger-tapping sequence, with a delay compared to the first real amplitude decrement. On the other hand, higher threshold values caused the detection of very small amplitude changes, which might appear due to the normal movement variability.

An example of the detection of the amplitude decrement is given in Figure 7.4. In the example, the threshold TH_α was set based on the angle value of the first tap. The thresholding criteria were satisfied for all other taps in the finger-tapping sequence; however, the second tap was the first tap with an angle below the threshold value, and therefore, the result was $i_{dec} = 2$.

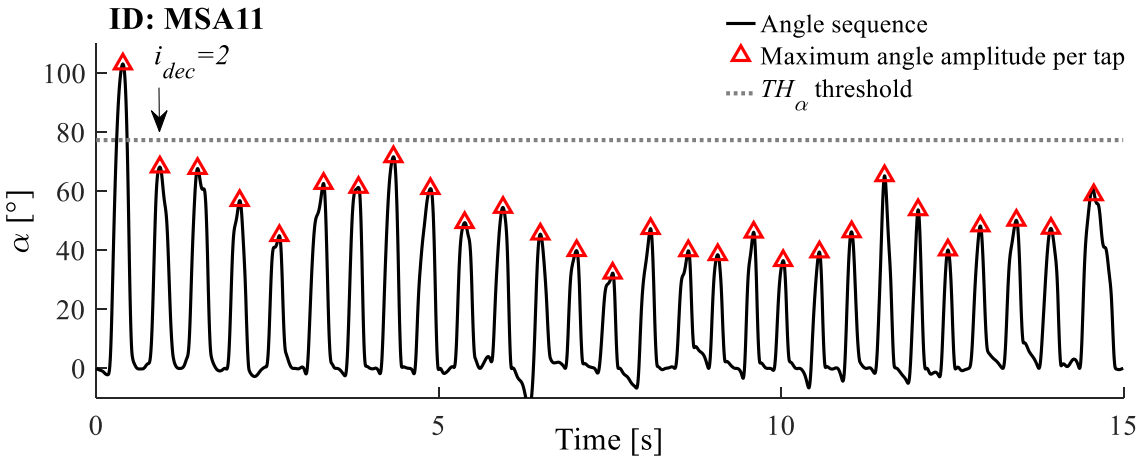

Figure 7.4 Procedure for detection of taps showing significant decrement in the angle amplitude values. Angle sequence is represented with a solid black line, whereas the extracted tapping angle amplitudes were marked with red triangles. The threshold TH_α for detection of amplitude decrement is represented with a dotted grey line. An example is given for one MSA patient.

7.1.4.4. Hesitations and freezes

Hesitations and freezes represent a very important part of the bradykinesia evaluation. They are demonstrated as breaks or irregularities of the regular movement rhythm, which can occasionally appear in the finger-tapping performance. In order to quantify these movement irregularities, the continuous wavelet transform (CWT) was applied. Wavelet analysis has already proven to be a useful tool for analysis of transient changes and spikes in rhythmic behaviour [139], [140], and as such, it was selected for detection and localization of disturbances in the rhythmic finger-tapping performance.

CWT represents a time-frequency analysis method that is suitable for the analysis of signals with both faster and slower changes, which represents its main advantage compared to other time-frequency analysis techniques (such as Short Time Fourier Transform) [17]. In order to determine the spectral characteristics of the signal, a probing function is applied. Various functions can be used as the probing function; however, all of them have one main characteristic - by translating and scaling, they adapt to the shape of the original signal. In this way, the concept of CWT is introduced. The basic wavelet function must take on an oscillatory form, which is why this analysis method is called the "wavelet" transform. CWT is defined with the Equation (7.1) [17]:

$$W(a,b) = \int_{-\infty}^{\infty} x(t) \frac{1}{\sqrt{|a|}} \psi^* \left(\frac{t-b}{a} \right) dt \tag{7.1}$$

where a performs time scaling of the probing function ψ, and b controls the translation of this function. The probing or wavelet function is marked with ψ, whereas $x(t)$ represents the signal, which is analysed. The normalization factor is denoted by $\frac{1}{\sqrt{|a|}}$, whereas the operator * indicates complex conjugation. Since the energy of the wavelet function is dependent on the scale, the normalization factor allows the energy of the wavelet function to be the same for each value of the parameter a. The result of the CWT $W(a,b)$ is represented with the correlation coefficients of the probing function and the signal being analysed. These coefficients are called wavelet coefficients.

Depending on the value of the parameter a, certain features of the wavelet function ψ can be achieved [17]:

- For $|a| > 1$ function ψ is stretched along the time axis,
- For $|a| < 1$ function ψ is compressed along the time axis,
- For $|a| < 0$ function ψ is flipped around the time axis.

For $a = 1$ and $b = 0$, the wavelet function is given in its basic form, and it is called *mother wavelet.*

By selecting the appropriate value of the scaling and translation parameters, the basic function can adjust to any change that occurs in the signal. Information about the frequency content of the signal is presented through the obtained coefficients. These coefficients have a stronger response to the changes that are on the same scale as the wavelet function, or that resemble it. Therefore, CWT maps the signal to the time-scale domain. Small scales correspond to high frequencies, which make them suitable for describing fast changes in signals, and vice versa.

If the wavelet function is appropriately selected, the original signal can be reconstructed from the obtained coefficients, using the following Equation [17]:

$$x(t) = \frac{1}{C} \int_{a=-\infty}^{\infty} \int_{b=-\infty}^{\infty} W(a,b)\psi_{a,b}(t)da\,db \tag{7.2}$$

where C represents admissibility condition, and it is given as [17]:

$$C = \int_{-\infty}^{\infty} \frac{|\psi(\omega)|^2}{|\omega|} \mathrm{d}\omega \tag{7.3}$$

The wavelets are well localized, but not perfectly localized in either scale and time domain. The time range of the wavelet can be specified as [17]:

$$\Delta t_\psi = \sqrt{\frac{\int_{-\infty}^{\infty} (t-t_0)^2 \left|\psi(\frac{t}{a})\right|^2 dt}{\int_{-\infty}^{\infty} \left|\psi(\frac{t}{a})\right|^2 dt}} \tag{7.4}$$

where t_0 represents center time or the first moment of the wavelet. The time range is defined as the square root of the second moment of the wavelet about its time center, Equation (7.4) [17]. Time center can be calculated as:

$$t_0 = \sqrt{\frac{\int_{-\infty}^{\infty} t \left|\psi(\frac{t}{a})\right|^2 dt}{\int_{-\infty}^{\infty} \left|\psi(\frac{t}{a})\right|^2 dt}} \tag{7.5}$$

The frequency range is given similarly:

$$\Delta\omega t_\psi = \sqrt{\frac{\int_{-\infty}^{\infty} (\omega-\omega_0)^2 |\Psi(\omega)|^2 d\omega}{\int_{-\infty}^{\infty} |\Psi(\omega)|^2 d\omega\, a}} \tag{7.6}$$

where $\Psi(\omega)$ is a representation of the wavelet function $\psi(\frac{t}{a})$ in a frequency domain, and ω_0 represents its center frequency. Similarly, the center frequency can be calculated as [17]:

$$\omega_0 = \sqrt{\frac{\int_{-\infty}^{\infty} \omega|\psi(\omega)|^2 d\omega}{\int_{-\infty}^{\infty}|\psi(\omega)|^2 d\omega}} \tag{7.7}$$

The time and frequency ranges of the specific wavelet function family can be obtained by using the Equations (7.5) and (7.7). By scaling the wavelet function with the parameter a, the time range is modified as $\Delta t_\psi(a) = |a|\Delta t_\psi$. Similarly, the frequency range is changed as $\Delta\omega_\psi(a) = \Delta\omega_\psi/|a|$. The product of the time and frequency range is constant and does not depend on the scale. Additionally, the two ranges are inversely related: increasing the time range $\Delta t_\psi(a)$ decreases the frequency range $\Delta\omega_\psi(a)$, and vice versa. The correlation between these ranges defines the time-frequency resolution of the CWT [17].

In this study, CWT was applied to the dominant component of the relative angular velocity ω_{rd}. The fast Fourier transform-based algorithm was used. The mother wavelet function was selected from the complex Morlet family. The center frequency was set to 1 Hz, and the time-frequency resolution was given a value of 0.7. A matrix of complex CWT coefficients was obtained as a result and used for further analysis. CWT maps the signal into the time-scale domain. The signal representation in the time-scale domain is called a *scalogram*. It is a colour-coded representation of the calculated CWT coefficients. An example of a scalogram is given in Figure 7.5, together with the analysed signal. In the shown example, the jet colour map is applied. Lower values of the CWT coefficients are presented with colder colours, with dark blue hue for the lowest values. Warmer colours are used for higher values, with vibrant yellow for presenting the highest coefficients.

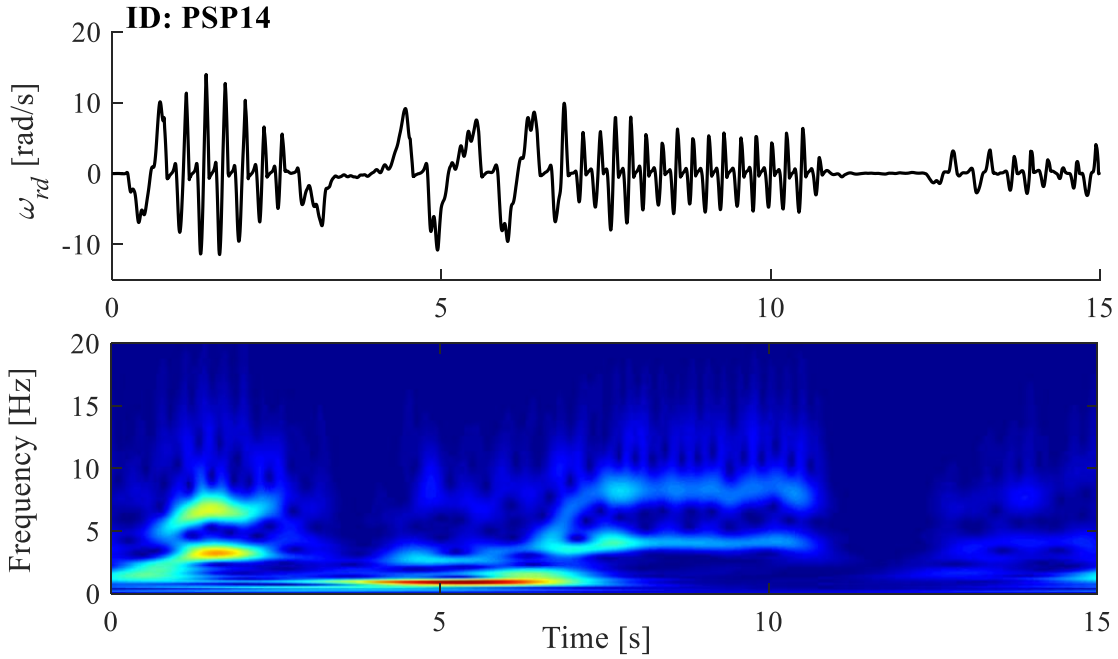

Figure 7.5 The dominant component of the relative angular velocity ω_{rd} (upper panel), and a scalogram of the calculated CWT coefficients, presented using the jet colourmap (lower panel). An example is given for one PSP patient.

By summing the values of the CWT coefficients perpendicular to the time axis, a new characteristic was obtained and referred to as a cross-sectional area (CSA_T). Afterwards, CSA_T was normalized and expressed as a percentage of the CSA_T maximum value. By calculating the introduced characteristic, temporal changes of the finger-tapping activity were described. The samples of the CSA_T characteristic were compared with two thresholds: $TH_{50} = 50\%$ of the average CSA_T value, and $TH_{25} = 25\%$ of the average CSA_T value. Samples valued below the threshold TH_{25} were considered as part of freezing sequences. Similarly, samples with values above the threshold TH_{25}, but below the threshold TH_{50} were assigned to hesitation sequences. A limitation was applied to the detected hesitation sequences: if a hesitation sequence lasted at least three times longer than the person's average finger-tapping cycle duration then this sequence was observed as a freezing sequence. Furthermore, sequences shorter than one half of the person's average finger-tapping cycle duration were discarded from further analysis. The number of hesitation sequences H_{num} and the number of freezing sequences F_{num} were provided as the final parametric results. By using the thresholds that were based on the average value of the CSA_T characteristic, adaptive thresholding was achieved, and detection of signal irregularities was adjusted to the inherent properties of each individual signal. In this way, the signal parts with noteworthy power drops (compared to the average performing power) were determined as irregularities. The threshold values were verified and tested through an extensive analysis of the used signal database. Additionally, neurologists visually inspected video recordings and confirmed all detected irregularities.

An example of the introduced CSA_T characteristic is given in Figure 7.6, together with the analysed signal. The threshold values were presented with horizontal lines of different texture and greyscale colour: solid light grey marked the average CSA_T value, dashed darker grey showed TH_{50} threshold, whereas the darkest grey dotted line represented TH_{25}. Detected irregularities were bounded with dotted red vertical lines and labelled with "H" for hesitations, and "F" for freezes.

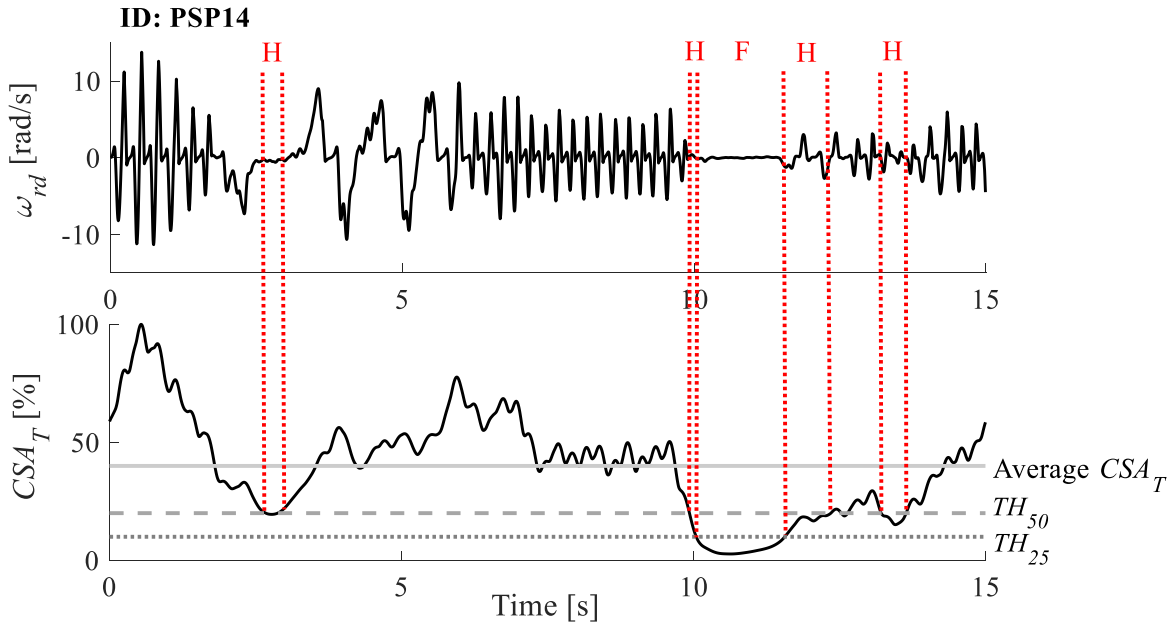

Figure 7.6 Procedure for detection of irregularities, presented with the dominant component of the relative angular velocity ω_{rd} (upper panel), and the calculated CSA_T characteristic (lower panel). The light grey solid horizontal line showed the average CSA_T value. Thresholds TH_{50} and TH_{25} were marked with dashed and dotted grey horizontal lines, respectively. Similarly, red vertical lines bound areas detected as hesitations ("H") and freezes ("F"). An example is provided for one PSP patient.

7.1.4.5. Speed

The speed of repetitive movements represents an important criterion for the evaluation of bradykinesia symptom. In the case of the finger-tapping movement, neurologists evaluate how fast subjects tap their fingers. For faster movements, a larger number of repetitions is executed during the 15 s long finger-tapping test, and vice versa. In this sense, speed can be evaluated by observing the number of performed taps and their duration. Still, this approach only gives a rough estimate of speed, which can be very variable from tap to tap. Because of that, in this study, changes in the tapping rhythm were observed on the level of each individual sample. In order to achieve that, the calculated matrix of the CWT coefficients was used for the detection of the most prominent frequency for each time step. A vector of the CWT coefficients (corresponding to one sample) was extracted from the matrix. The dominant frequency was computed as the frequency at which the highest coefficient was located for that time sample. This procedure was repeated for all time samples. In this way, a new sequence was obtained describing the change of the dominant finger-tapping frequency over time (or instantaneous finger-tapping frequency) and referred to as $f^{(i)}$. The final parametric result was calculated as the average value of the extracted sequence of the tapping frequency and marked as $f_{av}^{(i)}$.

An example of the procedure for calculating the introduced metric is shown in Figure 7.7. The scalogram of the analysed signal is presented, together with the procedure for detecting the instantaneous finger-tapping frequency. On the smaller upper panel, the CWT coefficients for the i^{th} time sample are presented. The dominant frequency is calculated from the extracted vector of coefficients using the described procedure and marked as $f_i^{(i)}$.

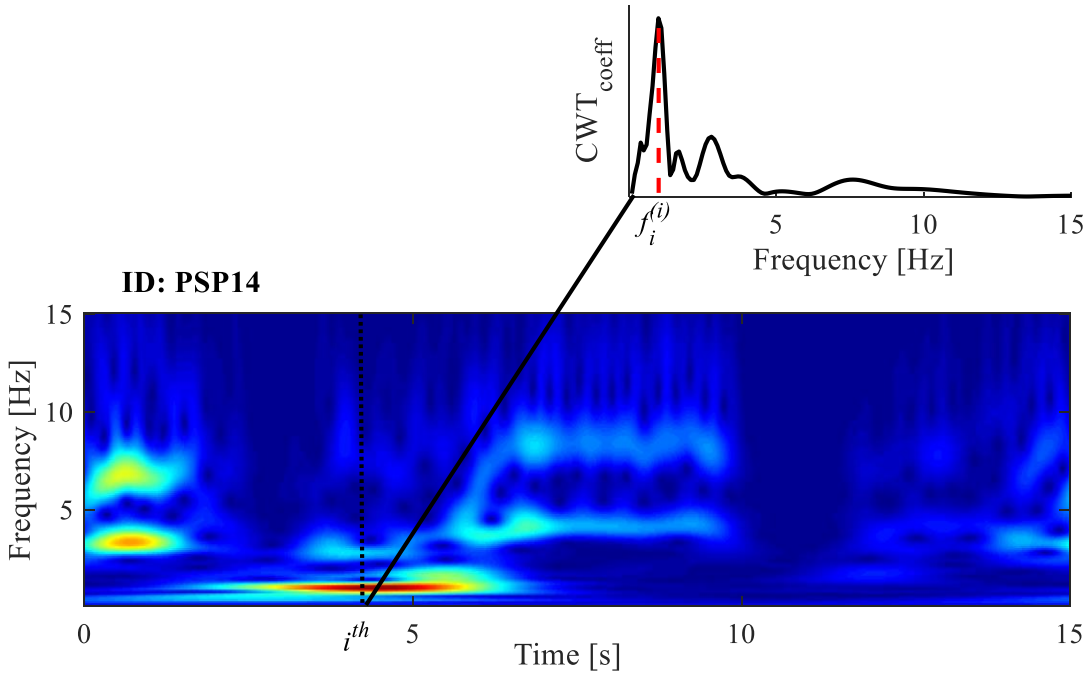

Figure 7.7 Procedure for calculating the instantaneous finger-tapping frequency. A scalogram of CWT coefficients was presented on the lower panel. The vector of coefficients at the i^{th} sample was marked with dashed black line on the scalogram and then visualized on the smaller upper panel. The most prominent frequency (at which the highest coefficient was detected for i^{th} sample) was labelled with red dashed line (marked as $f_i^{(i)}$.). An example is provided for one PSP patient.

7.1.4.6. Additional movement characteristics

Previously introduced parametrization described essential properties of the finger-tapping movement. These movement characteristics are observed and evaluated in clinical practice by neurologists, and they are of crucial importance for the evaluation of patients' state, symptom severity, and disease progression. Therefore, the abovementioned analysis and introduced metrics represent a foundation of the analysis for the evaluation of bradykinesia severity (later referred to as "basic feature set"). However, during the extensive analysis of the used signal database, some other movement properties were noticed. Because of that, a more detailed and profound analysis of the finger-tapping movement was performed (later referred to as "additional feature set") [141], [142].

7.1.4.6.1. Movement intra-variability

By observing movement sequences of different subjects, it was shown that some subjects performed the finger-tapping test more consistently from tap to tap compared to others. The amplitude and the rhythm of their finger-tapping was uniform, and without movement irregularities during the period of 15 s. On the other hand, there were some subjects who performed the finger-tapping test very differently throughout the recorded movement sequence: significant changes of tapping amplitude or rhythm, or appearance of several hesitations or freezes. Therefore, those subjects performed the finger-tapping movement with more expressed intra-variability. In order to quantify movement variability from tap to tap, a method based on Welch's estimation of power spectral density (PSD) was applied to the dominant component of the relative angular velocity ω_{rd} [143]. This method applies the fast Fourier transform to the shorter segments of the analysed signal and estimates the power spectral density by averaging modified periodograms of these shorter segments. It was already applied in the literature for the assessment of intra-gait variability [144].

Prior to estimating the power spectral density, the analysed signal was standardized by dividing it with its standard deviation. In this study, PSD estimation was performed using a window size of 800 samples, with an overlap of 50% between the consecutive windows. FFT length was set to be two times the power of 2 higher of the signal length. For the most prominent peak, two features were extracted: 1) width of the peak – calculated at the half of the peak's maximum amplitude (referred to as w_{PSD} [Hz]); 2) slope of the peak – calculated from the point located at the half of the peak's maximum amplitude to the point of the maximum peak's amplitude (referred to as s_{PSD} [psd/Hz]) [144]. Smaller values of the slope and higher values of the width feature indicate greater intra-variability and vice versa. Two examples are presented in Figure 7.8. Recorded movement sequences are presented on the left, whereas their power spectral densities and calculated metrics are shown on the right. The patient on the upper panel had a consistent finger-tapping performance. The second patient performed more variably from tap-to-tap, with significant amplitude and rhythm changes after the 7th second. For both patients, the calculated metrics confirmed these conclusions, with the higher peak width w_{PSD} and lower peak slope s_{PSD} for the second patient compared to the first patient.

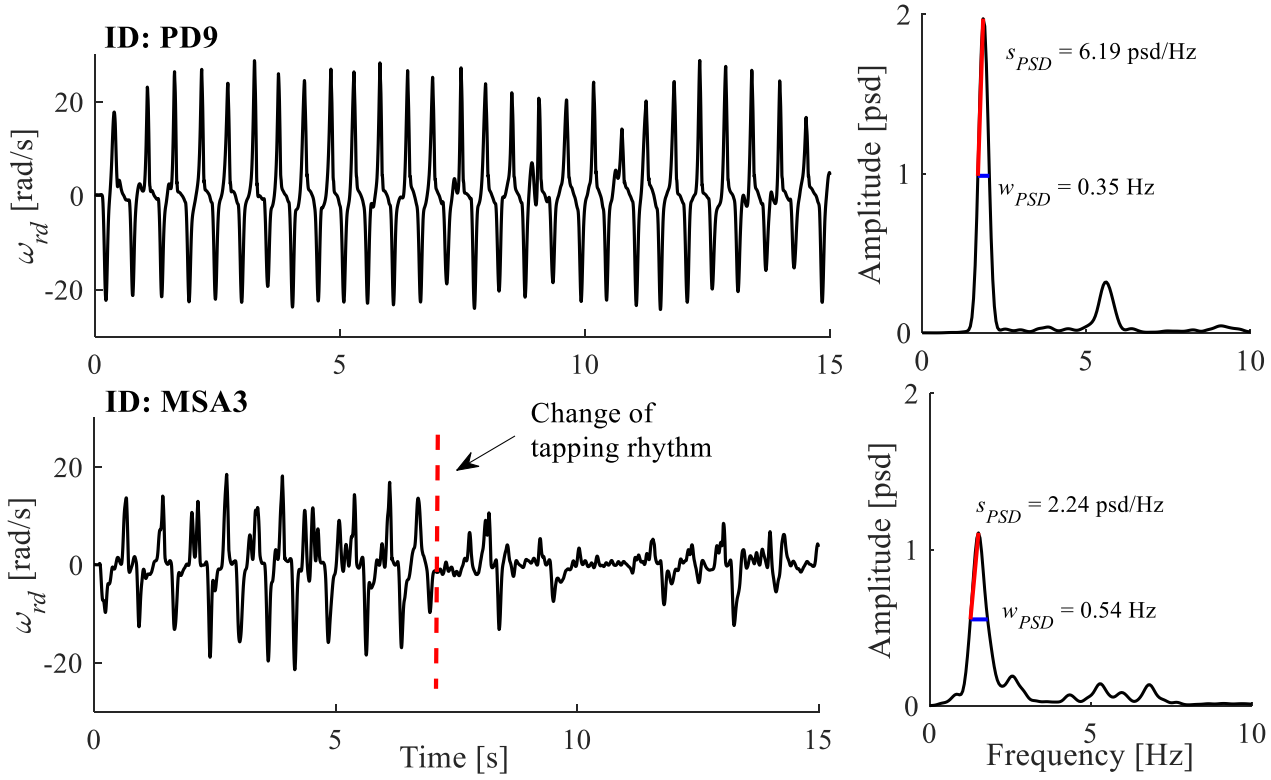

Figure 7.8 Presentation of the dominant component of the relative angular velocity ω_{rd} (on the left) with the calculated power spectral density function and derived features (on the right). In the graphs on the right, red lines mark peak slopes, whereas blue lines show peak width. Examples are provided for one PD patient (upper panel), and one MSA patient (lower panel).

7.1.4.6.2. Movement smoothness

Another specific movement characteristic was observed in the recorded signals. It was noticed that some patients performed the finger-tapping movement with certain "shaking" while opening and closing the fingers, usually as a consequence of another parkinsonian symptom – tremor. These changes were different from the standard hesitations and freezes. While hesitations and freezes caused breaks in the subject's normal finger-tapping rhythmicity, these new changes did not alter the rhythmicity, but they changed the shape of the finger-tapping pattern. In those cases, finger taps were bumpier and less smooth compared to others. An example of a short finger-tapping sequence containing such changes is shown in Figure 7.9. Red ellipse shows one of these "bumps" that may appear in the signal.

Smoothness generally represents a very important movement property, and it was observed in many studies. In the literature, different solutions were presented for evaluating the smoothness. In this study, two techniques were applied to the dominant component of the relative angular velocity ω_{rd}.

One of them is the Spectral Arc (SPARC) method [145]. SPARC method was already implemented for evaluating the smoothness of different sensorimotor behaviour [146], [147]. It is based on the calculation of the arc length of the Fourier spectrum of the analysed signal. The arc length is computed within the selected frequency range [145]. The final measure of the signal smoothness is expressed as the negative logarithm of the calculated arc length. In this study, arc length was calculated in the frequency range from 0.05 Hz to 20 Hz, since it was shown that significant

frequency content of the finger-tapping movement does not exceed the limit of 20 Hz. Using the markers of the maximum opening and closing angular velocity (red circular and squared markers in Figure 7.9), rising and decreasing edges of individual taps were extracted from the analysed signal. The SPARC measure was calculated separately for the rising and decreasing edges, and the result represented the sum of these two SPARC measures. The procedure was repeated for each individual finger-tapping cycle. The final measure of smoothness was given as the average value of the smoothness values obtained for the individual cycles and referred to as s_{SPARC}. Higher values of the parameter indicated smoother movements, and vice versa.

Other smoothness measure observed the analysed signal in the time domain. Once again, rising and decreasing edges of the finger-tapping sequence were extracted using the maximum opening and closing angular velocity markers. For each edge, a count of smaller bumps or peaks was detected. The obtained values for the rising and decreasing edges were summed for each individual finger-tapping cycle, and then averaged for all individual cycles, providing the final measure of the signal smoothness, marked as $s_{PEAKS.}$

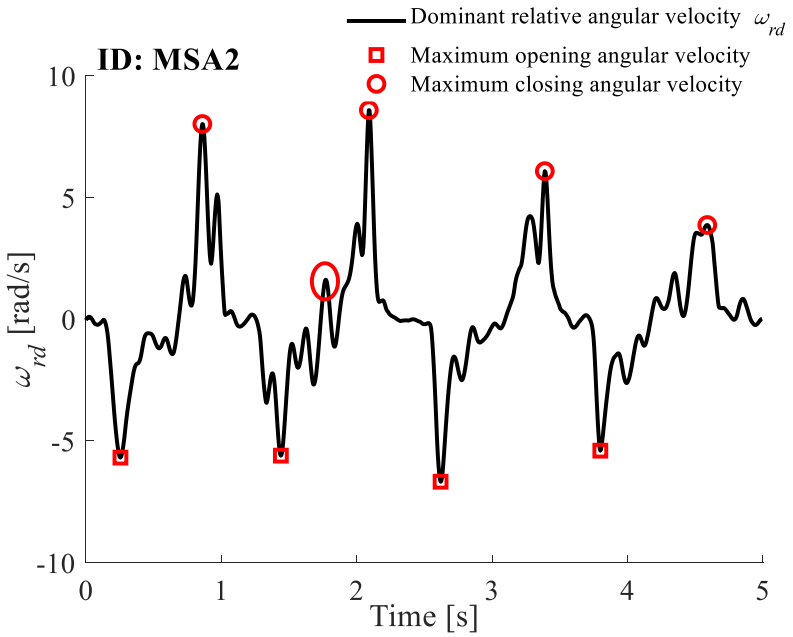

Figure 7.9 Short sequence of the dominant component of the relative angular velocity ω_{rd}, with three consecutive taps. Red circular markers show maximum closing angular velocity per each tap, whereas red squares represent maximum opening angular velocity per each tap. Red ellipse shows a "bump" in the signal. An example is given for one MSA patient.

7.1.5. Expert system for prediction of motor scores

Due to the nature of the observed problem, an expert system was developed for the prediction of clinical scores. The presented expert system utilized the basic feature set (previously defined in this Chapter), theoretical knowledge in this field, and a set of expert rules that completely objectified the instructions provided within the UPDRS scale for assigning the scores.

The basic feature set evaluated movement characteristics that were observed in the clinical practice, including the finger-tapping amplitude (quantified with α_{av}), the finger-tapping speed (quantified with $f_{av}^{(i)}$), the amplitude decrement (quantified with i_{dec}), and the number of hesitations (quantified with H_{num}) and freezes (quantified with F_{num}). These features were provided in a form

that was completely understandable and intuitive for the physicians. The additional feature set evaluated other movement characteristics (intra-variability and smoothness), which provided a more detailed assessment and insight into disease and symptoms progress. However, these features were not observed within the expert system since they quantified movement properties that were not analysed nor included in the instructions provided in the UPDRS test.

7.1.5.1. Knowledge base

In clinical practice, the finger-tapping movement is used and examined as part of the bradykinesia severity assessment. The knowledge base was developed according to the detailed instructions and evaluation criteria from the UPDRS scale, Part III – Motor examination, task 3.4 Finger tapping [42] are presented in Table 7.2.

Table 7.2 The evaluation criteria for the finger-tapping test, as provided in the UPDRS scale, Part III – Motor examination, task 3.4 Finger tapping.

Score	**Movement characteristic**		
	Rhythm	**Amplitude decrement**	**Interruptions**
0 – Normal	Fast movement with large amplitude	None	None
1 – Slight	Slight slowing	Amplitude decrements around the tenth tap	1 – 2 hesitations
2 – Mild	Mild slowing	Amplitude decrements midway through a 10-tap sequence	3 – 5 hesitations
3 – Moderate	Moderate slowing	Amplitude decrements after the first tap	More than 5 hesitations or at least one freeze
4 – Severe	Cannot or can only barely perform movement due to highly expressed slowing, interruptions or decrements		

Although clinical knowledge is unambiguously determined for certain criteria (amplitude decrement and hesitations/freezes), this is not the case for movement speed and amplitude (they are evaluated based on examiner's experience). Furthermore, the instructions indicate that the lowest score is assigned to "normal" finger-tapping movements, without deeper explanations and numerical values that could describe this type of movement in detail. Therefore, the knowledge base was extended with some additional information that was collected and extracted using the unsupervised learning process and basic feature set.

The first step was to define feature values that could be considered as "normal" or reference. Because of that, the subset of the input feature set corresponding to healthy subjects with no signs of bradykinesia (scored with 0 by both neurologists) was extracted.

During the examination of the signals and video recordings, it was noticed that subjects performed the finger-tapping movement in two ways. One batch of subjects performed the finger-tapping test with the largest amplitude at the highest possible speed that allowed such wide tapping. Others tapped their fingers at their fastest pace, but with lower amplitudes. The selected subset of healthy subjects was divided into two clusters using the k-means algorithm: cluster C_1– „wider and

slower, " and cluster C_2– „narrower and faster" finger-tapping performance. The k-means algorithm divides data to exactly k clusters that are defined by their centroids [148]. Firstly, k initial centroids are chosen, and each observation is assigned to the closest cluster based on the calculated point-to-centroid distances. The observations are reassigned to a different cluster if that decreases sum of squares of all point-to-centroid distances within one cluster. New centroids are then calculated as the average of all observations within the corresponding clusters. The procedure is repeated when cluster assignments stop changing, or the algorithm reaches maximum number of iterations.

The clustering was performed using the features describing the finger-tapping amplitude and speed (α_{av} and $f_{av}^{(i)}$, respectively). The coordinates of the two cluster centers were then applied for discriminating the two types of finger-tapping performance. Fifty percent of the observations were randomly selected from all three patient groups and assigned to the testing group. Each testing observation was then assigned to one of these two clusters based on the calculated Euclidian distance between the cluster centers and the coordinate pair $(\alpha_{av}, f_{av}^{(i)})$ of that observation.

The scores given by the specialists were provided as the final score evaluating the overall regularity of the finger-tapping movement. Therefore, these scores did not provide information about the individual aspects and characteristics of the examined finger-tapping performance. Because of that, the unsupervised learning algorithm was applied for analysing the intrinsic properties of the features and finding a natural grouping among analysed data. By using the k-means algorithm, the values of one of the features (α_{av} or $f_{av}^{(i)}$) assigned to one of two clusters (C_1 or C_2) were additionally split into four clusters, which corresponded to 0-3 scores. Although a finger-tapping movement can be evaluated with five scores, the data was divided into four clusters, because the highest score is given to patients that can barely perform the task, and such movement is affected by several types of disruptions simultaneously. The decision boundaries were then calculated using the coordinates of the cluster centers (c_1, c_2, c_3, c_4) as follows:

$$b_i = \frac{c_i + c_{i+1}}{2};\ i = 1,2,3 \tag{7.8}$$

where and c_i and c_{i+1} represented centers of two neighbouring clusters, and b_i represented the calculated boundary separating the two succeeding scores. The procedure was repeated for both features α_{av} and $f_{av}^{(i)}$ and both clusters C_1 and C_2, separately (1: C_1 and α_{av}, 2: C_2 and α_{av}, 3: C_1 and $f_{av}^{(i)}$, 4: C_2 and $f_{av}^{(i)}$). This clustering resulted in four sets of decision boundaries, each comprising three values. The decision boundaries were chosen from those four sets for each observation individually. Decision boundaries for the features i_{dec} and H_{num}, F_{num} features were defined to match the specifications given within the UPDRS scale (as presented in Table 7.2).

7.1.5.2. Inference process

The inference process started with calculating the patient's data with the previously described procedure for the extraction of basic features. Afterwards, the patient's speed and amplitude data is assigned to one of these two clusters, based on the Euclidian distance of the coordinate pair $(\alpha_{av}, f_{av}^{(i)})$ to the centers of the clusters C_1 and C_2: if the coordinate pair is closer to the center of the cluster

C_1, then this observation was assigned to the cluster C_1, and vice versa. The decision boundaries ($b_{\alpha 1,2,3}$ and $b_{f1,2,3}$) were then selected for the corresponding cluster.

A block diagram of the developed and implemented reasoning is presented in Figure 7.10. The first part of the decision-making process consisted of four blocks (marked with dashed black lines). The inputs to these four blocks were $\alpha_{av}, f_{av}^{(i)}, i_{dec}$ and H_{num}, F_{num} features. Each block implemented a defined set of rules and calculated a score for one individual movement characteristic: amplitude, speed, amplitude decrement, and movement interruptions. Therefore, the outputs from these blocks included four sub-scores: S_α, S_f, S_{dec}, and S_{HF}, respectively. If the sub-score "3 – Moderate" was obtained for at least three out of four movement characteristics, then the final score S_{FT} was set to "4 – Severe". Otherwise, the final score S_{FT} was computed as the maximum obtained sub-score among the four sub-scores evaluating the individual movement properties.

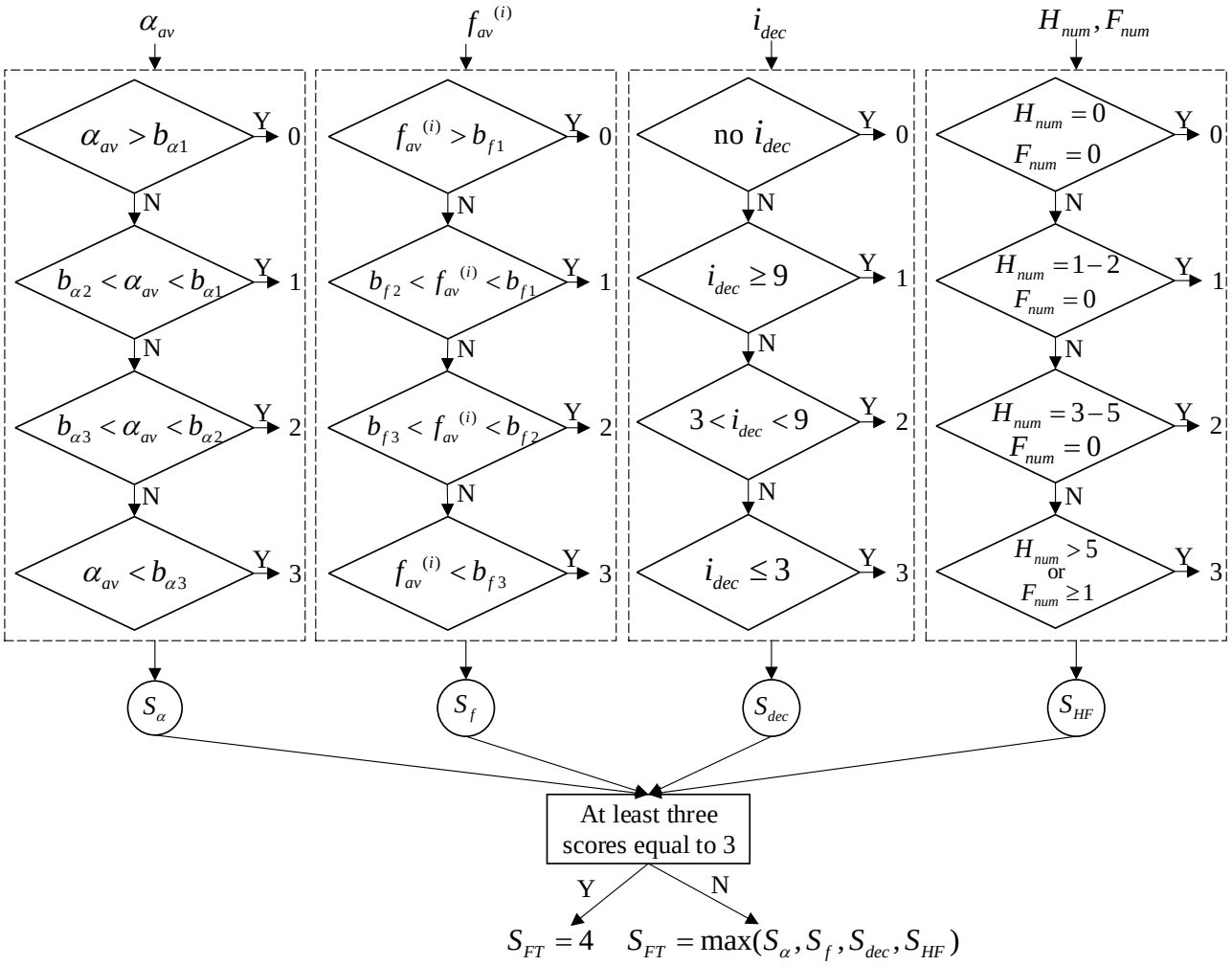

Figure 7.10 Block diagram of the developed and implemented reasoning. The decision-making process was divided into four blocks (marked with dashed black rectangles). The inputs to these four blocks were features: $\alpha_{av}, f_{av}^{(i)}, i_{dec}$ and H_{num}, F_{num}, respectively. Each block implemented a different set of rules and calculated a sub-score for one individual movement characteristic (amplitude, speed, amplitude decrement, and movement interruptions, respectively). The final score was calculated based on the sub-score values.

7.1.6. Statistical analysis and evaluation of the expert system

The agreement between the scores given by two neurologists was calculated using Cohen's kappa coefficient, which provided a measure of the intra-rater reliability. For each feature, two groups were compared using the corresponding statistical test. The test was applied based on data distribution. If both groups being compared satisfied the normal distribution, the independent t-test for two samples was applied. Otherwise, the Mann-Wilcoxon test was used. The normality of the data was found by observing several parameters simultaneously, including data skewness and kurtosis z-values, the Shapiro-Wilk test p-value, and histograms, normal Q-Q plots and box plots. For $p < 0.05$, the null hypothesis that two groups had the same mean rank was rejected. In that case, it was found that the two groups were showing statistically significant differences. Statistical analysis was performed in IBM SPSS Statistics v26.0 (IBM, Armonk, New York, U.S.A.).

In order to evaluate the efficiency of the proposed method, the scores given by the expert system were compared to those provided by the two specialists. The results were presented using the confusion matrix and the accuracy metric. The accuracy Ac [%] was calculated as the percentage of scores that were equally signed by the expert system and neurologists. Confusion matrix (or a contingency table) represents an evaluation approach that contains information about the true and predicted scores [149]. It is usually presented as a matrix, where cells on the main diagonal represent the percentage of correctly assigned scores, and other cells mark the error or percentage of incorrectly predicted scores. Two evaluation scenarios were analysed: using all observations (later referred to as "Case I") and using only observations that were equally scored by both neurologists (later referred to as "Case II").

7.2. Results

In this study, 111 recordings were analysed in total, which included 26 recordings from 13 PD patients, 34 recordings from 17 MSA patients, 27 recordings from 14 PSP patients, and 24 recordings from 12 healthy controls. Examples of the recorded finger-tapping movement are given in Figure 7.11, for one subject from all four participant groups.

HC subject tapped with the highest speed and the biggest amplitude. This movement was much more vigorous compared to the performance of the three patients (the fastest tap is accentuated with red colour). Also, HC performed the finger-tapping consistently throughout the 15 s of the test. Although they were in the same stage of the disease development (H&Y=2), three patients had very different finger-tapping movement patterns. Among all three patients, the PD patient had the most vigorous performance, with some changes in the standard rhythmicity (or insecurities) around the 12^{th} and 14^{th} s (marked with red ellipses). The finger-tapping pattern of the PD patient had the most similar shape with HC. In contrast, MSA had a consistent tapping, but the corrupted pattern – it contained a lot of bumps in the signal (marked with red rectangle), as a consequence of the hand tremor which was visible during the recording. The most changeable movement was seen in the PSP patient. This patient performed the finger-tapping with very variable rhythm and amplitude. The shape of the finger-tapping changed throughout the sequence (the point of visible change of rhythm is marked with red dashed line): at the beginning, his/her taps looked more like normal finger-tapping, whereas later in the sequence, his/her taps were more irregular with expressed bumps and insecurities while performing the movement (shown with red rectangle).

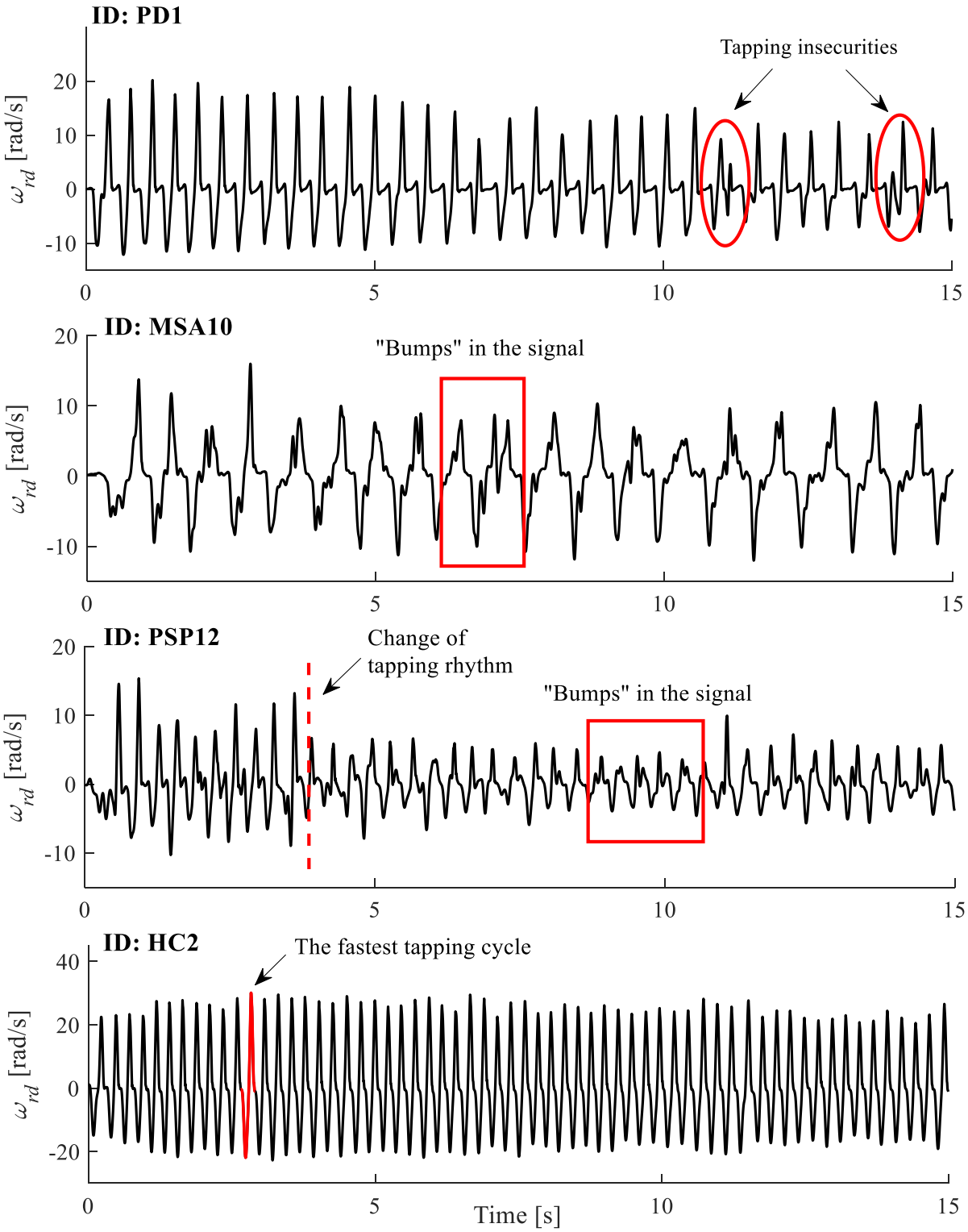

Figure 7.11 Representation of the dominant component of the relative angular velocity ω_{rd}, recorded during the repetitive finger-tapping movement. Examples are given for one PD patient (first panel), one MSA patient (second panel), one PSP patient (third panel), and one HC subject (fourth panel). Three patients were in the second stage of disease severity (H&Y=2).

Descriptive statistics (average±std) for the basic and additional feature sets are shown in Table 7.3 and Table 7.4, for each subject group separately. Table 7.5 presents the results of the performed statistical analysis.

Table 7.3 Descriptive statistics (average±std) for the basic feature set, presented for each subject group separately.

Feature	PD	MSA	PSP	HC
$f_{av}^{(i)}$ [Hz]	2.04±0.87	1.71±1.26	2.37±1.11	3.32±0.89
α_{av} [°]	63.08±8.54	56.27±36.11	44.87±31.74	80.48±26.55
i_{dec} [#]	5.00±5.66	4.03±4.74	5.62±4.88	11.00±10.99
H_{num} [#]	0-4	0-7	0-4	/
F_{num} [#]	0	0-2	0-1	/

PD – Parkinson's disease patients; MSA – Multiple system atrophy patients; PSP – Progressive supranuclear palsy patients; HC – Healthy controls.

HC performed finger-tapping movement with the highest speed and amplitude, as shown with α_{av} and $f_{av}^{(i)}$ parameters. The slowest tapping was detected in MSA patients, whereas PSP patients performed the finger-tapping with the highest frequency. However, the amplitude in PSP patients was significantly lower compared to PD patients, who performed the widest finger taps. This disproportion in the values for the tapping amplitude and speed for the PD and PSP groups confirmed the need for distinguishing two types of the finger-tapping movement (described by clusters C_1 and C_2). Results for the amplitude decrement provided comparable results between three groups. HC also experienced some decrease in the tapping amplitude; however, this was noticeable much later in the finger-tapping sequence (on average after the 10th tap). None of the HC subjects experienced any movement irregularities. On the other hand, patients from all three groups showed some episodes of hesitations (the largest number of hesitations in one movement sequence was seen in the MSA group). Freezes were detected only in patients with atypical forms of parkinsonism (MSA and PSP patient groups).

Table 7.4 Descriptive statistics (average±std) for the additional feature set, presented for each subject group separately.

Feature	PD	MSA	PSP	HC
w_{PSD} [Hz]	0.48±0.17	0.46±0.15	0.51±0.18	0.42±0.06
s_{PSD} [psd/Hz]	3.07±1.79	3.20±1.75	2.59±1.59	3.90±1.24
s_{SPARC}	-6.91±0.63	-7.60±1.52	-6.59±0.58	-6.55±0.24
s_{PEAKS}[#]	2.83±1.60	5.75±4.31	2.43±1.60	1.52±0.38

PD – Parkinson's disease patients; MSA – Multiple system atrophy patients; PSP – Progressive supranuclear palsy patients; HC – Healthy controls.

The features w_{PSD} and s_{PSD} showed that HC subjects performed the finger-tapping test with the smallest tap-to-tap variability. For PD and MSA patients, comparable results were obtained. The most prominent intra-variability was established in PSP patients, who, on average, had the highest value for the peak's width and the lowest value for the peak's slope, compared to the other three subject groups. Both features for smoothness quantification showed that HC performed the finger-tapping movement with the utmost easiness. Among all patient groups, MSA patients had the bumpiest and the least smooth performance.

Table 7.5 The results of the performed statistical analysis for comparison of two groups and features from both feature sets, separately.

Feature	Compared groups					
	PD-MSA	**PD-PSP**	**PD-HC**	**MSA-PSP**	**MSA-HC**	**PSP-HC**
$\boldsymbol{\alpha_{av}}$	0.230	0.017	0.053	0.221	0.009	0.001
$\boldsymbol{f_{av}^{(i)}}$	0.033	0.239	<0.001	0.008	<0.001	0.005
$\boldsymbol{i_{dec}}$	0.496	0.164	0.113	0.009	0.023	0.663
$\boldsymbol{H_{num}}$	0.862	0.836	/	0.710	/	/
$\boldsymbol{F_{num}}$	/	/	/	0.430	/	/
$\boldsymbol{w_{PSD}}$	0.849	0.212	0.824	0.106	0.727	0.025
$\boldsymbol{s_{PSD}}$	0.925	0.317	0.090	0.223	0.070	0.005
$\boldsymbol{s_{SPARC}}$	0.029	0.005	0.012	<0.001	0.001	0.802
$\boldsymbol{s_{PEAKS}}$	0.006	0.282	<0.001	0.001	<0.001	0.016

PD-MSA – Comparison of the PD and MSA groups; PD-PSP – Comparison of the PD and PSP groups; PD-HC – Comparison of the PD and HC groups; MSA-PSP – Comparison of the MSA and PSP groups; MSA-HC – Comparison of the MSA and HC groups; MSA-PSP – Comparison of the MSA and PSP groups; PD – Parkinson's disease patients MSA – Multiple system atrophy patients; PSP – Progressive supranuclear palsy patients; HC – Healthy controls.

Features showing the most expressed statistically significant differences between the compared groups were those describing the finger-tapping speed and movements smoothness ($f_{av}^{(i)}$, s_{SPARC}, s_{PEAKS}). For features describing movement variability, significant differences ($p < 0.05$) were seen only for the comparison of PSP patients, and HC subjects. H_{num} and F_{num} showed no differences between the compared groups.

The scores given by the two neurologists are provided in Table 7.6, together with the results of Cohen's Kappa statistics describing the agreement between the given scores. For patient groups, the scores are presented separately for the less and more-affected hand and averaged for all patients in the group. In the case of the HC group, the scores were averaged for both hands and all subjects.

As shown in Table 7.6, there were some discrepancies between the results given by two neurologists (more prominent for MSA and PSP groups). This result is also confirmed by Cohen's Kappa coefficient $\kappa = 0.79$, showing a moderate level of agreement between the scores given by the two neurologists.

Table 7.6. Descriptive statistics (average±std, median) for the finger-tapping scores given by two neurologists, presented separately for the less and more affected hand and each subject group.

Group	Statistics	FT_{N1} scores		FT_{N2} scores	
		Less AH	**More AH**	**Less AH**	**More AH**
PD	Average±std	1.67±0.89	2.17±0.94	1.75±0.97	2.17±0.94
	Median	2	2	2	2
MSA	Average±std	2.31±0.70	2.81±0.54	2.38±0.72	2.81±0.54
	Median	2	3	2.5	3
PSP	Average±std	2.17±0.94	2.62±0.77	2.08±0.79	2.77±0.73
	Median	2.5	3	2	3
HC	Average±std	0.44±0.63		0.50±0.73	
	Median	0		0	
Total agreement		**κ=0.79**			

PD – Parkinson's disease patients; MSA – Multiple system atrophy patients; PSP – Progressive supranuclear palsy patients; HC – Healthy controls; FT_{N1} scores – Scores given by the first neurologist; FT_{N2} scores – Scores given by the second neurologist; Less AH – The less affected hand; More AH – The more affected hand.

In Figure 7.12, the features representing the finger-tapping frequency $f_{av}^{(i)}$ and angle α_{av} are scattered as the function of the calculated scores. Two performance clusters are presented using markers of different colours and shapes. Both tapping frequency $f_{av}^{(i)}$ and angle α_{av} features show a decline in values with higher scores, which is in agreement with the clinical UPDRS criteria for evaluation of the finger-tapping and related movements. Furthermore, movement sequences assigned to the cluster C_1 are characterized by a lower tapping frequency $f_{av}^{(i)}$ and higher tapping angles α_{av} compared to the cluster C_2.

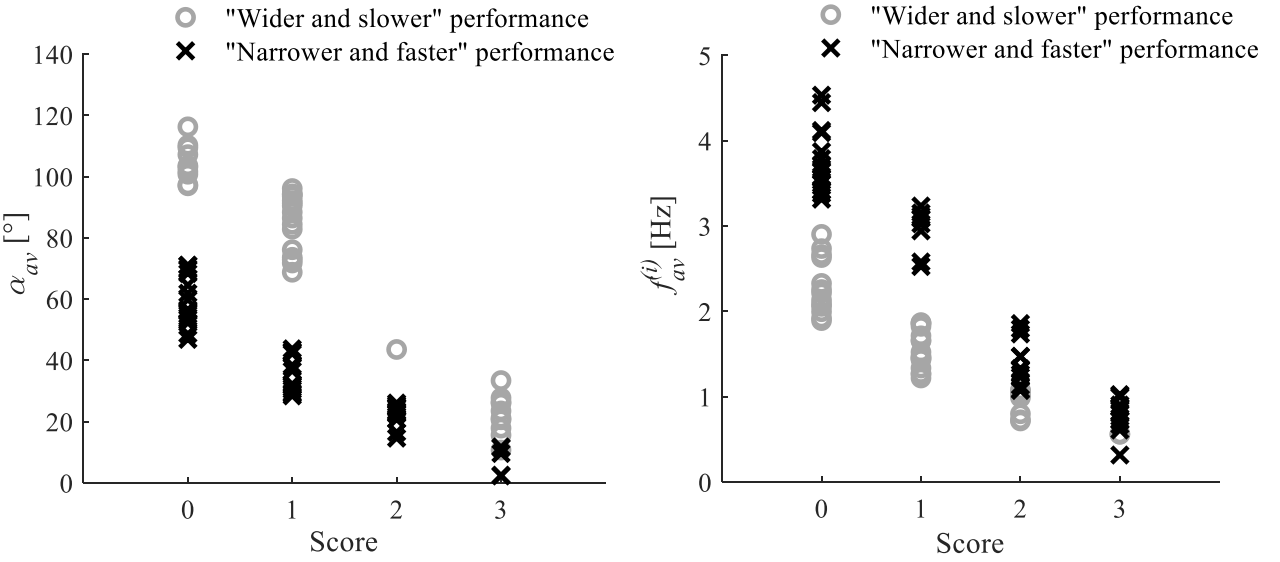

Figure 7.12 Dependence of feature α_{av} values on calculated scores (left), and feature $f_{av}^{(i)}$ values and calculated scores (right). Observations from two different clusters are shown with colour- and shape-coded representation: grey circles show observations from the cluster C_1 ("wider and slower" finger-tapping performance), and black crosses mark samples from the cluster C_2 ("narrower and faster" finger-tapping performance).

The results of the expert system, expressed through the Ac metric, are presented in Table 7.7, for each patient group separately, as well as summarized for all patients. In the left column, the results are shown for the first evaluation scenario, Case I, which included all observations (87 observations in total, PD: 26, MSA: 34, PSP: 27). The shown results were averaged for both raters. In the right column, the results are presented for the second evaluation scenario, Case II, including only the observations equally scored by both raters (76 observations in total, PD: 25, MSA: 29, PSP: 22). For both evaluation scenarios, results are also presented by a confusion matrix in Figure 7.13.

Table 7.7 Results of the expert system presented through the Ac metric, for each patient group and in total. The results are provided for two evaluation scenarios: 1) when all observations were included in the evaluation (Case I), and 2) when only observations equally scored by both neurologists were included in the evaluation (Case II).

Group	***Ac*** [%]	
	Case I	**Case II**
PD	82.69±2.72	84.00
MSA	82.36±8.32	89.65
PSP	83.76±7.86	90.91
Total	83.33±6.50	88.16

PD – Parkinson's disease patients; MSA – Multiple system atrophy patients; PSP – Progressive supranuclear palsy patients.

		Output				
		0	1	2	3	4
Target	0	100	0.0	0.0	0.0	0.0
	1	0.0	85.2	14.8	0.0	0.0
	2	0.0	5.7	84.9	9.4	0.0
	3	0.0	2.4	13.1	82.1	2.4
	4	0.0	0.0	0.0	25	75

		Output				
		0	1	2	3	4
Target	0	100	0.0	0.0	0.0	0.0
	1	0.0	84.6	15.4	0.0	0.0
	2	0.0	4.8	90.4	4.8	0.0
	3	0.0	2.7	5.4	89.2	2.7
	4	0.0	0.0	0.0	25	75

Figure 7.13 Confusion matrix for Case I - all observations included in the evaluation (left), and Case II - only observation equally evaluated by both raters included in the evaluation (right). The fields on the diagonal present the percentage [%] of accurately assigned scores, whereas the fields outside the diagonal present the percentage [%] of wrongly predicted scores.

The expert system provided scores that matched the scores estimated by the neurologists with good accuracy. For the first evaluation technique, Case I, with all observations included in the analysis, similar results were obtained for all three patient groups, showing accuracy above 82%. The results were improved for the second evaluation technique, Case II, when only observations equally scored by both raters were included, showing matching of almost 90% between the scores given by the expert system and those estimated by the neurologists. Furthermore, based on the results provided

in Figure 7.13, it can be seen that the scores provided by the expert system and the scores estimated by the neurologist did not exceed a difference of one score (except for one patient).

Example results of the developed support for the evaluation of bradykinesia severity are presented in Figure 7.14. The finger-tapping amplitude sequence is presented, together with the detected movement disturbances (amplitude decrement and movement irregularities) and calculated features describing basic movement characteristics. For comparison, the example is provided for two patients (one MSA and one PSP patient) who were equally evaluated by both raters and developed expert system (score S_{FT}).

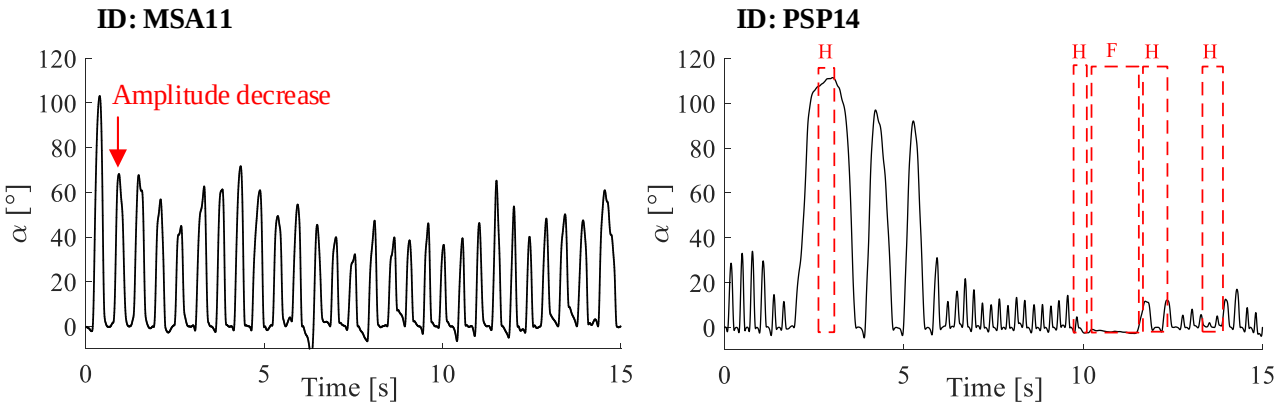

$\alpha_{av} = 53.44 \pm 15.01\ °$

$f_{av}^{(i)} = 1.86 \pm 0.17$ Hz

$i_{dec} = 2$

$H_{num} = 0,\ F_{num} = 0$

$\boldsymbol{S_{FT} = 3}$

$\alpha_{av} = 23.49 \pm 26.42\ °$

$f_{av}^{(i)} = 1.87 \pm 1.58$ Hz

$i_{dec} = 5$

$H_{num} = 4,\ F_{num} = 1$

$\boldsymbol{S_{FT} = 3}$

Figure 7.14 Example results of the developed support for the evaluation of bradykinesia severity. It comprises a graphical representation of the calculated finger-tapping amplitude sequence with marked disruptions (amplitude decrement and rhythm irregularities), calculated features describing different movement characteristics, and the score provided by the expert system. The example is provided for one MSA patient (left), right hand, and one PSP patient (left), right hand.

7.3. Discussion

This chapter presents a new method for the evaluation of the bradykinesia symptom. The method was developed and validated on the example of the finger-tapping movement, which is a standardized motor test for the evaluation of bradykinesia severity. Results include a new parametrization that describes important biomechanical movement properties and completely quantifies clinical evaluation criteria. This parametrization included two feature sets: basic and additional. The basic feature set comprised metrics that quantified movement characteristics, which are visually observed in the clinical practice and used for evaluation of patients' symptoms and degree of their motoric impairment. However, during the extensive analysis of the used signal database, some other movement properties were noticed and included in the analysis. The metrics quantifying movement variability and smoothness were developed and included as the additional feature set.

Although additional features target some movement characteristics that are not observed nor included in the clinical examination, the use of both feature sets enables more detailed movement analysis, providing deeper insight into the development of some other symptoms (such as tremor).

The continuous wavelet analysis was used for describing temporal changes of the dominant finger-tapping frequency, which gave an estimation of the tapping speed on the level of one sample. It was also successfully applied for the detection and localization of movement irregularities (hesitations and freezes) that might endanger the normal movement rhythmicity. The amplitude was quantified with the tapping angle, which was calculated by integrating the dominant component of the relative angular velocity of two fingers, following the procedure described in the Chapter 6. Significant amplitude drops were detected using a thresholding technique, which represented a new way for quantifying the amplitude decrement criterion. Welch's estimation of the power spectral density was used to evaluate the finger-tapping intra-variability. The width and slope of the most dominant peak in the power spectral density provided a measure of a tap-to-tap variability. Movement smoothness was assessed and quantified using two different measures: one implemented on a signal representation in the frequency domain as the length of the spectral arc length, and other calculated as the number of signal "bumps" in the time series.

The designed parametrization and medical knowledge defined in the UPDRS scale represented the basis for the development of a new expert system for the prediction of clinical scales and severity of symptoms. The expert system implemented simple decision rules that objectified and matched the standardized UPDRS criteria. Decision boundaries for the tapping amplitude and speed criteria were defined using a clustering technique and the testing data that was obtained from healthy controls and randomly selected patients. In this way, decision boundaries were not defined empirically nor linearly; they were established based on natural grouping of some randomly selected testing data. This approach distinguished two types of the finger-tapping movement: "wider and slower" (cluster C_1, grey circles in Figure 7.12) or "narrower and faster" (cluster C_2, black crosses in Figure 7.12). Each movement type was described with two sets of boundaries. The reasoning process included selection of corresponding boundaries for each patient individually, based on the type of their movement. Decision boundaries for the other two movement properties (amplitude decrement and hesitations/freezes) completely matched decision rules defined in the UPDRS scale.

The efficiency of the proposed expert system was evaluated for the entire range of finger-tapping bradykinesia severity scores (0-4). In the literature, most studies included severity stages up to 3, indicating that the highest scores were given to patients that cannot execute the task at all. However, in this study, three patients that barely managed to perform the finger-tapping movement were included. Their performance was poor and influenced by multiple movement disruptions simultaneously (visible for one or both of their hands), and therefore evaluated with the highest bradykinesia severity score (4).

The obtained results were compared with the scores provided by two neurology specialists. The expert system predicted the scores with overall accuracy Ac of 83.33±6.50% (averaged for both raters). On the level of the individual patient groups, accuracy Ac was 82.69±2.72%, 82.36±8.32%, and 83.76±7.86% for PD, MSA, and PSP groups, respectively. By analysing only observations that were equally evaluated by both neurologists, the accuracy of the expert system Ac achieved 88.16%. On the level of the individual patient groups, the accuracy was 84.00%, 89.65%, and 90.91% for PD, MSA, and PSP patients, respectively. In the latter case, the expert system predicted the wrong scores

for only nine observations (out of 76 observations). The expert system provided very good results for patients with idiopathic PD, but also for the patients with atypical forms of parkinsonism who may perform finger-tapping movements differently compared to the PD patients [71]. The predicted scores and clinical scores did not exceed a difference of one score (as shown in the confusion matrices in Figure 7.13), except for one PD patient. In that case, the expert system predicted the score lower (for two values) than the scores given by both raters. By recording and analysing the data from the larger pool of subjects, decision boundaries could be fine-tuned providing even better results.

Example results of the developed clinical support for two patients are presented in Figure 7.14. The first patient performed wider and slower finger taps (quantified with higher values for the α_{av} feature and lower values for the $f_{av}^{(i)}$ feature). Furthermore, during the performance, this patient experienced significant amplitude decrement after the first tapping cycle (quantified with the i_{dec} feature), which represented the criterium for assigning the score $S_{FT} = 3$. The second patient performed the finger-tapping with more considerable variations in speed and amplitude, with the appearance of four hesitations and one freeze. A large number of irregularities resulted in the score $S_{FT} = 3$. Although their performances were different, both patients were equally scored not only by the expert system but also by both neurologists. Based on the instructions provided in the UPDRS scale, one score is given if any of the evaluation criteria is satisfied (tapping amplitude, speed, amplitude decrement, or hesitations/freezes). In the case when different patients satisfy different criteria for obtaining the same score, their performances cannot be compared. This raises a question: is a scale with only four grades sufficient for evaluating such complex movements? In order to solve this problem, in the literature, continuous scoring is proposed for the evaluation of repetitive movements. Although such solutions provide more thorough scoring, the continuous evaluation does not correspond to a standardized clinical scoring system and, therefore, may be confusing and not fully applicable for physicians. Because of that, the presented expert system can provide the final score, but also scores for individual movement properties. Furthermore, the result of the developed support includes graphical representation of the movement amplitude, together with metrics describing important movement properties. The metrics are provided in a form that is intuitive and understandable for the potential end-users (neurologists). In this way, the results of the different or the same patient can be compared.

The list of subjects included patients with idiopathic Parkinson's disease and two types of atypical parkinsonism, as well as healthy controls. The inclusion of different forms of parkinsonism (both typical and atypical) allowed developed analysis and metrics to be examined for different symptom manifestations. In addition, the calculated parameters showed some differences between groups (especially visible for the features describing finger-tapping speed and movement smoothness), which proved their potential for distinguishing patients with different forms of parkinsonism. Furthermore, by applying the developed analysis to the recordings of healthy subjects, it was possible to test and determine the normal characteristics of the tapping movement.

Although the movement analysis and expert system were validated on the example of the finger-tapping movement, developed decision support is completely applicable and adjustable for all clinically relevant repetitive movements that are used for evaluation of bradykinesia symptom. The evaluation criteria are the same for these movements (which besides finger-tapping includes hand opening-closing, hand pronation-supination, and foot-tapping), and therefore the developed analysis can be easily adapted and applied for all these movements.

8. Decision support system for assessment of patients with neurodegenerative disorders: Presentation of results on the example of one patient

The results of the developed support are presented on the example of one male patient (ID: M.M.). In 2015, the patient came to the Clinic of Neurology, Clinical Centre of Serbia, School of Medicine, University of Belgrade, Belgrade, Serbia. At the time, he was 64 years old, with no other medical history. During the visit, the gait of this patient was recorded using the wearable wireless sensors system. The patient M.M. walked along a straight path for 8 s. The observed and processed walking sequence had 14 feature dimensions including normalized ground reaction force GRF_N, 3 accelerometer axes $a_{x,y,z}$ and 3 gyroscope axes $\omega_{x,y,z}$, as shown in Figure 8.1. The data was fed to developed deep learning models: long short-term memory network and convolutional neural network. In Figure 8.1 right panel, the results of the decision support are presented in the form of a probability that that patient had PD, separately for the LSTM and CNN models.

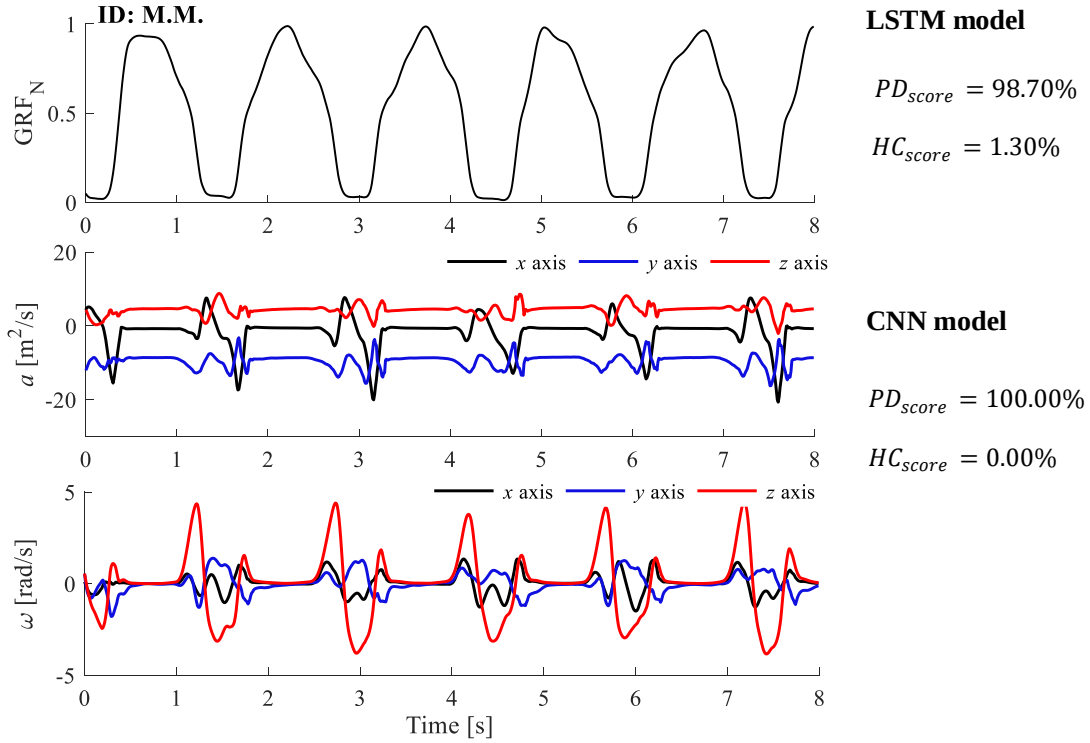

Figure 8.1 Presentation of the recorded walking sequence (data recorded from the more affected leg), together with the results given by the two deep learning models.

As shown, both models suggested that the patient M.M. had PD, with high probability (98.7% by the LSTM and 100% by the CNN model). The output given by the decision support based on deep learning models was presented in a way that is intuitive and understandable for the clinicians. The results agreed and supported the diagnosis given by two specialists in movement disorders.

A severe progression of the disease was observed in the following years, with more expressed bradykinesia symptom. During the visit to the Clinic of Neurology, the examination of the patient's motor abilities was executed. The patient performed the finger-tapping test for 15 s following the instructions provided in the UPDRS test and the measurement procedure (as introduced in Chapter 6). The movement was recorded with a miniature inertial sensor system and processed using the developed method for the objective movement analysis (as defined in Chapters 6 and 7). The symptom severity was evaluated using the developed expert system for the prediction of clinical scores (as shown in Figure 8.2).

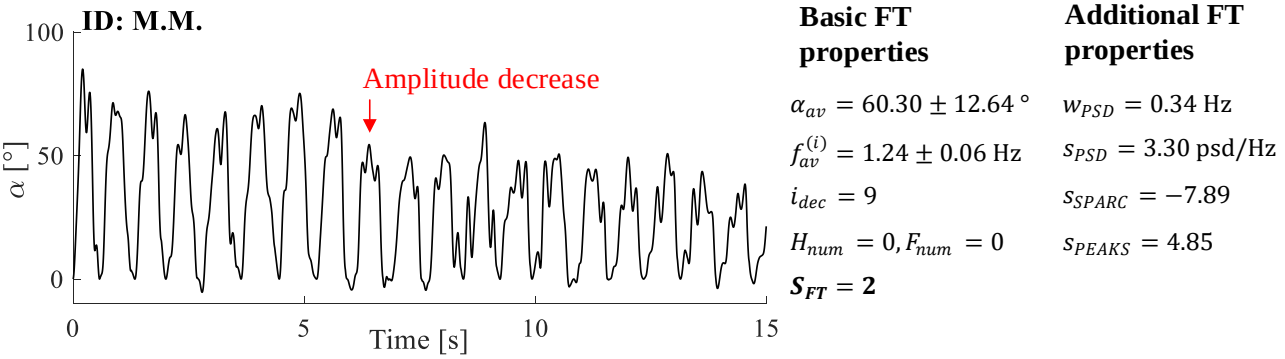

Figure 8.2 Presentation of the calculated finger-tapping movement amplitude, together with the metric describing important biomechanical properties and bradykinesia severity score.

During the examination, the patient performed wider but slower finger taps, with no hesitations nor freezes. The significant decrement in the movement amplitude was visible after the 9th tap. The decision support system predicted the bradykinesia severity score of $S_{FT} = 2$. Additional movement properties are shown as well, including features describing smoothness and intra-variability of the movement. Although the movement was not smooth, its variability was not significantly expressed. This indicated the presence of another symptom during the examination – tremor. In this way, a detailed and precise analysis of the movement is given as the output of the developed decision support, providing detailed insight into the patient's motor state and abilities.

9. Conclusion

9.1. Contribution of dissertation

The contribution of the research presented in this thesis primarily includes the research and development of a new intelligent clinical decision support system. The presented tool provides an objective, automatic and precise assessment of patients with neurodegenerative diseases, supporting disease recognition and evaluation of symptom severity in these patients. Analysis of repetitive hand and leg movements represents the basis of the developed system. The observed movements are part of standardized clinical motor tests or everyday activities.

The system has a high practical value. Movement patterns are captured using small, lightweight, and simple wireless wearable sensors. The necessary measurement systems do not require complicated set-up and can be easily applied in both clinical and everyday environments. Although in this system custom-made sensors are used, the designed DSS can be applied with any sensors that allow recording of inertial or force data in the same manner.

The system is a hybrid; different parts of the system apply diverse types of reasoning. Intelligent algorithms are carefully selected and designed to meet all the necessary requirements of the desired clinical decision support, type of performed movement analysis, and expected outcomes. The whole processing is automatic, repeatable and does not require any manual work or engineering skills of potential end-users to implement it.

The system is designed as a suggestion DSS – the clinical staff can seek for an assistance or a consultation while assessing the patients with neurodegenerative disorders. Because of that, the result is presented in a form that is intuitive and understandable for the potential end-users. It includes a graphical presentation of the analysed signals and parametric values that describe important movement properties and provide a diagnostic recommendation or symptom severity score.

Objective and automatic decision support for recognizing patients in the early stage of the disease development

The first part of the developed support is dedicated to the provision of objective identification of PD based on the intelligent and automatic analysis of the human gait. The support was developed using the nonknowledge-based reasoning, since it does not require any apriori knowledge about the observed problem.

For that purpose, deep learning models were designed. The initial database was augmented with walking segments of different sizes, which were segmented using two different techniques. The augmentation strategies provided several datasets (containing from a few hundred to a few thousand samples) for training and testing. The models were evaluated on a subject level: model performance was tested using data from a previously unseen subject. In this way, it was assured that the deep learning algorithms learned features that described subjects' health status and not some other intrinsic properties of the subject's gait related to their identity.

Developed deep learning models distinguished PD patients from healthy controls with high accuracy (above 90%). Recognition of PD patients in the early stage of the disease development was also performed with very good accuracy (above 80%). Although LSTM models are designed to find long-term dependencies in data, CNN outperformed LSTM for both classification tasks, proving great capabilities of these deep learning algorithms.

In addition to high accuracy results, the performed study has another important contribution – examination of the influence that walking duration and conditions might have on the efficiency of designed models. Although recognition of PD is based on very short sequences, and for those, high accuracy results are obtained, longer walking sequences would probably contribute to even better identification of PD in the early stage of the disease, especially in the case of the LSTM network. Walking segments that were recorded with a cognitive occupation were in larger percent correctly classified. These results showed that cognitive load while walking caused meaningful changes in the gait and contributed to more efficient early PD recognition. The literature already suggested that executive functions are impaired early in PD, which is demonstrated in an inability to separate the cognitive resources that are required for the simultaneous performance of different activities [150]. The obtained results complied with these conclusions and showed possible directions for the future development of the objective and automatic diagnosis of patients with neurodegenerative disorders.

The developed and presented method is the first that implements deep learning algorithms for automatic and objective early PD recognition, based on gait data recorded with wireless, wearable sensors. One may wonder why this is important. Deep learning algorithms process raw data; they do not require a high level of engineering skills for developing features that can capture desired patterns and subtle changes in data. In the practical sense, developed DL models have high potential – they can be easily applied for new previously unseen data; they are repeatable, automatic and do not require complicated data processing or apriori medical knowledge. The output is provided in the form of a probability that a person might have Parkinson's disease. The designed models are not too complex, which is especially notable for the LSTM model, which required training of only 56,301 parameters. Therefore, developed models can be easily applied to some mobile or web platforms and accessible for a large number of potential users.

Furthermore, the designed support is based on one of the most common everyday human activities – walking. Having a tool that can detect the appearance of one of the most common neurodegenerative disorders based on just a few strides may contribute to more efficient and widespread early recognition of this disease and consequently improve disease treatment and progress monitoring from its early stage. Additionally, the gait data is recorded with simple, inexpensive instrumentation that does not require a complicated set-up, and it can be applied at any time and any place. Therefore, presented support has high applicability and potential for the provision of automatic

and objective recognition of PD in the clinical environment, but also for the everyday self-management of healthy people that might have a predisposition to develop this disease.

A better understanding of analysed motor patterns and specific changes that may be visible in the recorded signals

The second part of the decision support system allows assessment of the bradykinesia severity using repetitive hand and leg movements. These movements represent standardized clinical motor tests, and they are of crucial importance for evaluating PD symptoms.

Firstly, the method for capturing and calculating the amplitude of these movements is defined and presented. The method includes the definition of the measurement procedure and instrumentation, as well as the algorithm for calculating the movement amplitude. The procedure for recording movements is simple, repeatable, and in agreement with the standardized clinical testing protocols. The measurement system is lightweight, easy to mount, and does not interrupt subjects' natural performance. The algorithm for calculating the movement amplitude was initially developed and validated for the finger-tapping test [134]. In this thesis, the algorithm is extended to the other three movements as well: hand opening/closing, hand pronation/supination, and toe-tapping. The particularly significant contribution is a detailed analysis of the motion patterns, which included a definition of movement phases, and characteristic changes that are related to specific movement events, such as "zero posture" of the fingers or hand, maximum amplitude, moments representing the transitions between the successive phases, and others. The preformed analysis served as the basis for the development of a new algorithm for the segmentation of these repetitive movements, which is automatic and precise, and it can be applied for both normal and endangered movement patterns because it is adaptive to the intrinsic movement properties. The performed detailed analysis represents a significant basis for further analysis of these important hand and leg movements.

New metrics describing important biomechanical movement properties

Performed analysis of fast repetitive hand and leg movements resulted in new metrics. Feature extraction is fully automatized, simple, repeatable, and does not require any manual or individual processing. Signal processing techniques were carefully selected for each feature individually. The developed parametrization has two sets. The first, basic set, comprises features that completely quantify standardized movement properties: amplitude, speed, amplitude decrement, and hesitations/freezes that may appear during the performance. For that purpose, time-frequency analysis, numerical analysis and thresholding techniques were applied. Designed parameters are presented in a form that is intuitive and understandable for physicians. The feature extraction is adaptable to the inherent properties of each individual signal. Therefore, developed movement analysis can be easily applied to new signals that were not used during the design and validation of the method itself.

The metrics are complemented with some additional features describing other movement properties as well. These motion characteristics do not represent part of the standardized clinical evaluation; however, during the extensive search and examination of the used database, some specifics in the movement patterns were observed that might be of interest to neurologists for the long-term monitoring of patients and comparison with other patients. These include smoothness of the movement and movement intra-variability, which were described with some simple and

repeatable signal processing techniques. The features were designed with a time- and frequency-domain signal processing techniques.

Furthermore, the results of the statistical analysis showed that the developed metrics have great potential for differential diagnosis of parkinsonism and related disorders.

Automatic prediction of clinical scores based on the expert system

Developed support implements a new expert system for the prediction of clinical scores and symptom severity. The expert system predicted scores with high accuracy of 88.16% for comparison with the reference data given by two specialists in movement disorders.

Although machine learning algorithms could predict scores with high accuracy, in that case, prediction of scores would require the use of labels that are visually estimated by neurologists. As it was already mentioned, evaluation efficiency severely depends on the examiner's knowledge and experience, and therefore, the decision-making process is prone to subjectivity. The use of subjectively estimated labels can cause subjectivity in the learning model and its results as well. Because of that, this thesis offers a different approach to solve this problem. Since UPDRS scale encompasses domain-specific knowledge that is expressed though the clinical evaluation criteria, prediction of clinical scores was performed using the knowledge-based reasoning. The expert rules for the discrete movement properties (the serial number of the tap with significant amplitude drop and the number of hesitations/freezes) completely matched clinical rules and instructions for assigning scores. In the case of continuous features (such as the amplitude and speed), the medical knowledge does not comprise precisely defined criteria. Because of that, decision boundaries were defined using a clustering technique. The clustering allowed the definition of expert rules based on a natural grouping of data that was obtained from healthy subjects and randomly selected pool of patients. In addition to the score describing the bradykinesia severity, the system can also output the sub-scores evaluating the individual movement properties. Therefore, all movement characteristics are considered simultaneously for providing the final score.

Furthermore, this is the only solution that observes the natural inter-subject diversity of these movements. The extensive search and analysis of the used database showed that subjects perform the finger-tapping movement in two different ways: 1) wider but slower finger taps and 2) narrower but faster finger taps. When reasoning, the presented expert system also considers the type of movement, and based on that, applies the corresponding set of decision boundaries. In this way, the patient's understanding of the given task does not influence the decision-making process. The whole procedure is objective and automatic – the movement is automatically assigned to one movement type, and the corresponding set of decision boundaries is selected.

The result of the support comprises a graphical presentation of the calculated movement amplitude, detected movement irregularities and disturbances, calculated feature sets describing important movement properties, and scores for prediction of symptom severity. Developed support represents a valuable and practical tool that can assist neurologists. It provides an automatic and objective assessment of bradykinesia, evaluation of symptom severity through prediction of clinical scores, monitoring of disease progress and response to therapy, and comparison with other patients.

The expert system was validated on the example of the finger-tapping test; however, it is fully applicable for other bradykinesia related movements as well. Instructions for evaluating these four

movements are the same, including movement properties that should be observed and rules for assigning scores. The movements differ only in the manner how movements are performed, and their amplitude is observed, which is also analysed in this thesis. Therefore, although the expert system was only validated on the example of the finger-tapping test, the developed analysis and expert system are fully adaptable and applicable for other movements as well, proving the high practical value of the developed support.

Validation of the developed decision support system on different groups of subjects

The intelligent algorithms, developed and presented in this thesis, were validated on several groups of subjects. The patient groups reflected many features of real clinical cases, which enabled the examination of the developed algorithms for a wide range of movement impairments. Data recorded on healthy subjects allowed the definition of "normal" or reference movement patterns. Designed deep learning models were cross-validated using the gait data recorded from PD patients in different stages of the disease development. The particular focus was given to identifying patients with PD in its early stage when symptoms endangering their gait are not significantly expressed and visible.

Objective and automatic support for the assessment of bradykinesia symptom was validated on the pool of patients, that included patients with several neurodegenerative disorders, more specifically typical and atypical forms of parkinsonism, patients in different stages of the disease, and different stages of the bradykinesia severity (ranging from normal to severely impaired motions). The developed and presented movement analysis, and expert system gave high accuracy results for all patient groups, regardless of the disease stage and bradykinesia severity, showing the great practical potential of developed support for patients with different types of parkinsonism and different symptom manifestations. Most studies only included patients evaluated with the test score up to 3. In this thesis, several patients with the highest degree of bradykinesia severity were included. Those patients performed the finger-tapping test very badly, expressing multiple movement disturbances simultaneously. This caused their movement to be scored with the highest score, by both neurologists and the expert system. In this way, the applicability of the developed support was examined for the full range of scores 0-4.

9.2. Perspective and future research

Extension of the developed system for other neurodegenerative disorders or tasks

The obtained results gave potential directions for the future improvement and extensions of the developed decision support system. The support will be extended to other neurodegenerative disorders as well. This advancement primarily includes the differentiation of typical and atypical forms of parkinsonism. In this thesis, it was shown that developed analysis of bradykinesia has great diagnostic potential. These results represent a significant basis for future research, which will be directed towards designing appropriate features that can capture significant patterns in movement data and contribute to the precise differentiation of these patient groups. Furthermore, obtained results showed that cognitive dual-tasking and longer sequences might play a significant role in the precise early PD identification. Due to that, an effort will be put in developing experimental protocols that can contribute to even better identification of PD patients in the early stage of disease development or differential diagnosis with other neurodegenerative disorders.

As for the expert system, planned extensions include validation of developed algorithms on other bradykinesia related movements: hand opening/closing, hand pronation/supination and toe-tapping. Furthermore, expansion of the entire system is planned, which will include the development of an objective and automatic support for the assessment of other PD symptoms, such as tremor, rigidity, postural instability, and others.

Collaboration with other groups for more widespread validation of the developed system

The main limitation of the developed system is a relatively small number of included subjects. This represents the burning issue in the field of sensor-derived assessment of patients with neurodegenerative disorders. Most research groups working in this field have collaboration with medical institutions and put a lot of effort and resources to collect enough data for developing and validating their intelligent algorithms. Data acquisition typically requires a lot of time and results with only a few dozen of analysed patients, which is not enough to have a clinically acceptable system. Therefore, the validation of developed decision support would benefit from increased and widespread collaboration among different research groups in the world. Aligning experiment protocols, validating algorithms using data recorded with measurement systems of different manufacturers or from patients of different demographic features, and sharing data among researchers would provide a good basis for the development of large-scale databases and more precise and clinically acceptable systems.

Development of an intuitive graphical interface

In the future, a developed decision support system should be developed in the form of a mobile or web application. This advancement would enable the system to be used by a larger number of users, and it would additionally improve the accessibility and practical value of the developed support.

The software application should have an intuitive and simple graphical interface, protected with a password. It should provide a graphical presentation of recorded signals, numerical results of features, diagnostic recommendations, scores and sub-scores, and statistical analysis. Furthermore, the collected data should be saved for later analysis and monitoring and exported in a form that is suitable for reporting and compatible with local electronic health records.

References

[1] B. Eta S., *Clinical decision support systems*. New York: Springer Science+ Business Media, LLC., 2007.

[2] M. A. Musen, B. Middleton, and R. A. Greenes, "Clinical decision-support systems," in *Biomedical Informatics: Computer Applications in Health Care and Biomedicine: Fourth Edition*, 2014.

[3] J. P. Shim, M. Warkentin, J. F. Courtney, D. J. Power, R. Sharda, and C. Carlsson, "Past, present, and future of decision support technology," *Decis. Support Syst.*, vol. 33, no. 2, pp. 111–126, Jun. 2002.

[4] M. M. Baig, H. GholamHosseini, A. A. Moqeem, F. Mirza, and M. Lindén, "A Systematic Review of Wearable Patient Monitoring Systems – Current Challenges and Opportunities for Clinical Adoption," *J. Med. Syst.*, vol. 41, no. 7, pp. 1–9, Jul. 2017.

[5] S. C. Mukhopadhyay, "Wearable sensors for human activity monitoring: A review," *IEEE Sensors Journal*, vol. 15, no. 3. Institute of Electrical and Electronics Engineers Inc., pp. 1321–1330, 2015.

[6] A. M. Sabatini, "Inertial sensing in biomechanics: A survey of computational techniques bridging motion analysis and personal navigation," in *Computational Intelligence for Movement Sciences: Neural Networks and Other Emerging Techniques*, 2006.

[7] A. Wang, G. Chen, J. Yang, S. Zhao, and C. Y. Chang, "A Comparative Study on Human Activity Recognition Using Inertial Sensors in a Smartphone," *IEEE Sens. J.*, vol. 16, no. 11, pp. 4566–4578, Jun. 2016.

[8] S. Russel and P. Norvig, *Artificial intelligence—a modern approach 3rd Edition*. 2012.

[9] P. Jackson, *Introduction to Expert System*. Addison-Wesley Longman Publishing Co., Inc.75 Arlington Street, Suite 300 Boston, MAUnited States, 1998.

[10] J. P. Ignizio, "A brief introduction to expert systems," *Comput. Oper. Res.*, vol. 17, no. 6, pp. 523–533, Jan. 1990.

[11] G. Schreiber *et al.*, *Knowledge Engineering and Management: the CommonKADS Methodology*. MIT press, 2000.

[12] B. G. Buchanan and E. A. Feigenbaum, "Dendral and Meta-Dendral," in *Readings in Artificial Intelligence*, Elsevier, 1981, pp. 313–322.

[13] E. H. Shortliffe, "Computer-based medical consultations: MYCIN." American Elsevier Publishing Co. New York, 1976.

[14] P. E. Hart, R. O. Duda, and M. T. Einaudi, "PROSPECTOR-A computer-based consultation system for mineral exploration," *J. Int. Assoc. Math. Geol.*, vol. 10, no. 5, pp. 589–610, Oct. 1978.

[15] I. Goodfellow, Y. Bengio, A. Courville, and Y. Bengio, *Deep learning*. Cambridge: MIT press, 2016.

[16] M. Sokolova and G. Lapalme, "A systematic analysis of performance measures for classification tasks," *Inf. Process. Manag.*, vol. 45, no. 4, pp. 427–437, Jul. 2009.

[17] J. L. Semmlow and B. Griffel, *Biosignal and Biomedical Image Processing*. CRC press, 2014.
[18] Y. Lecun, Y. Bengio, and G. Hinton, "Deep learning," *Nature*, vol. 521, no. 7553. Nature Publishing Group, pp. 436–444, 27-May-2015.
[19] A. Krizhevsky, I. Sutskever, and G. E. Hinton, "ImageNet Classification with Deep Convolutional Neural Networks," in *Advances in neural information processing systems*, 2012, pp. 1097–1105.
[20] C. Farabet, C. Couprie, L. Najman, and Y. Lecun, "Learning hierarchical features for scene labeling," *IEEE Trans. Pattern Anal. Mach. Intell.*, vol. 35, no. 8, pp. 1915–1929, 2013.
[21] T. Mikolov, A. Deoras, D. Povey, L. Burget, and J. Černocký, "Strategies for training large scale neural network language models," in *2011 IEEE Workshop on Automatic Speech Recognition and Understanding, ASRU 2011, Proceedings*, 2011, pp. 196–201.
[22] G. Hinton *et al.*, "Deep neural networks for acoustic modeling in speech recognition: The shared views of four research groups," *IEEE Signal Process. Mag.*, vol. 29, no. 6, pp. 82–97, 2012.
[23] M. Abbasi and S. K. Sweden, "Clinical Decision Support Systems: A discussion on different methodologies used in Health Care," *Marlaedalen University Sweden*. 2006.
[24] W. H. Organization, "mHealth: new horizons for health through mobile technologies.," *mHealth new horizons Heal. through Mob. Technol.*, 2011.
[25] B. Martínez-Pérez, I. De La Torre-Díez, M. López-Coronado, B. Sainz-De-Abajo, M. Robles, and J. M. García-Gómez, "Mobile clinical decision support systems and applications: A literature and commercial review," *J. Med. Syst.*, vol. 38, no. 1, pp. 1–10, Jan. 2014.
[26] J. B. Martin, "Molecular basis of the neurodegenerative disorders," *New England Journal of Medicine*, vol. 340, no. 25. Massachusetts Medical Society , pp. 1970–1980, 24-Jun-1999.
[27] E. Ray Dorsey *et al.*, "Global, regional, and national burden of Parkinson's disease, 1990–2016: a systematic analysis for the Global Burden of Disease Study 2016," *Lancet Neurol.*, vol. 17, no. 11, pp. 939–953, Nov. 2018.
[28] "Statistical Office of the Republic of Serbia." [Online]. Available: https://publikacije.stat.gov.rs/G2017/Pdf/G20171175.pdf. [Accessed: 21-Aug-2020].
[29] E. R. Dorsey *et al.*, "Projected number of people with Parkinson disease in the most populous nations, 2005 through 2030," *Neurology*, vol. 68, no. 5, pp. 384–386, Jan. 2007.
[30] W. Dauer and S. Przedborski, "Parkinson's disease: Mechanisms and models," *Neuron*, vol. 39, no. 6. Cell Press, pp. 889–909, 11-Sep-2003.
[31] J. Jankovic, "Parkinson's disease: Clinical features and diagnosis," *Journal of Neurology, Neurosurgery and Psychiatry*, vol. 79, no. 4. BMJ Publishing Group, pp. 368–376, 01-Apr-2008.
[32] A. Samii, J. G. Nutt, and B. R. Ransom, "Parkinson's disease," in *Lancet*, 2004.
[33] A. Berardelli, J. C. Rothwell, P. D. Thompson, and M. Hallett, "Pathophysiology of bradykinesia in parkinson's disease," *Brain*, vol. 124, no. 11. Oxford University Press, pp. 2131–2146, 01-Nov-2001.
[34] M. Pistacchi *et al.*, "Gait analysis and clinical correlations in early Parkinson's disease," *Funct. Neurol.*, vol. 32, no. 1, p. 28, 2017.
[35] M. M. Hoehn and M. D. Yahr, "Parkinsonism: Onset, progression and mortality.," *Neurology*, vol. 50, no. 2, p. 318, 1998.
[36] W. Poewe and G. Wenning, "The differential diagnosis of Parkinson's disease," *Eur. J. Neurol.*, vol. 9, no. s3, pp. 23–30, Nov. 2002.
[37] M. J. Armstrong and M. S. Okun, "Time for a New Image of Parkinson Disease," *JAMA Neurology*. American Medical Association, 2020.
[38] A. J. Hughes, S. E. Daniel, L. Kilford, and A. J. Lees, "Accuracy of clinical diagnosis of idiopathic Parkinson's disease: A clinico-pathological study of 100 cases," *J. Neurol. Neurosurg. Psychiatry*, vol. 55, no. 3, pp. 181–184, Mar. 1992.
[39] C. H. Adler *et al.*, "Low clinical diagnostic accuracy of early vs advanced Parkinson disease: Clinicopathologic study," *Neurology*, 2014.

[40] C. G. Goetz *et al.*, "*Movement* Disorder Society Task Force report on the Hoehn and Yahr staging scale: Status and recommendations The *Movement* Disorder Society Task Force on rating scales for Parkinson's disease," *Mov. Disord.*, vol. 19, no. 9, pp. 1020–1028, Sep. 2004.
[41] R. M. of the U. D. C. Fahn, S; Elton, "The Unified Parkinson's Disease Rating Scale," *Recent Dev. Park. Dis. Vol 2*, pp. 153–163, 293–304, 1987.
[42] C. G. Goetz *et al.*, "MDS-UPDRS," 2008.
[43] D. Bone, C. C. Lee, T. Chaspari, J. Gibson, and S. Narayanan, "Signal Processing and Machine Learning for Mental Health Research and Clinical Applications [Perspectives]," *IEEE Signal Processing Magazine*, vol. 34, no. 5. Institute of Electrical and Electronics Engineers Inc., 01-Sep-2017.
[44] M. Belić, V. Bobić, M. Badža, N. Šolaja, M. Đurić-Jovičić, and V. S. Kostić, "Artificial intelligence for assisting diagnostics and assessment of Parkinson's disease—A review," *Clinical Neurology and Neurosurgery*, vol. 184. Elsevier B.V., p. 105442, 01-Sep-2019.
[45] M. Little, P. McSharry, E. Hunter, J. Spielman, and L. Ramig, "Suitability of dysphonia measurements for telemonitoring of Parkinson's disease," *Nat. Preced.*, pp. 1–1, Sep. 2008.
[46] A. Tsanas, M. A. Little, P. E. McSharry, and L. O. Ramig, "Accurate telemonitoring of parkinsons disease progression by noninvasive speech tests," *IEEE Trans. Biomed. Eng.*, vol. 57, no. 4, pp. 884–893, Apr. 2010.
[47] C. R. Pereira *et al.*, "A new computer vision-based approach to aid the diagnosis of Parkinson's disease," *Comput. Methods Programs Biomed.*, vol. 136, pp. 79–88, Nov. 2016.
[48] A. Naseer, M. Rani, S. Naz, M. I. Razzak, M. Imran, and G. Xu, "Refining Parkinson's neurological disorder identification through deep transfer learning," *Neural Comput. Appl.*, vol. 32, no. 3, pp. 839–854, Feb. 2020.
[49] C. Lainscsek *et al.*, "Finger tapping movements of Parkinson's disease patients automatically rated using nonlinear delay differential equations," *Chaos An Interdiscip. J. Nonlinear Sci.*, vol. 22, no. 1, p. 013119, Mar. 2012.
[50] F. Wahid, R. K. Begg, C. J. Hass, S. Halgamuge, and D. C. Ackland, "Classification of Parkinson's disease gait using spatial-temporal gait features," *IEEE J. Biomed. Heal. Informatics*, 2015.
[51] A. Procházka, O. Vyšata, M. Vališ, O. ̊upa, M. Schätz, and V. Mařík, "Bayesian classification and analysis of gait disorders using image and depth sensors of Microsoft Kinect," *Digit. Signal Process. A Rev. J.*, 2015.
[52] C. G. Pachón-Suescún, J. O. Pinzón-Arenas, and R. Jiménez-Moreno, "Abnormal gait detection by means of LSTM," *Int. J. Electr. Comput. Eng.*, vol. 10, no. 2, pp. 1495–1506, 2020.
[53] S. Arora *et al.*, "Detecting and monitoring the symptoms of Parkinson's disease using smartphones: A pilot study," *Park. Relat. Disord.*, 2015.
[54] N. Kostikis, D. Hristu-Varsakelis, M. Arnaoutoglou, and C. Kotsavasiloglou, "A smartphone-based tool for assessing parkinsonian hand tremor," *IEEE J. Biomed. Heal. Informatics*, 2015.
[55] L. Fraiwan, R. Khnouf, and A. R. Mashagbeh, "Parkinsons disease hand tremor detection system for mobile application," *J. Med. Eng. Technol.*, 2016.
[56] V. N. Bobić, M. D. Đurić-Jovičić, S. M. Radovanović, N. T. Dragašević, V. S. Kostić, and M. B. Popović, "Classification of parkinsonism based on foot tapping test," in *5th International Conference on Electrical, Electronic and Computing Engineering*, 2018, pp. BTI1-5.
[57] M. D. Djurić-Jovičić *et al.*, "Implementation of continuous wavelet transformation in repetitive finger tapping analysis for patients with PD," in *2014 22nd Telecommunications Forum, TELFOR 2014 - Proceedings of Papers*, 2014.
[58] M. Delrobaei, S. Tran, G. Gilmore, K. McIsaac, and M. Jog, "Characterization of multi-joint upper limb movements in a single task to assess bradykinesia," *J. Neurol. Sci.*, vol. 368, pp. 337–342, Sep. 2016.
[59] A. Garza-Rodríguez, L. P. Sánchez-Fernández, L. A. Sánchez-Pérez, C. Ornelas-Vences, and M. Ehrenberg-Inzunza, "Pronation and supination analysis based on biomechanical signals

from Parkinson's disease patients," *Artif. Intell. Med.*, vol. 84, pp. 7–22, Jan. 2018.
[60] J. Stamatakis *et al.*, "Finger Tapping Clinimetric Score Prediction in Parkinson's Disease Using Low-Cost Accelerometers," *Comput. Intell. Neurosci.*, vol. 2013, pp. 1–13, 2013.
[61] F. Cuzzolin *et al.*, "Metric learning for Parkinsonian identification from IMU gait measurements," *Gait Posture*, 2017.
[62] W. Zeng, F. Liu, Q. Wang, Y. Wang, L. Ma, and Y. Zhang, "Parkinson's disease classification using gait analysis via deterministic learning," *Neurosci. Lett.*, 2016.
[63] I. El Maachi, G. A. Bilodeau, and W. Bouachir, "Deep 1D-Convnet for accurate Parkinson disease detection and severity prediction from gait," *Expert Syst. Appl.*, vol. 143, p. 113075, Apr. 2020.
[64] S. Patel *et al.*, "Monitoring motor fluctuations in patients with parkinsons disease using wearable sensors," *IEEE Trans. Inf. Technol. Biomed.*, 2009.
[65] A. M. S. Muniz *et al.*, "Comparison among probabilistic neural network, support vector machine and logistic regression for evaluating the effect of subthalamic stimulation in Parkinson disease on ground reaction force during gait," *J. Biomech.*, 2010.
[66] M. Djurić-Jovičić, M. Belić, I. Stanković, S. Radovanović, and V. S. Kostić, "Selection of gait parameters for differential diagnostics of patients with de novo Parkinson's disease," *Neurol. Res.*, 2017.
[67] L. Giancardo *et al.*, "Computer keyboard interaction as an indicator of early Parkinson's disease," *Sci. Rep.*, 2016.
[68] T. D. Pham, K. Wardell, A. Eklund, and G. Salerud, "Classification of short time series in early Parkinson's disease with deep learning of fuzzy recurrence plots," *IEEE/CAA J. Autom. Sin.*, vol. 6, no. 6, pp. 1306–1317, Nov. 2019.
[69] C. Gao *et al.*, "Objective assessment of bradykinesia in Parkinson's disease using evolutionary algorithms: Clinical validation," *Transl. Neurodegener.*, 2018.
[70] M. A. Lones *et al.*, "Evolving classifiers to recognize the movement characteristics of parkinson's disease patients," *IEEE Trans. Evol. Comput.*, 2014.
[71] M. Djurić-Jovičić *et al.*, "Finger tapping analysis in patients with Parkinson's disease and atypical parkinsonism," *J. Clin. Neurosci.*, vol. 30, pp. 49–55, Aug. 2016.
[72] Z. Lin *et al.*, "Quantification of Parkinsonian Bradykinesia Based on Axis-Angle Representation and SVM Multiclass Classification Method," *IEEE Access*, vol. 6, pp. 26895–26903, 2018.
[73] N. Piro *et al.*, "Analysis and Visualization of 3D Motion Data for UPDRS Rating of Patients with Parkinson's Disease," *Sensors*, vol. 16, no. 6, p. 930, Jun. 2016.
[74] C. Ornelas-Vences, L. P. Sánchez-Fernández, L. A. Sánchez-Pérez, and J. M. Martínez-Hernández, "Computer model for leg agility quantification and assessment for Parkinson's disease patients," *Med. Biol. Eng. Comput.*, vol. 57, no. 2, pp. 463–476, Feb. 2019.
[75] M. Djuric-Jovicic *et al.*, "Finger and foot tapping sensor system for objective motor assessment," *Vojnosanit. Pregl.*, vol. 75, no. 1, pp. 68–77, 2018.
[76] H. Jeon *et al.*, "Automatic classification of tremor severity in Parkinson's disease using awearable device," *Sensors (Switzerland)*, 2017.
[77] G. Rigas *et al.*, "Assessment of tremor activity in the parkinsons disease using a set of wearable sensors," *IEEE Trans. Inf. Technol. Biomed.*, 2012.
[78] J. C. van den Noort *et al.*, "Quantification of Hand Motor Symptoms in Parkinson's Disease: A Proof-of-Principle Study Using Inertial and Force Sensors," *Ann. Biomed. Eng.*, vol. 45, no. 10, pp. 2423–2436, Oct. 2017.
[79] S. H. Roy *et al.*, "High-resolution tracking of motor disorders in Parkinson's disease during unconstrained activity," *Mov. Disord.*, 2013.
[80] D. J. Cook, M. Schmitter-Edgecombe, and P. Dawadi, "Analyzing activity behavior and movement in a naturalistic environment using smart home techniques," *IEEE J. Biomed. Heal. Informatics*, 2015.
[81] Y. Sano *et al.*, "Quantifying Parkinson's disease finger-tapping severity by extracting and

synthesizing finger motion properties," *Med. Biol. Eng. Comput.*, vol. 54, no. 6, pp. 953–965, Jun. 2016.
[82] J. M. Hausdorff, A. Lertratanakul, M. E. Cudkowicz, A. L. Peterson, D. Kaliton, and A. L. Goldberger, "Dynamic markers of altered gait rhythm in amyotrophic lateral sclerosis," *J. Appl. Physiol.*, vol. 88, no. 6, pp. 2045–2053, Jun. 2000.
[83] C. Tucker *et al.*, "A data mining methodology for predicting early stage Parkinson's disease using non-invasive, high-dimensional gait sensor data," *IIE Trans. Healthc. Syst. Eng.*, 2015.
[84] M. Alam, T. Tabassum, K. Munia, and K. Tavakolian, "A Quantitative Assessment of Bradykinesia Using Inertial Measurement Unit Performance Measurement View project Signal-Image Processing View project," 2017.
[85] B. E. Sakar *et al.*, "Collection and analysis of a Parkinson speech dataset with multiple types of sound recordings," *IEEE J. Biomed. Heal. Informatics*, vol. 17, no. 4, pp. 828–834, 2013.
[86] "The HandPD dataset." [Online]. Available: http://wwwp.fc.unesp.br/~papa/pub/datasets/Handpd/. [Accessed: 28-Sep-2020].
[87] C. R. Pereira, S. A. T. Weber, C. Hook, G. H. Rosa, and J. P. Papa, "Deep learning-aided Parkinson's disease diagnosis from handwritten dynamics," in *Proceedings - 2016 29th SIBGRAPI Conference on Graphics, Patterns and Images, SIBGRAPI 2016*, 2017, pp. 340–346.
[88] "Gait in Parkinson's Disease v1.0.0." [Online]. Available: https://physionet.org/content/gaitpdb/1.0.0/. [Accessed: 28-Sep-2020].
[89] "Gait in Neurodegenerative Disease Database v1.0.0." [Online]. Available: https://physionet.org/content/gaitndd/1.0.0/. [Accessed: 28-Sep-2020].
[90] E. Rovini, C. Maremmani, and F. Cavallo, "How wearable sensors can support parkinson's disease diagnosis and treatment: A systematic review," *Frontiers in Neuroscience*. 2017.
[91] W. L. Zuo, Z. Y. Wang, T. Liu, and H. L. Chen, "Effective detection of Parkinson's disease using an adaptive fuzzy k-nearest neighbor approach," *Biomed. Signal Process. Control*, vol. 8, no. 4, pp. 364–373, Jul. 2013.
[92] M. Shahbakhi, D. T. Far, and E. Tahami, "Speech Analysis for Diagnosis of Parkinson's Disease Using Genetic Algorithm and Support Vector Machine," *J. Biomed. Sci. Eng.*, vol. 07, no. 04, pp. 147–156, Mar. 2014.
[93] W. R. Adams, "High-accuracy detection of early Parkinson's Disease using multiple characteristics of finger movement while typing," *PLoS One*, 2017.
[94] E. Abdulhay, N. Arunkumar, K. Narasimhan, E. Vellaiappan, and V. Venkatraman, "Gait and tremor investigation using machine learning techniques for the diagnosis of Parkinson disease," *Futur. Gener. Comput. Syst.*, vol. 83, pp. 366–373, Jun. 2018.
[95] A. Zhao, L. Qi, J. Li, J. Dong, and H. Yu, "A hybrid spatio-temporal model for detection and severity rating of Parkinson's disease from gait data," *Neurocomputing*, vol. 315, pp. 1–8, Nov. 2018.
[96] C. R. Pereira *et al.*, "Handwritten dynamics assessment through convolutional neural networks: An application to Parkinson's disease identification," *Artif. Intell. Med.*, vol. 87, pp. 67–77, May 2018.
[97] J. F. Reyes, J. Steven Montealegre, Y. J. Castano, C. Urcuqui, and A. Navarro, "LSTM and Convolution Networks exploration for Parkinson's Diagnosis," in *2019 IEEE Colombian Conference on Communications and Computing, COLCOM 2019 - Proceedings*, 2019, pp. 1–4.
[98] A. Johri and A. Tripathi, "Parkinson Disease Detection Using Deep Neural Networks," in *2019 12th International Conference on Contemporary Computing, IC3 2019*, 2019, pp. 1–4.
[99] A. L. T. Tavares *et al.*, "Quantitative measurements of alternating finger tapping in Parkinson's disease correlate with UPDRS motor disability and reveal the improvement in fine motor control from medication and deep brain stimulation," *Mov. Disord.*, vol. 20, no. 10, pp. 1286–1298, Oct. 2005.
[100] O. Bazgir, S. H. Habibi, L. Palma, P. Pierleoni, and S. Nafees, "A classification system for

assessment and home monitoring of tremor in patients with Parkinson's disease," *J. Med. Signals Sens.*, 2018.
[101] S. K. Patrick, A. A. Denington, M. J. A. Gauthier, D. M. Gillard, and A. Prochazka, "Quantification of the UPDRS rigidity scale," *IEEE Trans. Neural Syst. Rehabil. Eng.*, vol. 9, no. 1, pp. 31–41, 2001.
[102] H. Dai, H. Lin, and T. C. Lueth, "Quantitative assessment of parkinsonian bradykinesia based on an inertial measurement unit," *Biomed. Eng. Online*, vol. 14, no. 1, p. 68, Dec. 2015.
[103] Z. Lin, H. Dai, Y. Xiong, X. Xia, and S.-J. Horng, "Quantification assessment of bradykinesia in Parkinson's disease based on a wearable device," in *2017 39th Annual International Conference of the IEEE Engineering in Medicine and Biology Society (EMBC)*, 2017, pp. 803–806.
[104] T. Q. Mentzel *et al.*, "Reliability and validity of an instrument for the assessment of bradykinesia," *Psychiatry Res.*, vol. 238, pp. 189–195, Apr. 2016.
[105] J.-W. Kim *et al.*, "Quantification of bradykinesia during clinical finger taps using a gyrosensor in patients with Parkinson's disease," *Med. Biol. Eng. Comput.*, vol. 49, no. 3, pp. 365–371, Mar. 2011.
[106] S. Memar, M. Delrobaei, M. Pieterman, K. McIsaac, and M. Jog, "Quantification of whole-body bradykinesia in Parkinson's disease participants using multiple inertial sensors," *J. Neurol. Sci.*, vol. 387, pp. 157–165, Apr. 2018.
[107] "Kinesia ONE^{TM}." [Online]. Available: https://glneurotech.com/kinesia/products/kinesia-one/. [Accessed: 13-May-2019].
[108] J. Perry, *Gait Analysis: Normal and Pathological Function*. Thorofare, NJ: Slack, 1992.
[109] P. Catalfamo, D. Moser, S. Ghoussayni, and D. Ewins, "Detection of gait events using an F-Scan in-shoe pressure measurement system," *Gait Posture*, vol. 28, no. 3, pp. 420–426, Oct. 2008.
[110] N. Haji Ghassemi *et al.*, "Segmentation of Gait Sequences in Sensor-Based Movement Analysis: A Comparison of Methods in Parkinson's Disease," *Sensors*, vol. 18, no. 2, p. 145, Jan. 2018.
[111] J. R. Rebula, L. V. Ojeda, P. G. Adamczyk, and A. D. Kuo, "Measurement of foot placement and its variability with inertial sensors," *Gait Posture*, vol. 38, no. 4, pp. 974–980, Sep. 2013.
[112] S. Jiang, X. Wang, M. Kyrarini, and A. Gräser, "A robust algorithm for gait cycle segmentation," in *25th European Signal Processing Conference, EUSIPCO 2017*, 2017, vol. 2017-January, pp. 31–35.
[113] H. Ying, C. Silex, A. Schnitzer, S. Leonhardt, and M. Schiek, "Automatic step detection in the accelerometer signal," in *IFMBE Proceedings*, 2007, vol. 13, pp. 80–85.
[114] J. Barth *et al.*, "Subsequence dynamic time warping as a method for robust step segmentation using gyroscope signals of daily life activities," in *Proceedings of the Annual International Conference of the IEEE Engineering in Medicine and Biology Society, EMBS*, 2013, pp. 6744–6747.
[115] M. E. Micó-Amigo *et al.*, "A novel accelerometry-based algorithm for the detection of step durations over short episodes of gait in healthy elderly," *J. Neuroeng. Rehabil.*, vol. 13, no. 1, p. 38, Apr. 2016.
[116] V. N. Bobic, M. D. Djuric-Jovicic, S. M. Radovanovic, N. T. Dragasevic, V. S. Kostic, and M. B. Popovic, "Challenges of Stride Segmentation and Their Implementation for Impaired Gait," in *Proceedings of the Annual International Conference of the IEEE Engineering in Medicine and Biology Society, EMBS*, 2018, vol. 2018-July, pp. 2284–2287.
[117] N. Jovicic, "Therapeutic FES with distributed units," 2010.
[118] M. Müller, "Dynamic Time Warping," in *Information Retrieval for Music and Motion*, Springer Berlin Heidelberg, 2007, pp. 69–84.
[119] P. Senin, "Dynamic Time Warping Algorithm Review," Honolulu, Hawaii, 2008.
[120] R. C. Staudemeyer and E. R. Morris, "Understanding LSTM -- a tutorial into Long Short-Term Memory Recurrent Neural Networks," Sep. 2019.

[121] Andrew Ng, “Week 5: Neural Networks: Learning [MOOC lecture],” in *Machine Learning*, Coursera, 2018.
[122] N. Srivastava, G. Hinton, A. Krizhevsky, and R. Salakhutdinov, “Dropout: A Simple Way to Prevent Neural Networks from Overfitting,” 2014.
[123] S. Ioffe and C. Szegedy, “Batch normalization: Accelerating deep network training by reducing internal covariate shift,” in *32nd International Conference on Machine Learning, ICML 2015*, 2015, vol. 1, pp. 448–456.
[124] S. J. S. Hochreiter, “LSTM CAN SOLVE HARD LO G TIME LAG PROBLEMS,” 1997.
[125] C. H. Adler *et al.*, “Low clinical diagnostic accuracy of early vs advanced Parkinson disease: Clinicopathologic study,” *Neurology*, vol. 83, no. 5, pp. 406–412, Jul. 2014.
[126] S. Radovanović, M. Jovičić, N. P. Marić, and V. Kostić, “Gait characteristics in patients with major depression performing cognitive and motor tasks while walking,” *Psychiatry Res.*, vol. 217, no. 1–2, pp. 39–46, Jun. 2014.
[127] M. Pistacchi *et al.*, “Gait analysis and clinical correlations in early Parkinson’s disease,” *Funct. Neurol.*, vol. 32, no. 1, p. 28, 2017.
[128] E. K. Antonsson and R. W. Mann, “The frequency content of gait,” *J. Biomech.*, vol. 18, no. 1, pp. 39–47, Jan. 1985.
[129] X. Glorot and Y. Bengio, “Understanding the difficulty of training deep feedforward neural networks,” 2010.
[130] N. E. Fritz, F. M. Cheek, and D. S. Nichols-Larsen, “Motor-Cognitive Dual-Task Training in Persons with Neurologic Disorders: A Systematic Review,” *Journal of Neurologic Physical Therapy*, vol. 39, no. 3. Lippincott Williams and Wilkins, pp. 142–153, 30-Jul-2015.
[131] M. Plotnik, N. Giladi, Y. Dagan, and J. M. Hausdorff, “Postural instability and fall risk in Parkinson’s disease: Impaired dual tasking, pacing, and bilateral coordination of gait during the ‘oN’ medication state,” in *Experimental Brain Research*, 2011, vol. 210, no. 3–4, pp. 529–538.
[132] G. Yogev, N. Giladi, C. Peretz, S. Springer, E. S. Simon, and J. M. Hausdorff, “Dual tasking, gait rhythmicity, and Parkinson’s disease: Which aspects of gait are attention demanding?,” *Eur. J. Neurosci.*, vol. 22, no. 5, pp. 1248–1256, Sep. 2005.
[133] S. Saeb, L. Lonini, A. Jayaraman, … D. M.-, and undefined 2017, “The need to approximate the use-case in clinical machine learning,” *academic.oup.com*, vol. 6, no. 5, 2017.
[134] M. Djurić-Jovičić *et al.*, “Quantification of Finger-Tapping Angle Based on Wearable Sensors,” *Sensors*, vol. 17, no. 2, p. 203, Jan. 2017.
[135] H. Ling, L. A. Massey, A. J. Lees, P. Brown, and B. L. Day, “Hypokinesia without decrement distinguishes progressive supranuclear palsy from Parkinson’s disease,” *Brain*, vol. 135, no. 4, pp. 1141–1153, Apr. 2012.
[136] H. Goldstein, C. Poole, and J. Safko, *Classical Mechanics* , vol. 32, no. 7. Addison Wesley: San Francisco, CA, USA, 2000.
[137] J. A. Nelder and R. Mead, “A Simplex Method for Function Minimization,” *Comput. J.*, vol. 7, no. 4, pp. 308–313, Jan. 1965.
[138] V. Bobić, M. Djurić-Jovičić, N. Dragašević, M. B. Popović, V. S. Kostić, and G. Kvaščev, “An Expert System for Quantification of Bradykinesia Based on Wearable Inertial Sensors,” *Sensors*, vol. 19, no. 11, p. 2644, Jun. 2019.
[139] L. Senhadji and F. Wendling, “Epileptic transient detection: wavelets and time-frequency approaches,” *Neurophysiol. Clin. Neurophysiol.*, vol. 32, no. 3, pp. 175–192, Jun. 2002.
[140] D. Gajic, Z. Djurovic, S. Di Gennaro, and F. Gustafsson, “Classification of EEG signals for detection of epileptic seizures based on wavelets and statistical pattern recognition,” *Biomed. Eng. - Appl. Basis Commun.*, vol. 26, no. 2, Mar. 2014.
[141] V. N. Bobić *et al.*, “Frequency analysis of repetitive finger tapping – extracting parameters for movement quantification,” in *Proc of the 3rd International Conference on Electrical, Electronic and Computing Engineering*, 2016, p. MEI2.2 1-MEI2.2 5.
[142] V. Bobic *et al.*, “Spectral parameters for finger tapping quantification,” *Facta Univ. - Ser.*

Electron. Energ., vol. 30, no. 4, pp. 585–597, 2017.
[143] P. D. Welch, "The Use of Fast Fourier Transform for the Estimation of Power Spectra: A Method Based on Time Averaging Over Short, Modified Periodograms," *IEEE Trans. Audio Electroacoust.*, vol. 15, no. 2, pp. 70–73, 1967.
[144] A. Weiss, S. Sharifi, M. Plotnik, J. P. P. Van Vugt, N. Giladi, and J. M. Hausdorff, "Toward automated, at-home assessment of mobility among patients with Parkinson disease, using a body-worn accelerometer," *Neurorehabil. Neural Repair*, vol. 25, no. 9, pp. 810–818, Nov. 2011.
[145] S. Balasubramanian, A. Melendez-Calderon, A. Roby-Brami, and E. Burdet, "On the analysis of movement smoothness," *J. Neuroeng. Rehabil.*, vol. 12, no. 1, pp. 1–11, Dec. 2015.
[146] S. Balasubramanian, A. Melendez-Calderon, and E. Burdet, "A robust and sensitive metric for quantifying movement smoothness," *IEEE Trans. Biomed. Eng.*, vol. 59, no. 8, pp. 2126–2136, 2012.
[147] V. Crocher, J. Fong, M. Klaic, D. Oetomo, and Y. Tan, "A tool to address movement quality outcomes of post-stroke patients," *Biosyst. Biorobotics*, vol. 7, pp. 329–339, 2014.
[148] A. K. Jain, "Data clustering: 50 years beyond K-means," *Pattern Recognit. Lett.*, vol. 31, no. 8, pp. 651–666, Jun. 2010.
[149] A. Tharwat, "Classification assessment methods," *Appl. Comput. Informatics*, 2018.
[150] J. M. Hausdorff, J. Balash, and N. Giladi, "Effects of Cognitive Challenge on Gait Variability in Patients with Parkinson's Disease," *J. Geriatr. Psychiatry Neurol.*, vol. 16, no. 1, pp. 53–58, Mar. 2003.

Biography

Vladislava Bobić was born on October 11, 1991, in Belgrade, where she finished elementary school and high school with excellent grades. She enrolled in the School of Electrical Engineering – University of Belgrade in 2010. In 2014, she graduated from the Department of Physical Electronics, majoring in Biomedical and Environmental Engineering, with an average grade of 9.33. She was awarded as the best graduate student of the department for the school year 2013/2014. In 2015, she completed master studies at the same faculty, on the module for Biomedical and Environmental Engineering. Afterwards, she enrolled in doctoral studies at the Department for System Control and Signal Processing. Her average grade during master and doctoral studies was 10.00.

During her bachelor and master studies, Vladislava was a recipient of several scholarships awarded by the Serbian Ministry of Education, Science and Technological Development (MPNTR), including the "Scholarship for Extremely Gifted Students" and the scholarship for doctoral students. During her doctoral fellowship, she was engaged on the MPNTR project #175090 "Motor and Non-Motor Symptoms of Parkinsonism: Clinical, Morphological, and Molecular-Genetic Correlations," PI prof. dr Vladimir Kostić. Since November 2016, Vladislava has been working as a researcher at the Innovation Center, School of Electrical Engineering in Belgrade (ICEF), engaged on the MPNTR project OI #175016 "Effects of assistive systems in neurorehabilitation: recovery of sensory-motor functions," PI prof. dr Mirjana Popović. So far, Vladislava has participated in 9 different research or commercial projects, including two projects of bilateral scientific cooperation with France and Germany. In addition to her research work, Vladislava also works as the ICEF's Operations Manager.

During her master and doctoral studies, Vladislava began her multidisciplinary research in the field of clinical engineering. Her research focuses on the development of new systems that can support the clinical decision-making process, as well as the assessment of patients with neurological disorders. Since 2014, she has participated in several scientific studies regarding the movement analysis in patients with neurodegenerative diseases, most notably Parkinson's disease. The results of her research have been presented in 14 papers, including – 3 papers in the international journals, one paper in a domestic journal, 9 papers at international conferences, one paper at a national conference. Her two publications from the international conference IcEtran (published in 2016 and 2018) were awarded as the best papers of the section.

образац изјаве о ауторству

Изјава о ауторству

Име и презиме аутора Владислава Н. Бобић

Број индекса 5014/2015

Изјављујем

да је докторска дисертација под насловом

"Систем за подршку одлучивању, евалуацију и праћење стања пацијената оболелих од неуродегенеративних болести"

(наслов на енглеском: "Decision support system for assessment of patients with neurodegenerative disorders")

- резултат сопственог истраживачког рада;
- да дисертација у целини ни у деловима није била предложена за стицање друге дипломе према студијским програмима других високошколских установа;
- да су резултати коректно наведени и
- да нисам кршио/ла ауторска права и користио/ла интелектуалну својину других лица.

Потпис аутора

У Београду, 14.12.2020.

Владислава Бобић

образац изјаве о истоветности штампане и електронске верзије докторског рада

Изјава о истоветности штампане и електронске верзије докторског рада

Име и презиме аутора Владислава Н. Бобић

Број индекса 5014/2015

Студијски програм Електротехника и рачунарство, Управљање системима и обрада сигнала

Наслов рада "Систем за подршку одлучивању, евалуацију и праћење стања пацијената оболелих од неуродегенеративних болести" (наслов на енглеском: "Decision support system for assessment of patients with neurodegenerative disorders")

Ментор др Горан Квашчев, ванредни професор

Изјављујем да је штампана верзија мог докторског рада истоветна електронској верзији коју сам предао/ла ради похрањивања у **Дигиталном репозиторијуму Универзитета у Београду.**

Дозвољавам да се објаве моји лични подаци везани за добијање академског назива доктора наука, као што су име и презиме, година и место рођења и датум одбране рада.

Ови лични подаци могу се објавити на мрежним страницама дигиталне библиотеке, у електронском каталогу и у публикацијама Универзитета у Београду.

Потпис аутора

У Београду, 14.12.2020.

Владислава Бобић

образац изјаве о коришћењу

Изјава о коришћењу

Овлашћујем Универзитетску библиотеку „Светозар Марковић“ да у Дигитални репозиторијум Универзитета у Београду унесе моју докторску дисертацију под насловом:

"Систем за подршку одлучивању, евалуацију и праћење стања пацијената оболелих од неуродегенеративних болести"

(наслов на енглеском: "Decision support system for assessment of patients with neurodegenerative disorders")

која је моје ауторско дело.

Дисертацију са свим прилозима предао/ла сам у електронском формату погодном за трајно архивирање.

Моју докторску дисертацију похрањену у Дигиталном репозиторијуму Универзитета у Београду и доступну у отвореном приступу могу да користе сви који поштују одредбе садржане у одабраном типу лиценце Креативне заједнице (Creative Commons) за коју сам се одлучио/ла.

1. Ауторство (CC BY)

2. Ауторство – некомерцијално (CC BY-NC)

3. Ауторство – некомерцијално – без прерада (CC BY-NC-ND)

4. Ауторство – некомерцијално – делити под истим условима (CC BY-NC-SA)

5. Ауторство – без прерада (CC BY-ND)

6. Ауторство – делити под истим условима (CC BY-SA)

(Молимо да заокружите само једну од шест понуђених лиценци.
Кратак опис лиценци је саставни део ове изјаве).

Потпис аутора

У Београду, 14.12.2020.

Владислава Бодић

1. **Ауторство**. Дозвољавате умножавање, дистрибуцију и јавно саопштавање дела, и прераде, ако се наведе име аутора на начин одређен од стране аутора или даваоца лиценце, чак и у комерцијалне сврхе. Ово је најслободнија од свих лиценци.

2. **Ауторство – некомерцијално.** Дозвољавате умножавање, дистрибуцију и јавно саопштавање дела, и прераде, ако се наведе име аутора на начин одређен од стране аутора или даваоца лиценце. Ова лиценца не дозвољава комерцијалну употребу дела.

3. **Ауторство – некомерцијално – без прерада**. Дозвољавате умножавање, дистрибуцију и јавно саопштавање дела, без промена, преобликовања или употребе дела у свом делу, ако се наведе име аутора на начин одређен од стране аутора или даваоца лиценце. Ова лиценца не дозвољава комерцијалну употребу дела. У односу на све остале лиценце, овом лиценцом се ограничава највећи обим права коришћења дела.

4. **Ауторство – некомерцијално – делити под истим условима**. Дозвољавате умножавање, дистрибуцију и јавно саопштавање дела, и прераде, ако се наведе име аутора на начин одређен од стране аутора или даваоца лиценце и ако се прерада дистрибуира под истом или сличном лиценцом. Ова лиценца не дозвољава комерцијалну употребу дела и прерада.

5. **Ауторство – без прерада**. Дозвољавате умножавање, дистрибуцију и јавно саопштавање дела, без промена, преобликовања или употребе дела у свом делу, ако се наведе име аутора на начин одређен од стране аутора или даваоца лиценце. Ова лиценца дозвољава комерцијалну употребу дела.

6. **Ауторство – делити под истим условима**. Дозвољавате умножавање, дистрибуцију и јавно саопштавање дела, и прераде, ако се наведе име аутора на начин одређен од стране аутора или даваоца лиценце и ако се прерада дистрибуира под истом или сличном лиценцом. Ова лиценца дозвољава комерцијалну употребу дела и прерада. Слична је софтверским лиценцама, односно лиценцама отвореног кода.